Biomechanics and Dynamics of Turning

Kevin Charles Flick

A dissertation submitted in partial fulfillment of the
requirements for the degree of

Doctor of Philosophy

University of Washington

2005

Program Authorized to Offer Degree:
Zoology

INFORMATION TO USERS

The quality of this reproduction is dependent upon the quality of the copy submitted. Broken or indistinct print, colored or poor quality illustrations and photographs, print bleed-through, substandard margins, and improper alignment can adversely affect reproduction.

In the unlikely event that the author did not send a complete manuscript and there are missing pages, these will be noted. Also, if unauthorized copyright material had to be removed, a note will indicate the deletion.

ProQuest Information and Learning Company
300 North Zeeb Road
P.O. Box 1346
Ann Arbor, MI 48106-1346

University of Washington
Graduate School

This is to certify that I have examined this copy of a doctoral dissertation by

Kevin Charles Flick

and have found that it is complete and satisfactory in all respects,
and that any and all revisions required by the final
examining committee have been made.

Chair of Supervisory Committee:

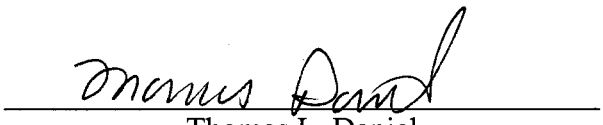

Thomas L. Daniel

Reading Committee:

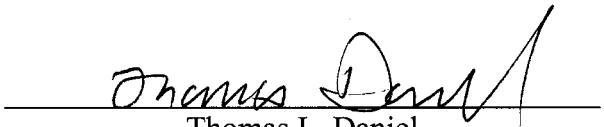

Thomas L. Daniel

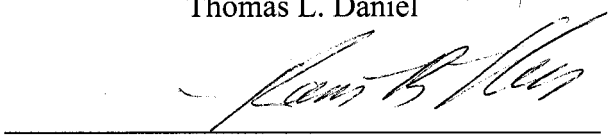

Raymond B. Huey

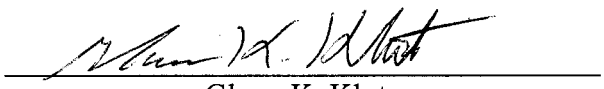

Glenn K. Klute

Date: 5/2/05

In presenting this dissertation in partial fulfillment of the requirements for the doctoral degree at the University of Washington, I agree that the Library shall make its copies freely available for inspection. I further agree that extensive copying of the dissertation is allowable only for scholarly purposes, consistent with "fair use" as prescribed in the U.S. Copyright Law. Requests for copying or reproducing of this dissertation may be referred to Proquest Information and Learning, 300 North Zeeb Road, Ann Arbor, MI, 48106-1364, to whom the author has granted "the right to reproduce and sell (a) copies of the manuscript in microform and/or (b) printed copies of the manuscript made from microform."

Signature 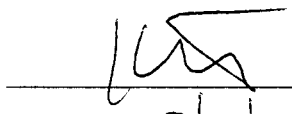

Date 5/2/05

University of Washington

Abstract

Biomechanics and dynamics of turning

Kevin Charles Flick

Chair of the Supervisory Committee:
Professor Thomas L. Daniel
Zoology

In chapter one, I examine the extent to which a pelagic marine gastropod, *Clione limacina*, turns by changing its wingstroke kinematics versus shifting its tail position as a rudder. I find that there is no evidence for tail-ruddering in free-swimming animals under the conditions tested. In response to tilting a tethered animal with respect to gravity, however, the wingstroke kinematics do change. Compared to its preferred head-up orientation, when the animal is tethered at 45° or 90°, the average wing position shifts ventrally by one body width.

In chapter two, I explore the effects of turning around a 90° corner for humans with and without lower-limb, below-knee amputations. I find that amputees appear to compensate for their limb loss by reducing the extent to which they shift their prosthetic limbs under their pelvis during a turn. I also find that there is no difference between intact and amputee subjects in the distribution of the body's total rotation between the two feet.

In chapter three (Flick, et al., 2005), we compare the mechanical performance of prosthetic rotation adaptors to data on ankle rotation in intact humans. We find that the human ankle varies in composite stiffness throughout the stride. While none of the

rotation adaptors tested varies its stiffness in the same pattern, most of them encompassed the range of human ankle rotation and torque.

In chapter four, I use a finite element model of the below-knee amputee's residual limb and prosthetic socket to predict the differences in tissue strain between walking straight and turning, both with and without a prosthetic rotation adaptor. There are differences in the absolute amounts of tissue strain and its rate of increase between walking straight and turning. The inclusion of a rotation adaptor has very little effect.

TABLE OF CONTENTS

LIST OF FIGURES

LIST OF TABLES

ACKNOWLEDGEMENTS

Countless people have made this work possible.

I have benefited tremendously from major contributions of time and effort, casual conversations in the hallways, much needed distractions, love, words of advice and warning, and more patience than imaginable.

Without the help of colleagues, friends, and family, I'd still be sitting in the lab.

Thank you.

My work was funded by the University of Washington Presidential Fellowship and the NIDRR Mary Switzer Fellowship awarded to me. I was also supported by grants awarded to Tom Daniel: the UW Komen Professorship, the MacArthur Fellowship, and an ONR Grant. The VA and Glenn Klute were also generous with their funding through their Center Grant and various Merit Review Projects.

DEDICATION

To Melissa.

Chapter One: Directional Control of Swimming in Marine Mollusc *Clione limacina*

INTRODUCTION

An organism maneuvers in the environment by generating forces with its body, utilizing whatever number and type of appendages it has. Each appendage may act in different modes (e.g. braking, propelling, providing turning forces), depending on its motion patterns. Most organisms simultaneously or alternately use different modes and/or appendages, each of which can be considered a locomotor mechanism. When and how they switch between these mechanisms depends on the external environment and the organism's need for maneuvering. For example, locusts maneuver via left/right forewing kinematic asymmetries, and lateral flexion of the abdomen and legs (Robertson and Johnson 1993). When the locust flies slowly, leg and abdomen flexion alter the direction of net force by shifting the animal's center of gravity with respect to the wingstroke plane (Zanker 1988). At high speeds, leg and abdominal flexion may also create torque by exposing different sides of the animal to aerodynamic pressure (Camhi 1970b; Gotz, Hengstenberg et al. 1979). In collision avoidance maneuvers, changes in the locusts' wingstroke kinematics were very predictable, while the leg and abdomen flexion was more variable. Thus locusts appear to vary the extent of abdominal ruddering as needed for maneuvers (Robertson and Johnson 1993).

The neural basis of locomotor control has been studied extensively in the shell-less marine gastropod, *Clione limacina*. *Clione* is capable of reacting to a number of environmental cues: temperature (Panchin, Arshavsky et al. 1995), gravity (Arshavsky,

Deliagina et al. 1991; Panchin, Arshavsky et al. 1995), touch (Arshavsky Yu, Beloozerova et al. 1985; Satterlie, Labarbera et al. 1985), and contact with prey (Arshavsky Yu, Beloozerova et al. 1985; Arshavsky, Deliagina et al. 1993). While it is clear that Clione senses its environment in at least these demonstrated ways, the connection between stimuli and natural behavior is unclear.

Also unclear are the locomotor mechanisms for turning, themselves. Specifically, the role of the wings in maneuvering is undecided. Anecdotal evidence suggests that *Clione* maneuvers by flexing its tail in the direction of a turn. The assumed mechanism is the same as ruddering a boat – a change in torque due to a different profile and different center of pressure on the animal (Satterlie, Labarbera et al. 1985; Panchin, Arshavsky et al. 1995). The most direct evidence for tail ruddering comes from a study (Deliagina, Arshavsky et al. 1998) showing increased activity in the motor neurons of the longitudinal tail muscles contralateral to the direction of an imposed tilt. They also demonstrated that motor output to the tail muscles could be used to right an isolated *Clione* CNS on a rotating platform under closed loop conditions. These findings are excellent neurobiological support for the ruddering hypothesis, however no whole-organism behavioral work has been done. Also, since no kinematic analysis of the wingstroke pattern exists, little can be said for the wings' role in maneuvering. Like the locust, *Clione* may also make use of multiple locomotor mechanisms.

Abdominal ruddering and/or changes in the wing kinematics are detectable with 3D video analysis techniques. If a freely swimming animal uses abdominal ruddering, its body angle should change before its heading changes (fig. 1.1). If the forward heading is

0^{o}, and if body curvature is measured as a change from 180^{o} (straight body), ruddering would be indicated as a decrease in curvature (down from 180^{o}) followed by an increase in heading angle (up from 0^{o}). In this case, heading would be negatively correlated with curvature, with some time lag. Additionally, since *Clione* is sensitive to gravity, potential changes in the wing kinematics could be detected by analyzing digitized the wingtip over time while changing the animal's angle with respect to gravity. Assuming that the animal would try to right itself to its preferred upright orientation (Deliagina, Arshavsky et al. 1998), it would use different wingstroke patterns at different angles.

In the present study I address two questions: 1) Is tail ruddering evident in free-swimming animals?, and 2) Do wingstroke patterns change in response to changes in body orientation with respect to gravity? I use a combination of theoretical and empirical approaches to address these questions. I will show results from predator prey interaction models, and data from both free-swimming and tethered animal experiments.

MATERIALS AND METHODS

Animal Background

The pteropod, *Clione limacina* (Class: Gastropoda, Order: Gymnosomata) is a free-swimming snail found in all northern oceans. Adults are entirely pelagic and swim by alternating dorsal and ventral flexions of its wings (parapodia). The parapodia flex back and forth in much the same way as birds and flying insects. The wing rotates around the base, alternating angle of attack, to provide lift on the up and down-strokes. The wings overlap at the end of each half-stroke on the ventral and dorsal sides (Satterlie, Labarbera

et al. 1985). The animals maintain a head-up posture at normal swimming speeds (1 to 3 body lengths per second), but perform tight turns and loops when startled or hunting (Arshavsky, Deliagina et al. 1993). Four of the seven muscle groups in each wing (two associated with each wing surface) are linked to "global" dorsal and ventral flexion. The other three may change the wing shape (span-wise length, chord-wise length, and wing thickness). Additionally, longitudinal muscles in the trunk are capable of bending the tail (Satterlie, Labarbera et al. 1985).

Animal Maintenance

Live adults (1-2.5 cm long) were collected in the spring and early summer of 2000 off the breakwater at the Friday Harbor Marine Laboratory, on Friday Harbor Island, Washington. I kept animals in 8-liter jars of 7-10°C (local water temperature) filtered seawater, which I changed at least once daily. Experiments were conducted in a 40-liter tank of fresh, filtered seawater at 10°C.

Video

Positional data were collected with two black and white Sony analog video cameras that captured either front and side, or front and top orthogonal views of the animal at 30 frames per second. Two video sources were synchronized and recorded on the same SVHS tape via a screen splitter. I digitized the video with Adobe Premier and analyzed the resulting coordinate data with custom software written in Matlab.

Experimental Design and Analysis: Tail-Ruddering

I filmed individual animals from the front and side (after a 30-minute acclimation period in the experimental tank) to test whether tail ruddering is used in freely swimming

animals. The cameras were positioned to capture the animal in the center of the tank in order to avoid possible wall effects. Video segments of the animal turning at approximately the same rate of angular change in heading were analyzed for any cross-correlation between the heading and body angle (see below).

For each frame of video data I digitized, the animal's head, anterior margin of the viscera and tail tip from both camera views (fig. 1.2). This generated a time series of 3D coordinates for each animal's head, center, and tail. Here, an interesting phenomenon arose in the analysis. If the animal swims forward with a fixed body angle while rotating around its long axis, the 3D planes of rotation are no longer independent from one another. Since the pressure on the bent trailing portion turns the whole animal, and the rotation causes the pressure to move around the direction of motion, the animal would travel in a spiral with no change in body angle. To eliminate the possibility of this effect, I projected the coordinates onto (and analyzed the data from the perspective of) the three orthogonal coordinate planes (XY, XZ, & YZ). This is as simple as viewing the animal perpendicularly to each plane and neglecting depth.

From the digitized body positions, I measured the body angle and heading (see figure 1). For the three turns digitized, I generated a cross-correlogram between the body angle and heading.

Experimental Design and Analysis: Wing Kinematics

To test the idea that *Clione* alters its wing kinematics for postural control, I elicited changes in the wingtip kinematics by changing the whole animal's orientation with respect to gravity. For these experiments, animals were glued with cyano-acrylate to a

0.5mm diameter wire on the dorsal midline, just posterior to the wings. Each of five animals was held in the center of the tank at 0° (upright), 45°, or 90° (horizontal, ventral side down).

For each frame of video data, I digitized the center of the animal's head and the wingtip. Between the head and the wing-base, the body does not flex appreciably while the animal swims, so the head coordinates were subtracted from the wing coordinates to remove body motion from the wingtip kinematics. Because each animal bent its body at a unique angle, coordinates were tilted in the XY plane so that the new Y-axis aligned with the animal's long axis, from the midsection to the tip of the head (fig. 1.2). Five animals were held at each of the three treatment angles. Roughly five-second segments, during which the animal flapped at a characteristic 2 to 3 Hz, were digitized for each trial. For analysis, the x, y and z coordinate time series for each wingstroke were cut from the original data and re-splined (Matlab cubic spline algorithm) with 100 points to account for slight variations in the duration of each wingstroke. All the re-splined wingstrokes were aligned in time and averaged across all animals for each treatment. The mean x, y, and z positions in time are shown with 95% confidence intervals (using the Bonferroni multiple-comparison correction: $\alpha_B = \alpha/g$; g=100) in figure 1.6.

Experimental Design and Analysis: Predator/Prey Simulation

As a theoretical addendum, I created a computer model of a predator/prey interaction. The model does not represent the behavior of either *Clione* or its prey, *Limacina*. The purpose of the model is to demonstrate the difficulty of visually detecting the difference between random and biased predatory behavior. The current opinion among most *Clione*

researchers is that *Clione* behaves randomly and may be aggregated with its prey by water currents. While this opinion may be correct, it is not based on any objective data, nor are there gastropods that do not utilize their chemoreceptive capacities for some non-random behavior. The 3D model establishes a 15cm radius sphere around a stationary prey (a point) inside which, the predator can "detect" the prey. For each trial, the predator starts 30 cm away from the prey and 15 cm from the signal boundary. During each second of the one-hour simulation, the predator can stay still or move one cm in either positive or negative X, Y or Z (seven possibilities). The predator is biased to continue in the same direction it was going when it detected the prey signal (got within 15cm of the prey). Outside the signal sphere, the predator has an equal likelihood of any of the seven movement possibilities. I ran 1000 trials of the model with each of three predator behaviors: zero bias (random, no effect of signal sphere), and 17% and 22% bias in favor of the direction the predator was moving upon signal encounter. See appendices A & B for the Matlab code.

RESULTS

Tail Ruddering

As described in the introduction, ruddering would emerge as a negative correlation of the heading with respect to curvature with a time lag. This would be evident in the graphs as a negative peak on the negative side of the time axis. Because each animal was turning in a different direction, which means a different angular change in each orthogonal plane, we do not expect this pattern for each animal in each plane. What we are looking for is that each animal would evidence a clear negative correlation in at least

one of the planes, but not necessarily all of them. There is no consistent pattern of that relationship, which suggests that the animals tested were not using tail ruddering (fig. 1.3)

Wing Kinematics

Over the range of tether angles tested there is variation in the mean position of the wingtip and some of the finer details of the wingtip paths. Compared to the 0° (upright) wingtip kinematics, the kinematics at 45° and 90° (horizontal) are shifted ventrally. As a consequence of the ventral shift in position, the ventral overlap of the wingtips is greater, and the dorsal overlap is lessened. Figure 1.4 gives a the general pattern for one animal, to give the reader a sense of the changes that will be discussed in more detail below.

Compared to the kinematics at 0° the same pattern emerges from the data pooled from all the animals. There is a ventral shift in the mean wingtip position of about one body-width at 45° and 90° (fig. 1.5). In the X-axis, a longer, ventrally shifted downstroke is evident at 45° and 90°. Additionally, the upstroke at 90° is shorter by 3mm and there is the dorsal crossover is lessened. The trajectories in the Y-axis are not significantly different, nor are the 0° and 45° trajectories in the Z-axis. However, the 90° trajectory in the Z-axis shows a more lateral shift (greater wing extension) in the downstroke, and a more medial upstroke. The normal period of dorsal crossover is marked by a more lateral position of the wingtip, another indicator that dorsal crossover is lessened. These results come from figure 1.6, in which regions of non-overlapping 95% confidence intervals are taken as significantly different.

Predator/Prey Model

The paths that the virtual predators take are visually indistinguishable from one another, yet the three conditions yield 30, 41, and 67 encounters per 1000 hunts, respectively (fig. 1.7). All three results are significantly different from one another (ANOVA, $p<0.0001$).

DISCUSSION

This study examined two aspects of *Clione's* maneuvering behavior. The first experiment was designed to evaluate the presence of tail ruddering in free-swimming animals. The second experiment was designed to examine whether or not there was a righting response in the wingstroke patterns response to changes in body orientation with respect to gravity. The results from the first experiment do not indicate tail ruddering over the range of swimming speeds and turning rates analyzed. The results from the second experiment show evidence for wingtip path modulation in response to changes in the animals' body angle with respect to gravity.

Clione can vary its swimming speeds from less than 1 body length per second to 4 body lengths per second. While turning in the free-swimming experiments, all of the animals in this experiment swam on the slow end of the speed range and turned with relatively large radii (~10 body lengths). When startled or stimulated by prey, *Clione* maintains a pronounced mid-body bend and swims its fastest while executing small radii turns (1 to 2 body lengths). These conditions are more favorable for ruddering than the conditions in this study. It is possible that the same velocity dependent effect of

abdominal ruddering in locusts also holds true for *Clione*. The effect of hydrodynamic drag on the tail is proportional to the projected surface area of the tail and the square of the animal's velocity. At the low swimming speeds in the current analysis, it may be the case that tail ruddering is generally ineffective, and that wing steering is the dominant mechanism.

The wing kinematic data demonstrate a probable posture correcting behavior. While the forces were not directly measured, we can infer the direction of the force changes by the changes in the wing kinematics. The major difference between 0° and either 45° or 90° is the ventral shift in the mean wing position. This indicates a shift in the whole wingstroke envelope to the ventral side, which moves the net anterior force to the ventral side, creating a restorative force towards the head-up posture. It is currently believed that the wings generate force in each half-stroke by traditional circulatory lift and that the wing generates increased early circulation by peeling away from the body (Satterlie, Labarbera et al. 1985) , similar to the insect "clap-and-fling" model (Bennett 1977). Because the wings come closer to the body at the end of the downstroke, they are in a position to generate early circulation by peeling away from the body, whereas they do not come near the body on the dorsal side. Compared to the downstroke, this mechanism causes increased circulation on the upstroke. This would act to further right the animal towards the ventral side.

The shift in amount of wingtip overlap suggests another possible force generation mechanism. When the wingtips overlap at the end of each wingstroke, they appear to create a pocket of water that is ejected downwards. This water jet would propel the

animal upwards and away from the side on which the jet was created. Because there is no overlap on the dorsal side and increased overlap on the ventral side, this mechanism would add to the restorative forces by creating another force on the ventral side to right the animal towards the head-up posture.

Pursuing the mechanisms for fine spatial and postural control in *Clione* begs the question of the animals' need for this control. Our best understanding of *Clione's* predatory capacity is that they switch to a more aggressive hunting behavior only after physical contact with their prey, a conclusion drawn from watching *Clione* behave in an aquarium with *Limacina*. However, subtle changes in behavior that may increase the average encounter rate with prey items would be difficult to detect by visual observation without quantifying the behavior in some way. The predator/prey computer model, while insufficient to describe the exact relationship between Clione and its prey, casts doubt on our ability to visually detect small biases that are result in higher prey encounter rates for a predator.

This research was intended to answer the following questions: "Does *Clione* Rudder?", "Does *Clione* steer with its wings?", and "Is it possible to model predatory behavior that is impossible to detect visually, yet confers an advantage to the predator?". On the basis of the data presented it is possible to answer all three questions: no, yes, and yes, respectively. The evidence against tail ruddering under these experimental conditions and the modeling support for biased behavior lend support to the evidence that Clione does indeed maneuver and does so at least in part with its wings. The evidence for changes in the wingstroke pattern reveals a novel control mechanism for the organism.

Given the wing musculature, shape changes can occur in all dimensions, giving rise to many different, and completely un-studied maneuvering control mechanisms.

NOTES TO CHAPTER ONE

Arshavsky, Y. I., T. G. Deliagina, et al. (1993). "Pharmacologically induced elements of the hunting and feeding behavior in the pteropod mollusk Clione limacina: I. Effects of GABA." Journal of Neurophysiology Bethesda **69**(2): 512-521.

Arshavsky, Y. I., T. G. Deliagina, et al. (1991). Locomotion of *Clione limacina* in relation to various types of behavior. Simpler nervous systems. D. A. Sakharov and W. Winlow. Manchester, UK, Manchester University Press: 290-315.

Arshavsky Yu, I., I. N. Beloozerova, et al. (1985). "Control of Locomotion in Marine Mollusk Clione-Limacina 1. Efferent Activity During Actual and Fictitious Swimming." Experimental Brain Research **58**(2): 255-262.

Bennett, L. (1977). "Clap And Fling Aerodynamics - Experimental Evaluation." Journal Of Experimental Biology **69**(AUG): 261-272.

Camhi, J. (1970b). "Sensory control of abdomen posture in flying locusts." Journal of Experimental Biology **52**: 533-537.

Deliagina, T. G., Y. I. Arshavsky, et al. (1998). "Control of spatial orientation in a mollusc." Nature London **393**(6681): 172-175.

Gotz, K., B. Hengstenberg, et al. (1979). "Optomotor control of wing beat and body posture in *Drosophila*." Biol Cybern **35**: 101-112.

Panchin, Y. V., Y. I. Arshavsky, et al. (1995). "Control of locomotion in marine mollusk Clione limacina: IX. Neuronal mechanisms of spatial orientation." Journal of Neurophysiology Bethesda **73**(5): 1924-1937.

Robertson, R. M. and A. G. Johnson (1993). "Collision Avoidance of Flying Locusts: Steering Torques and Behavior." J. exp. Biol. **183**: 35-60.

Satterlie, R. A., M. Labarbera, et al. (1985). "Swimming in the Pteropod Mollusk Clione-Limacina I. Behavior and Morphology." Journal of Experimental Biology **116**: 189-204.

Zanker, J. M. (1988). "How does lateral abdomen deflection contribute to flight control of *Drosophila melanogaster*?" J. Comp. Physiol. A **162**: 581-588.

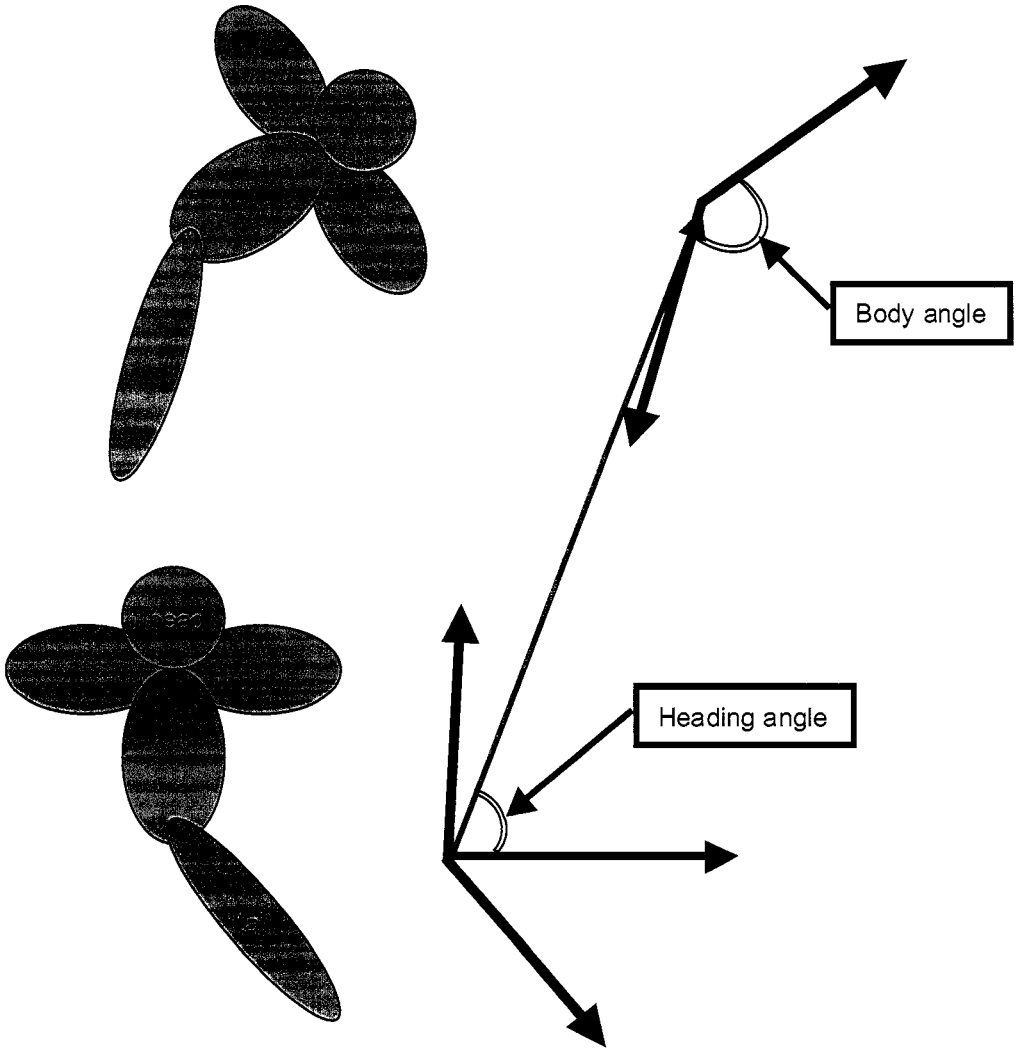

Figure 1.1. *Clione* body angle and heading diagram. A cartoon of the animal is on the left, with the body segments replaced by vectors on the right. The lower diagrams are one frame earlier than the upper diagrams.

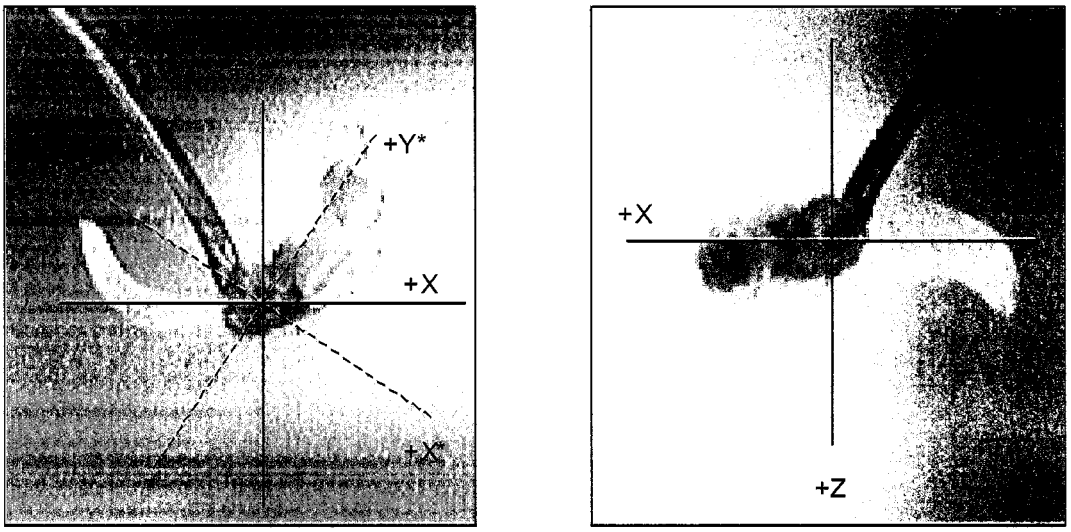

Figure 1.2. One video frame from the wing kinematics experiments. The left image is from the front of the tank and the right image is from above. On the left, the axes (X,Y) are originally aligned with the sides of the frame, and then transformed so that the animal's long axis became the Y-axis (X*,Y*). The Z-axis is the center of rotation.

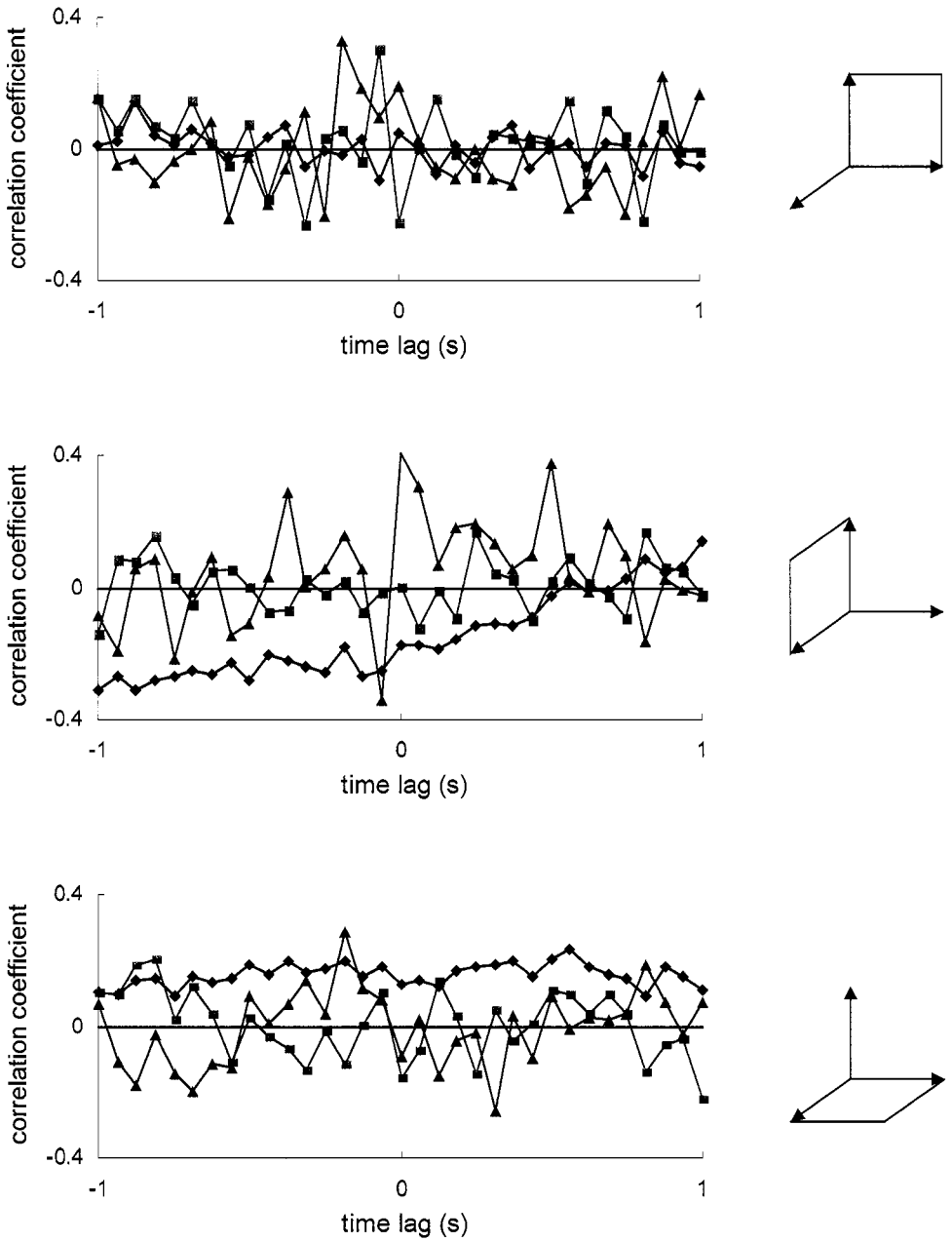

Figure 1.3. Body angle and heading correlation coefficients. Correlations in time between the animal's heading and body angle (fig. 1.1) for 3 free-swimming turns in three planes. blue diamonds: animal 1, red squares: animal 2, green triangles, animal 3

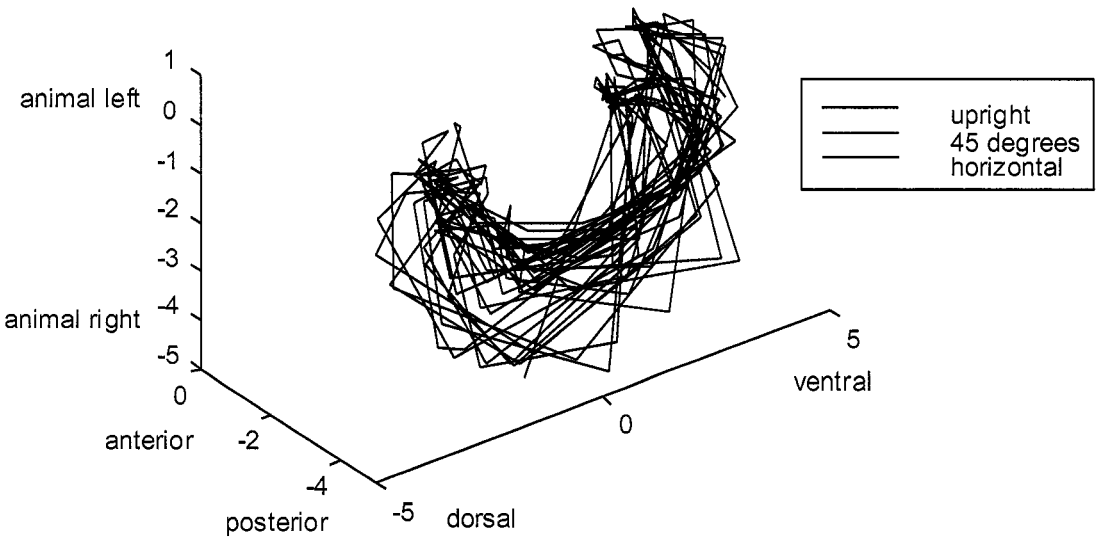

Figure 1.4. Sample *Clione* wingtip pattern. Wingtip relative to the animal's body for one animal tethered in three different positions relative to gravity. Axis dimensions are in mm.

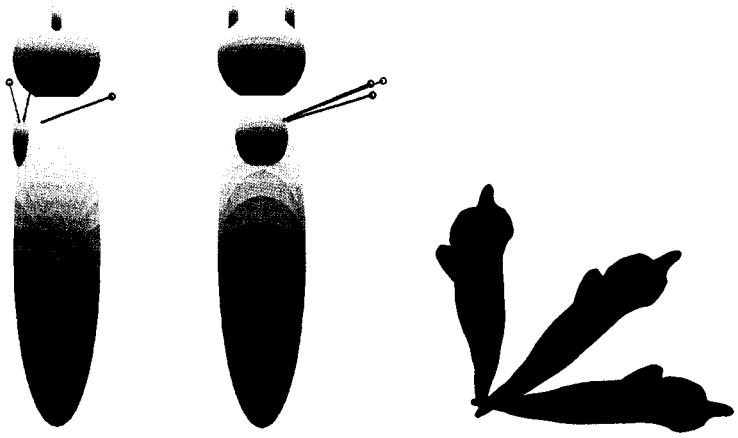

Figure 1.5. Mean wingtip positions. The left view is of the animal's left while the right view is of the ventral surface. The end of each ray indicates the mean wingtip position for each treatment (black: 0 degrees, blue: 45 degrees, red: 90 degrees). n=5 for each treatment

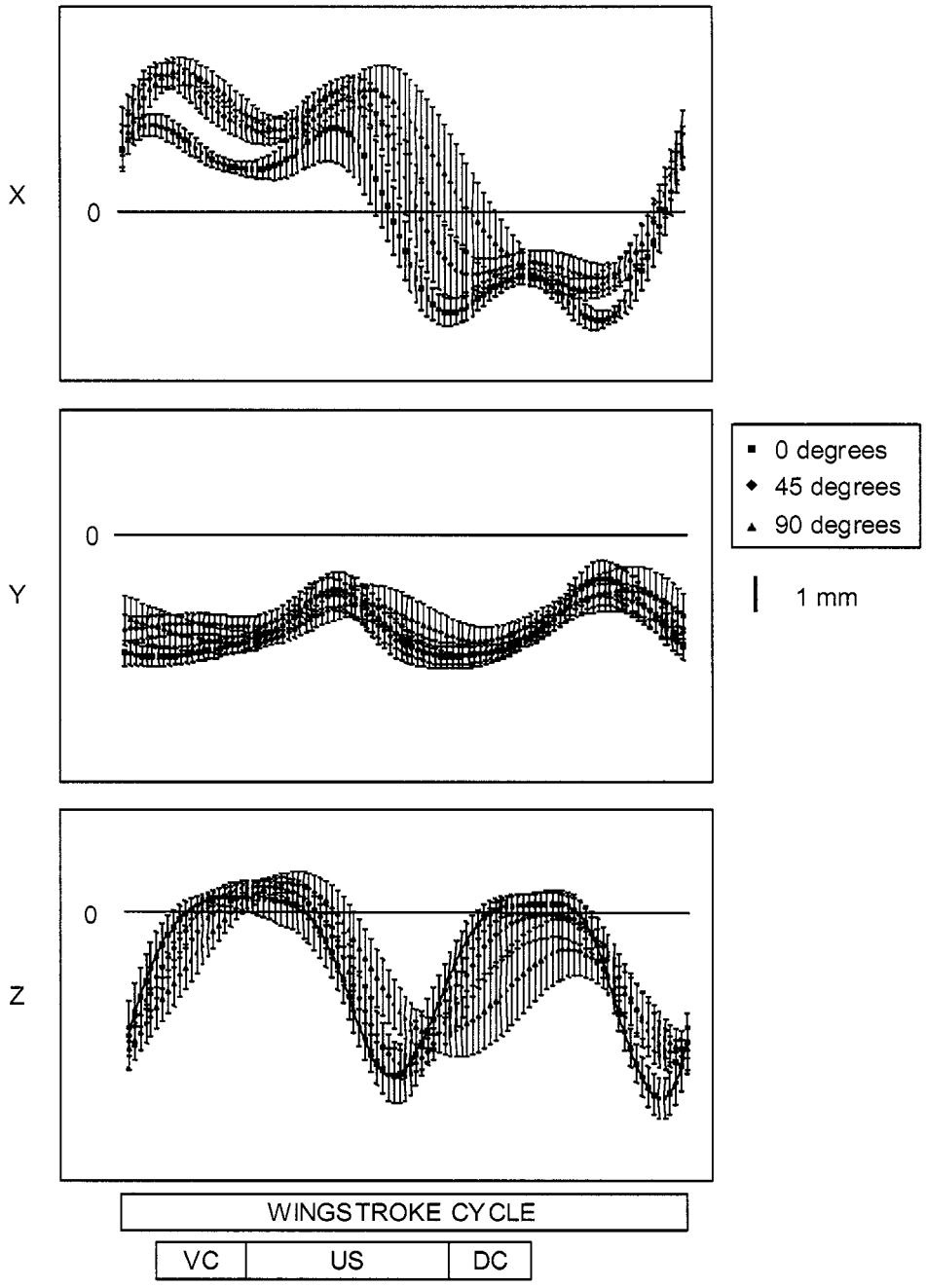

Figure 1.6. Wingtip coordinates for tethered animal experiments. The x-axis is non-dimensional time representing one wingstroke cycle. DC: dorsal crossover, US: upstroke, VC: ventral crossover. The unlabeled portion of the wingstroke is the upstroke. n=5 animals per angle; 32 wingstrokes at 0°, 31 at 45°, and 40 at 90°.

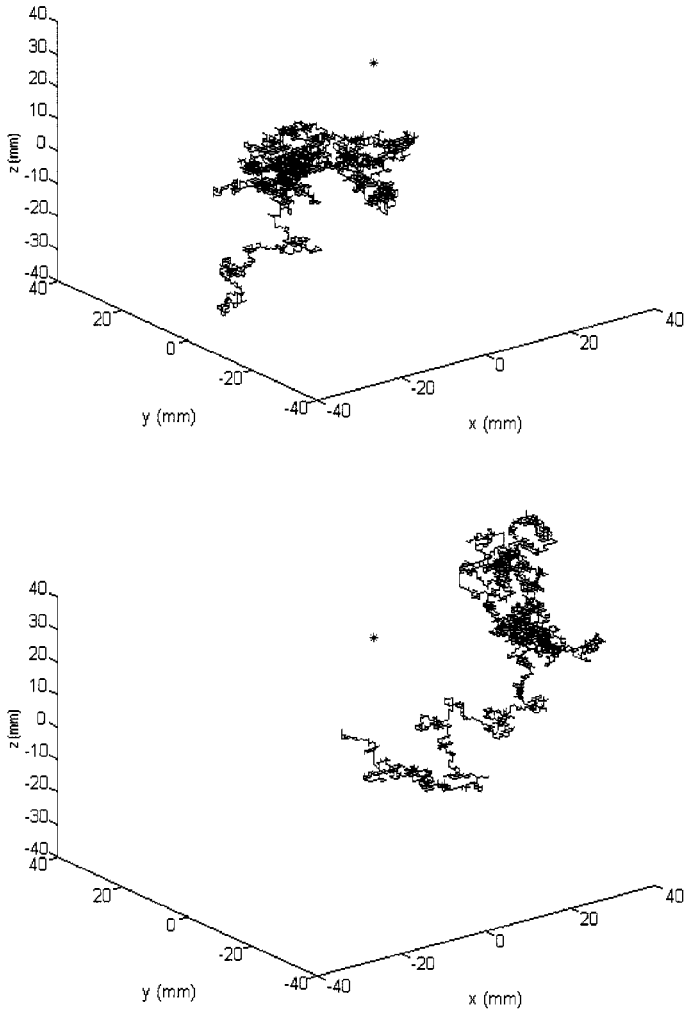

Figure 1.7. Model predator search paths. These images represent the pathway of a virtual Clione in blue relative to a prey item in red. The upper image is a biased pathway which results in a higher prey encounter on average, and the lower image is a random pathway.

Chapter Two: Biomechanics of human turning: amputee compensatory strategies

INTRODUCTION

Very little is known about the kinetics or kinematics of turning humans. The field of modern (synchronized, automated, computer based kinetics and kinematics) gait analysis dates back to the late 1980's. Since then, scientists interested in human gait have focused on walking straight forward on level ground. Despite the lack of attention, turning is a frequent activity that has high demands for balance and motor control. While turning is demanding for a person with two intact legs, it is more demanding for amputees. It makes sense to hypothesize that excessive residual limb strains, a predominant cause of residual limb pain and injury, are likely higher during turning. This research explores how amputees change their behavior depending on whether they are walking straight or turning.

What little evidence exists suggests that humans walk in short bouts with frequent turns. One study demonstrated that non-amputees take up to one turning step for every five straight steps (Sedgman, Goldie et al. 1994). Another study addressed this issue tangentially in amputees. The authors analyzed daily activity for ten below-knee amputees over one week and found that the distribution of the duration of walking bouts was shifted heavily towards short bouts (Klute, 2005). For this subject group, 75% of all walking bouts were four minutes or less (fig 2.1). We can assume that each of these walking bouts starts and ends with a change in posture or direction, which suggests that typical amputee gait is punctuated with many maneuvers.

Turning is not only a frequent activity, but also a challenging one. Relative to straight ahead walking, turning involves many changes in gait: 1. we move our center of mass relative to foot placement, often times going outside the base of support, leading to a statically unstable posture (Orendurff, Segal et al. 2005), 2. we lean to the inside of the turn to balance centripetal forces (Courtine and Schieppati 2003; Orendurff, Segal et al. 2005), 3. we slow down entering a turn and speed up coming out of it (Hase and Stein 1999), 4. we look towards our exit point, in a direction away from where our body is instantaneously heading (Imai, Moore et al. 2001; Courtine and Schieppati 2003), and 5. we change our stride length and stride frequency (Courtine and Schieppati 2003). All of these factors contribute to difficulty in turning for people impaired in any way. Additionally, falls while turning appear to be more consequential; a fall during a turn is 7.9 percent more likely to result in a hip fracture than a fall during straight walking (Cumming and Klineberg 1994). Anecdotally in our clinic at the VA, our amputee patients report that if they have trouble walking, they have it during turns, which suggests prosthetic design does not adequately solve these difficulties with turning gait.

In tackling the challenge of designing lower leg prostheses, it is important to consider how amputees use these devices. Given that what we know about gait comes mainly from studies on straight walking, we currently cannot design devices that specifically function well during maneuvering.

Amputees certainly adapt to their prostheses by developing compensatory strategies. For example, amputees reduce stance time on the residual limb and change the patterns of the location of the center of pressure on the foot during stance (Schmid, Beltrami et al.

2005). These compensatory mechanisms may reduce pain or injury on the residual limb in the short term, but they may induce secondary disabilities, such as joint pain or arthritis (Norvell, Czerniecki et al. 2005). Given these costs of compensatory mechanisms for amputees, it is critical to study these mechanisms as they relate to both walking straight and turning, so that future prostheses may be designed to allow amputees to walk without relying on potentially damaging altered behavior.

This study is designed to explore two possible compensatory mechanisms that amputees might use while turning. Subjects were challenged to execute a maneuver common in daily activities: turning 90° around a corner, either to the left or right. I investigated two hypotheses regarding amputees turning, both of which predicted that amputees would act to limit the forces on their residual limb. The first hypothesis had to do with the tendency to lean into a corner, which requires a lateral shift in foot placement relative to the pelvis. *I hypothesized that amputees modulate their medial-lateral foot placement more with their intact limb than their prosthetic limb.* The second hypothesis dealt with angular rotation in a corner. In rounding a 90° corner, the body undergoes roughly the same 90° rotation. *I hypothesized that amputees distribute the total rotation of the turn unevenly: by rotating the body more while in stance on the intact limb.* Both of these hypotheses were tested by analyses of kinematic data taken from human subjects walking around a typical hallway corner. The subject group included control subjects (both legs intact), left below-knee amputees (LBKs), and right below-knee amputees (RBKs).

MATERIALS AND METHODS

The data were taken from ten subjects: five bilaterally intact subjects, three left BK (below-knee) amputees, and two right BK amputees. The University of Washington human subjects institutional review board approved the protocol and all subjects gave their informed consent to participate. All subjects were free from musculoskeletal and neurological problems by self-report. Thirty-six reflective markers were placed on each subject according to the Plug-In-Gait model (Vicon, Oxford Metrics, Oxford, UK). A ten-camera Vicon 612 system recorded the three-dimensional marker coordinates at 120 Hz.

The experimental hallway consisted of sheets of plastic netting (1" square) stretched onto a frame of 1" diameter copper pipe. The wall was transparent to the cameras but visible to the subjects and could be felt on the skin if there was contact (see Appendix C for a validation of this method). Each of the four panels of the hallway corner measured 8" tall by 10" wide, and was connected to form a corner similar to what we encounter in typical daily activities. In accordance with ADA guidelines, and to make the hallway as realistic as possible, the walls were set 42" apart. Subjects were positioned 2 meters from the nearest edge of the first panel (the maximum distance possible in the lab) prior to starting each trial. Markers on the floor indicated the correct position of their feet for the start of each trial, and stopping point for the end of the trials (fig. 2.2).

Each subject performed twenty trials walking through the experimental hallway corner. The twenty trials were broken into four groups of five trials: turning left starting on the left foot, turning left starting on the right foot, turning right starting on the left

foot, and turning right starting on the right foot. This experimental design allowed for comparison between sound vs. prosthetic limb on the inside or outside of the turn. Each subject walked back and forth through the hallway several times to become accustomed to the task. The subjects were instructed to walk comfortably through the hallway at their own pace, in whatever way felt most comfortable. The trail was repeated if the subject accidentally made contact with the wall (by self-report).

The data were initially processed with Vicon's Workstation software, then exported as a text file for further analysis using custom software written in Matlab (see Appendix D). The timings of Toe-Off (TO), the time when a foot leaves the floor, and Heel-Strike (HS), the time when the foot contacts the floor, defined the phases of the gait cycle. The mean stride time for the control subjects in this experiment was approximately one second. To identify one turning stride per trial for analysis, I located the TO closest in time to ½ second before the pelvis crossed the center of the corner (defined as the line connecting the vertices of the corner frames). This TO defined the start of the stride, which continued through the next TO on the same side. This method divided one turning stride per trial into four phases: single limb support, double support, single limb support (on the contralateral limb) and double support. The remainder of the strides was identified as straight.

With regards to the two hypotheses, the kinematic data were analyzed for foot position relative to the pelvic center (PEL) and percentage of the turn accomplished on each leg and double support. Linear mixed effects models were used to determine if subject groups differed in HS placement and percent of angular change during the

different stance phases. Subject random effects were modeled for the first foot in the turn if the pattern of rotation by first foot in the turn varied by subject in a non-systematic manner. Left and right turning trials were combined because there was no effect of turn direction on any of the variables of interest. This produced groups by subject and inside vs. outside foot.

The walking velocities of the subjects were also calculated from the kinematic data for the pelvis. The comparison of turning vs. straight velocities is important for our understanding of the need to lean into the corner to counter centripetal forces. These velocity data were averaged for all trials (turn direction and lead foot combined) and the means were compared (ANOVA, Tukey HSD).

RESULTS

The data show significant differences, as predicted for the first hypothesis (that amputees alter their lateral foot placement more with their intact limb than their prosthetic limb). Compared to straight steps, HS position moves to the outside (along the X-axis, fig. 2.3) of the turn for turning steps (fig. 2.4, 2.5). This pattern was evident for both inside and outside feet, and all subject groups ($p < .0001$). There were no differences for changes between straight steps and turning steps along the Y-axis ($p > .4$). Control subjects shifted their inside feet more than their outside feet ($p < .05$), while amputees turning with the prosthesis on the inside shifted their inside feet less than their outside feet ($p < .05$). Compared to control subjects, both amputee groups shifted their inside feet less (fig. 2.6, $p = .015$). For all segments of the data collection (pre-turn, turn,

and post-turn) both LBKs and RBKs were slower than the control subjects ($p < .05$, fig. 2.8).

The data show no differences between subject groups for the second hypothesis (that amputees distribute the total rotation of the turn unevenly by rotating the body more while in stance on the intact limb). The only significant trend is that for all subject groups, more of the rotation occurs on the outside limb than on the inside limb ($p < .0001$).

DISCUSSION

This study was designed to investigate two possible compensatory mechanisms for amputees as they navigate corners. Both mechanisms might reduce potentially painful and injurious forces on residual limbs. The first mechanism involved amputees reducing the lateral force on the residual limb by keeping their residual limb and prosthesis more directly under the pelvis during turns. The second mechanism involved amputees reducing the torque on the residual limb by performing more of the rotation while in stance on the sound limb.

The general pattern for lateral foot shifts is that, compared to straight steps, both feet move to the outside of the turn during turning steps. The further the foot is shifted laterally, the more external forces it experiences (both due to twisting moments at the ankle, and lateral ground reaction forces). If amputees were trying to reduce these forces on their residual limbs, they should try to keep the residual limb more centered under the pelvis during turns (shift it less to the side). In fact, this is what they do. Amputees

turning with their prosthesis on the inside reverse the relationship shown by control subjects, who shift the inside feet more than their outside feet. When amputees turn with the prosthesis on the inside, they shift the inside foot *less* than the outside foot. When the prosthesis is on the outside of the turn, there is no change. This is explained by the fact that (again) for control subjects, the outside foot is shifted less than the inside foot. The amputees turning with their prosthesis on the outside, already experience a reduced shift on the prosthesis side, just because it happens to the on the outside.

At first glance, the lateral foot placement data appear confounded by the lower speeds of amputees. In all phases of the trial (pre-turn, turn, and post-turn, as defined in the methods), amputees are slower than control subjects (fig. 2.7). Slower velocities require less lean to counter centripetal forces. Less leaning means less of a lateral shift in foot placement relative to the pelvis. This would predict a reduction in lateral shift for amputees, simply because they are moving slower. There is a reduction in the foot shift between turning and straight steps for amputees compared to control subjects, but only for the inside feet. If the slower walking velocities accounted for the difference, I would expect to see less of a shift on both the inside and outside feet. Consequently, lower walking velocities do not appear to account for the changes in foot placement between control subjects and amputees.

The limb rotation mechanism arose from the hypothesized need for turning amputees to reduce torque on their residual limb. When a portion of the lower leg is removed, any degrees of freedom associated with it disappear as well. The human ankle rotates in the transverse plane (parallel to the ground) and can therefore accommodate some of the

rotation that occurs during single limb stance. A rigid pylon (which all test subjects wore) transfers all of the transverse rotation directly to the residual limb. I would expect that amputees would shift the bulk of the rotation for a given turn to their sound limb to avoid twisting their residual limb inside the prosthetic socket. In the case of this study, however, there is no evidence that amputees compensate for these transverse rotations. This means that all of the rotation that normally occurs in control subjects, occurs in amputee subjects as well, whether amputees lead into the corner on the intact or prosthetic limb.

Both the presence and absence of compensatory mechanisms indicate areas for further research. The fact that these data show a compensatory mechanism for lateral forces indicates the need to investigate not only the possible causes for that mechanism, but also any secondary injury that may arise from it. The lack of a compensatory mechanism for transverse rotations may mean that the amputees in this study felt no pain, and therefore no need to change their behavior in comparison to the control subjects. In that case, there would be no need to design prosthetic devices to help reduce the effect of rotational forces. However, it may also mean that the amputees are simply putting up with pain for which they have no behavioral solution, or that they are using a behavioral solution that we didn't detect.

In any case, further investigation is warranted; and we now have one clear guiding principle for novel prosthetic design: to eliminate the need for the compensatory mechanism to reduce lateral forces. Whether or not it is necessary to design towards reducing rotational forces will depend on the outcome of further study.

NOTES TO CHAPTER TWO

Courtine, G. and M. Schieppati (2003). "Human walking along a curved path. I. Body trajectory, segment orientation and the effect of vision." Eur J Neurosci **18**(1): 177-90.

Courtine, G. and M. Schieppati (2003). "Human walking along a curved path. II. Gait features and EMG patterns." Eur J Neurosci **18**(1): 191-205.

Hase, K. and R. B. Stein (1999). "Turning strategies during human walking." J Neurophysiol **81**(6): 2914-22.

Imai, T., S. T. Moore, et al. (2001). "Interaction of the body, head, and eyes during walking and turning." Exp Brain Res **136**(1): 1-18.

Norvell, D. C., J. M. Czerniecki, et al. (2005). "The prevalence of knee pain and symptomatic knee osteoarthritis among veteran traumatic amputees and nonamputees." Arch Phys Med Rehabil **86**(3): 487-493.

Orendurff, M. S., A. D. Segal, et al. (2005). "The kinematics and kinetics of turning: limb asymmetries associated with walking in a circular path." Gait & Posture **in press**.

Schmid, M., G. Beltrami, et al. (2005). "Centre of pressure displacements in trans-femoral amputees during gait." Gait & Posture **21**(3): 255-262.

Sedgman, R., P. Goldie, et al. (1994). "Development of a measure of turning during walking." Advancing Rehabilitation conference proceedings, La Trobe University, Melbourne, AU: 26-31.

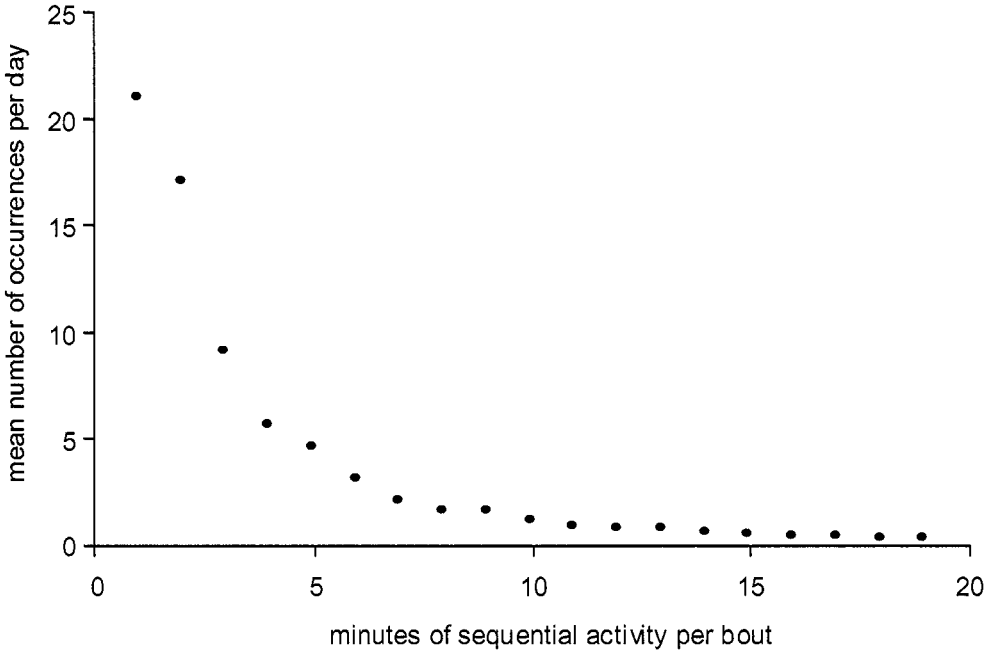

Figure 2.1: Duration of Walking Bouts. 10 below knee amputees using rigid pylons were recorded walking in their daily activities for 7 days. The x-axis indicates duration of walking bouts. The y-axis gives the mean number of occurrences per day, per amputee for the 7-day period.

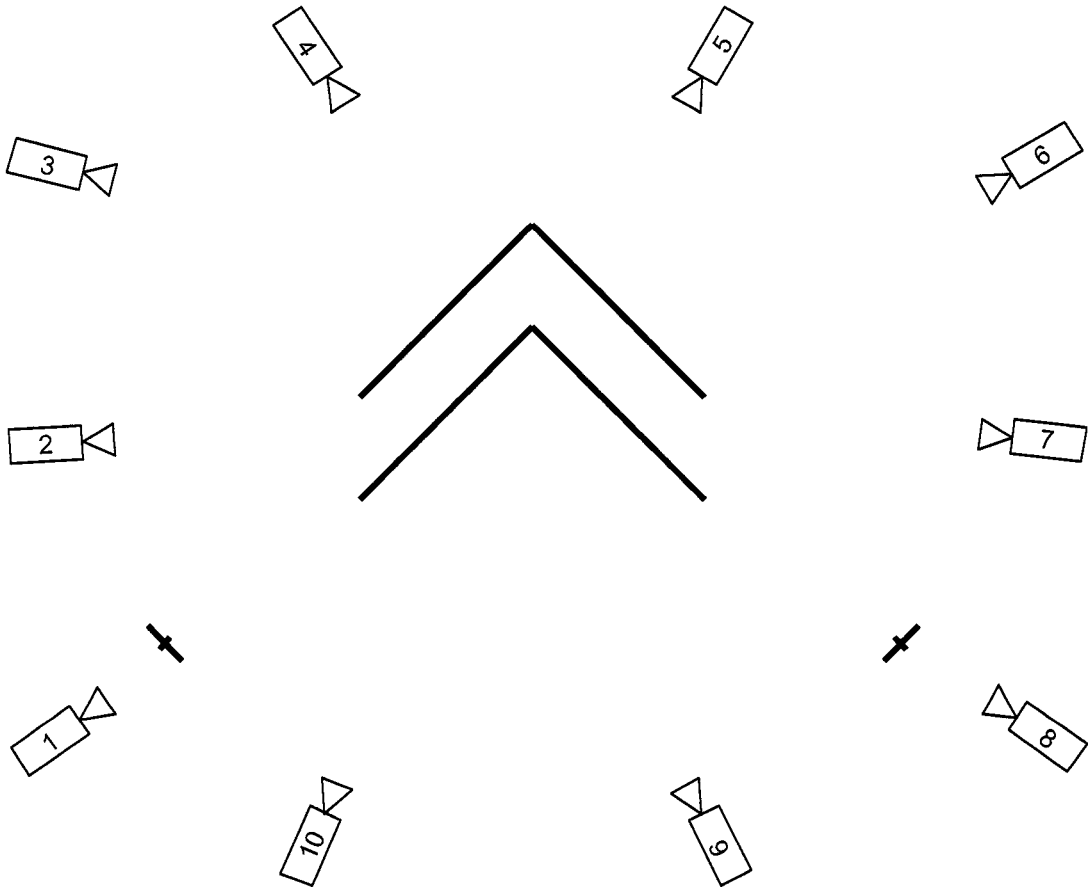

Figure 2.2: Motion Analysis Lab. Ten cameras surround the hallway corner. Subjects started and stopped at the purple crosses marked by tape on the floor.

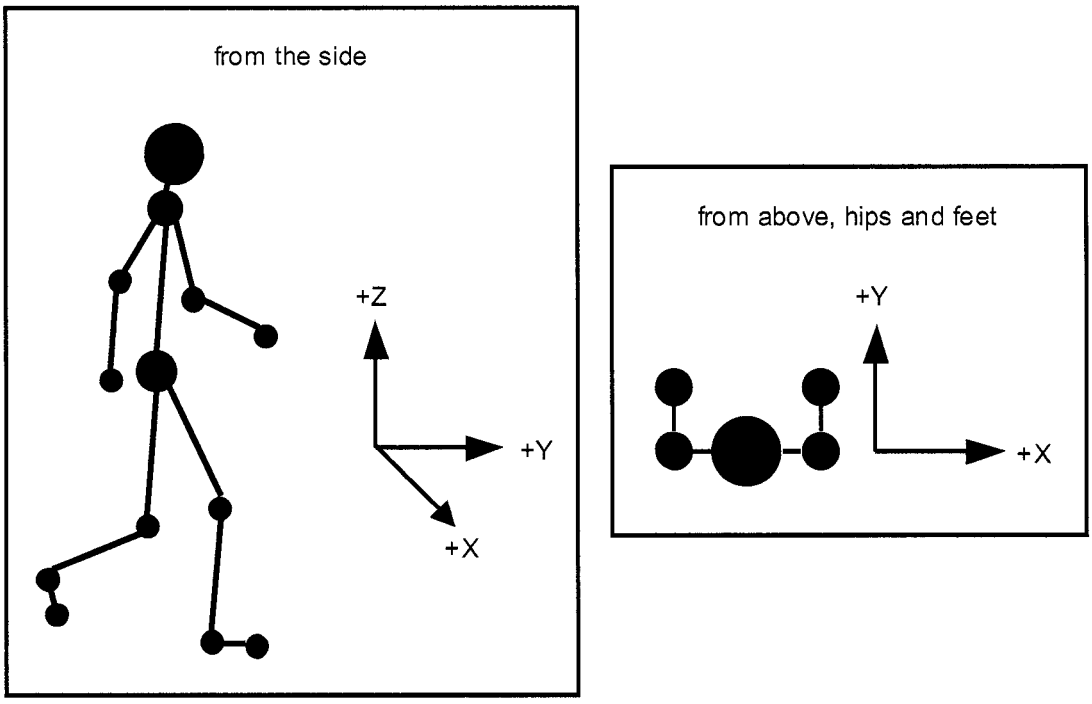

Figure 2.3: Direction Conventions

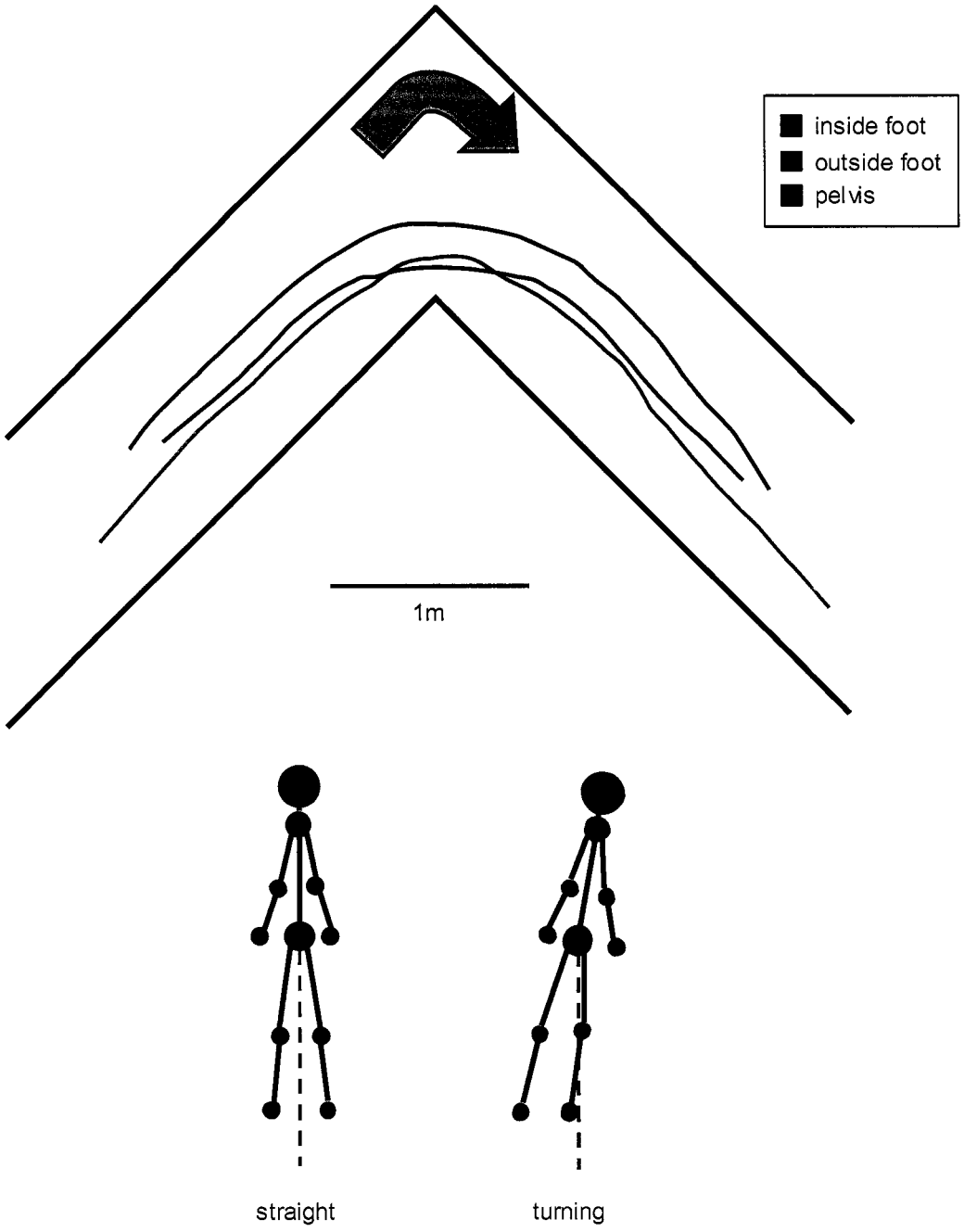

Figure 2.4: Pelvis and foot paths in turning. The upper illustration shows the paths of the pelvis, inside foot, and outside foot for one control subject during one right turn in the experimental hallway corner.

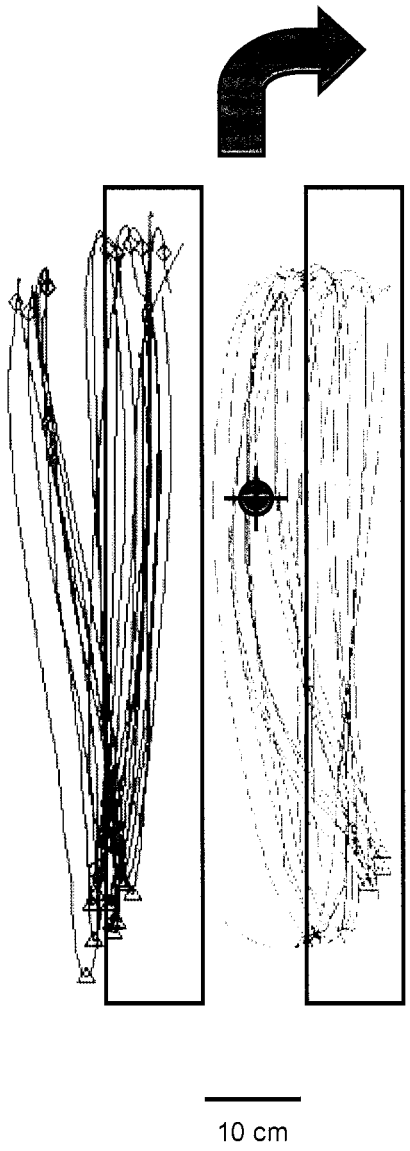

Figure 2.5: Foot paths for one subject. The paths of each foot (relative to the pelvis, and corrected for pelvic rotation) are shown of each foot. The center of the pelvis is marked by the gray circle/cross. These data include both straight steps and turning steps. The boxes indicate the approximate regions for the straight steps. Turning steps are shifted to the left, for a right turning lean. Left foot: blue, Right foot: red, heel-strikes: diamonds, toe-offs: triangles.

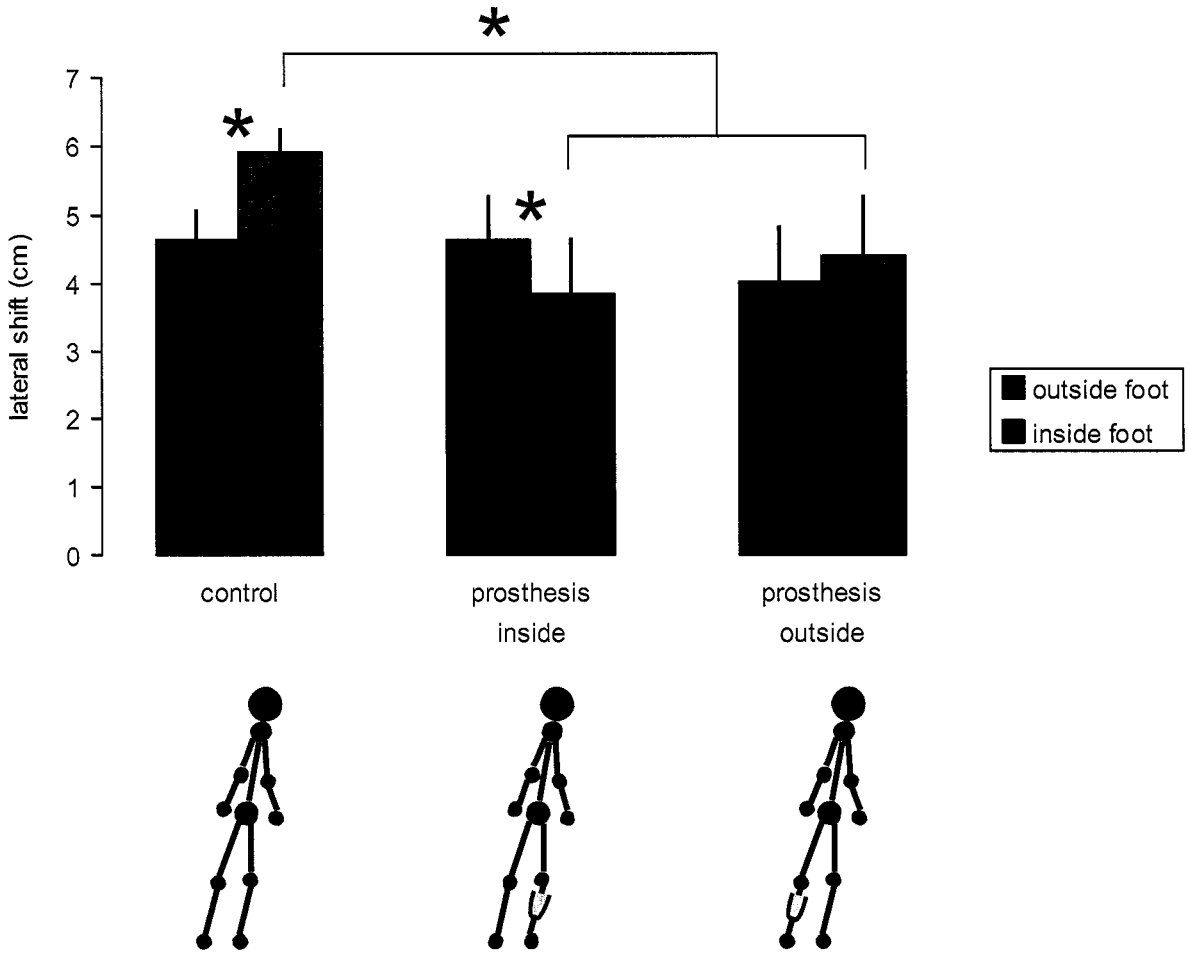

Figure 2.6: Lateral Foot Placement. The average absolute change in foot position with respect to the center of pelvis between walking straight and turning is plotted for each case. Error bars are plus/minus one standard deviation.

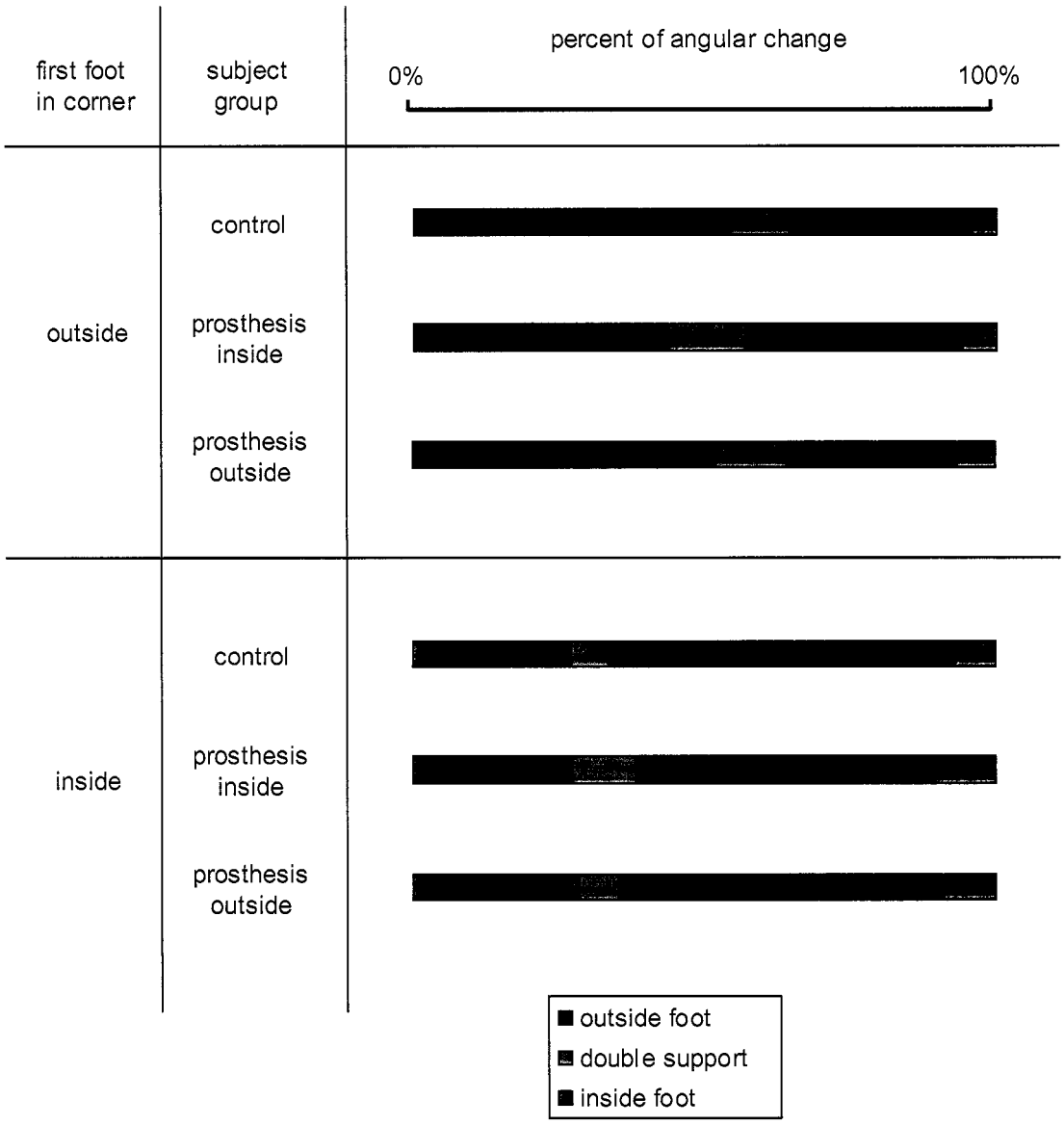

Figure 2.7: Percent of Turn on Each Leg. Each bar shows the mean percentage of total angular displacement for a given trial as accomplished on each limb and double support. The total angular displacement is normalized to give the same length bar in all cases. Rows represent the three subject groups. LBKs and RBKs are grouped together and classified by whether the prosthesis is on the inside or outside of the turn

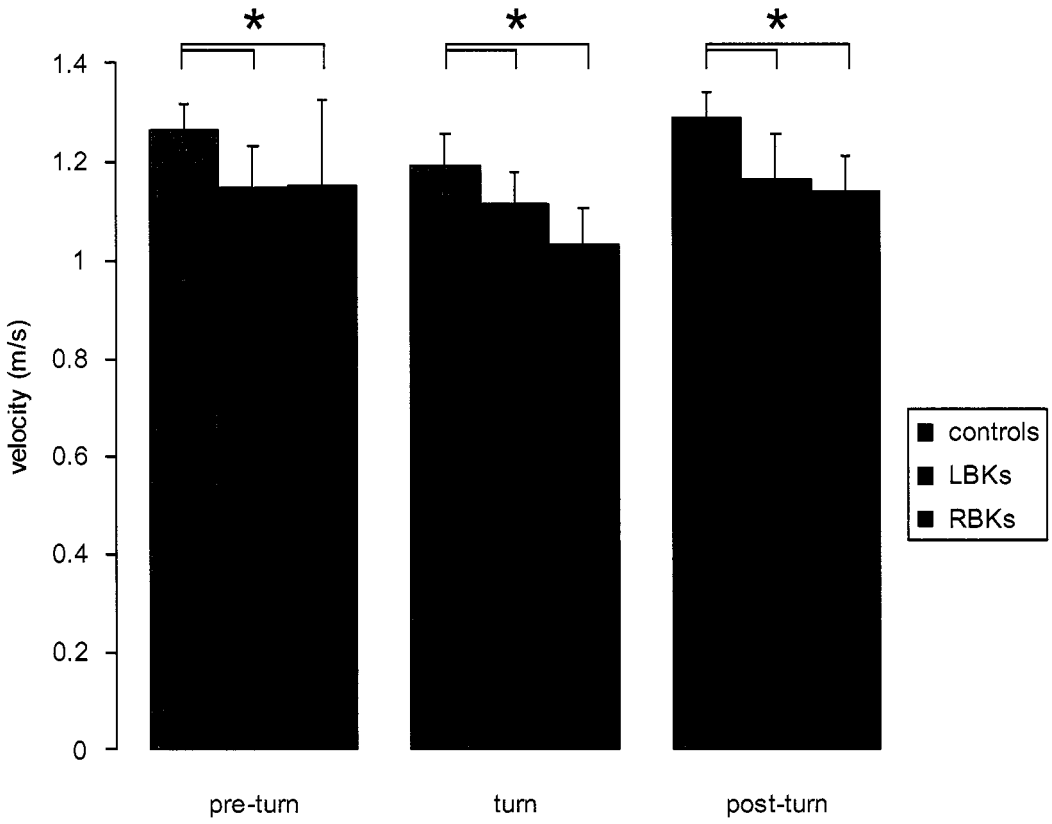

Figure 2.8: Corner Walking Velocities. Pre, turn, and post turn periods are defined as in the methods. Error bars are plus/minus one standard deviation.

Chapter Three: Comparison of human gait dynamics with prosthetic rotation adaptor performance

INTRODUCTION

For intact subjects while walking straight or turning, the leg acts as a system of rotating elements coupled in series, each doing some combination of elastic energy storage and release, torque transformation into motion in other planes, and torque transmission. The net torque results in transverse rotation of the foot (if it overcomes static friction with the substrate, or slides within the shoe), ankle and subtalar joint, tibia and fibula, knee, and hip. For the amputee, portions of this kinetic chain are replaced with the prosthesis. Whatever torque was applied to the biological structures that were removed, are now applied to the prosthesis and its interface with the residual limb. An intact leg is free to rotate in the transverse plane as described above, or to transmit the transverse rotation into motion in other planes; however, with the exception of the prosthetic foot rotating in the shoe, few lower limb prostheses allow for transverse rotation. Constrained rotation can increase residual limb shear stresses and, for some amputees, may be sufficiently uncomfortable to necessitate an altered gait. Given that discomfort and injury due to shear forces between the residual limb and the prosthetic socket are major complaints of amputees (Nielsen 1991; Legro, Reiber et al. 1999; Ehde, Czerniecki et al. 2000; Dillingham, Pezzin et al. 2001; Hagberg and Branemark 2001; Schoppen, Boonstra et al. 2001; Marshall, Jensen et al. 2002), it is important to minimize the shear forces in all planes of the socket/lining with respect to the residual limb.

While several products are currently available to reduce tissue loading in the transverse plane, little objective data exists documenting the effects of these devices

during turning gait or during typical activities of daily living. Lamoureux and Radcliffe (1977) explored several designs for a pylon device that allowed axial rotation. Using a prototype device, they conducted a treadmill experiment (n=2 transfemoral amputees) and found that pelvis rotation increased 6°, step length increased, and the shank externally rotated 8° over the foot during stance with the prototype in comparison to a standard pylon. In another study, Van der Linden *et al.* (2002) researched rotation adapters on two subjects walking at their self-selected speed. One subject showed greater axial rotation of the socket relative to the foot with the transverse plane rotation adapter. They concluded that the rotation adapter allowed the socket to rotate with the stump, which may imply that motion between the stump and socket was reduced. These studies illustrate some of the effects of rotation adaptors; yet, except for manufacturers' claims, there are no published reports on the influence of rotation adapters during more complex gait activities where torsional loads are expected to be higher than for linear walking. Aside from the manufacturers' product documentation, there is also no way to ascertain the differences between adaptors or between different elastomers used in the same adaptor. This study was conducted, with prosthetists in mind, to characterize the mechanical properties of the available adaptors and to raise the question of how exactly should a TRA respond to torque.

MATERIALS AND METHODS

The kinetic and kinematic data are taken from three intact subjects, each of whom performed five trials walking straight and turning to the right around a 1m-radius circle at

their self-selected speeds. All subjects gave their informed consent to participate in this study after the human subjects institutional review board governing this institution approved the protocol. All were free from musculoskeletal and neurological problems by self-report. Thirty-six reflective markers were placed on each subject according to the Plug In Gait model (Vicon, Oxford Metrics, Oxford, UK). A ten-camera Vicon 612 system recorded the three-dimensional coordinates of the markers at 120 Hz. A Kistler force plate (Winterthur, CH) mounted flush with the laboratory floor recorded the kinetic data at 600 Hz. Using the Vicon generated embedded coordinate axes, foot angle was defined as the angle between the heel to second ray axis and the axis through the ankle center perpendicular to the trans-malleolar axis (figure 1). Zero foot angle was recorded with the subject standing still, after receiving instructions to look straight ahead and to stand evenly on both feet. Internal rotation and torque are positive and external rotation and torque are negative. Torque is reported as moments generated by the subjects to counter environmental moments. The data include three conditions: right footstrikes during straight walking, right turns on the left foot, and right turns on the right foot. While it is becoming clear that there are asymmetries in lower limb function in able-bodied gait, there are no studies definitively linking symmetry to limb dominance or laterality in turning gait (for review, see Sadeghi, Allard et al. 2000). For the purposes of this study, we assume that the functional roles of the inside and outside legs during turning are the same, regardless of turn direction. To ensure a constant velocity, the subjects walked 5 to 6 steps (either straight or around the circle) prior to stepping on the force plate. The data were analyzed with Vicon's Workstation and Polygon software.

The Transverse Rotation Adaptor (TRA) performance data came from five transverse rotation adaptors that were purchased for testing (table 1) and assembled as necessary with standard pylons and tube clamp adapters. Each TRA has the same basic elements: upper and lower tubes or tube clamp adapters that rotate with respect to one another and a deformable elastomer or spring within a housing that connects them. Both Endolite TRAs use a white Delrin rod that is fabricated with thicker or thinner walls to vary the stiffness. The Delta Twist compresses urethane elastomers, and can be set to a different stiffness for internal and external rotation, while the 4R39 uses bevel washers under adjustable spring tension. The Century XXII compresses an elastomer sleeve mounted around an internal radial arm. The Delta Twist, TT Pylon, and Century XXII compress axially, in addition to rotating in the transverse plane.

Each TRA was mounted in a servo-hydraulic material testing system (MTS; Model 858 Bionix^{TM}; MTS System Corporation, Eden Prairie, MN). The long axis of the pylon and TRA was aligned with the MTS axis of rotation, with the TRA oriented upward (as if installed distally to the knee). Each elastomer for each TRA was tested over the full rotational range (from the users manuals) with no axial load, at 0.5 ^{o}/s, 60 ^{o}/s, and at 0.5 ^{o}/s with the elastomer removed (where possible) to quantify friction. The Otto Bock 4R39 has a non-removable spring and bevel-washer system that is adjusted with a screw; this TRA was tested in the middle and at the extremes of its stiffness. For the Century XXII, the angular range was established by rotating the TRA with the elastomer removed, noting the angles at which contact between the internal metal elements of the adaptor occurred. The full range, contact-to-contact, was $\pm 15^{o}$, so $\pm 13^{o}$ was used for

testing to avoid damaging the elastomer. For the TRAs with axial compression, an additional test of the middle stiffness elastomer was conducted at 0.5 °/s while the adaptor was axially loaded to 736N (75 kg, a representative mass for subjects who would use this TRA and elastomer). For all tests, the MTS was programmed to rotate, using displacement control, from center counterclockwise (from above) to the end of the range, then clockwise through the full range, then counterclockwise back to center. Repeatability was ensured by visual comparisons of multiple tests of each TRA (data not shown). The MTS sampling rate was 10 Hz for the 0.5°/s trials and 1000 Hz for the 60°/s trials. For the Endolite TRAs, multiplying the published stiffness values over the range of angular deformation generated an expected torque-deformation curve.

Since the integral of the curve on the portions acting against the elastomer is greater than the integral on the portions relaxing with the elastomer, the area within the loop (hysteresis loop) on the torque vs. deformation plot represents the total energy lost per cycle. The area within the loop when the TRA is tested at 0.5 °/s without an elastomer represents the energy lost to friction. The energy loss calculations were done with the public domain NIH Image program (developed at the U.S. National Institutes of Health and available on the Internet at http://rsb.info.nih.gov/nih-image/) by measuring the digitized areas within the torque vs. deformation curves.

RESULTS

The average torque vs. displacement curves for each subject over five trials were highly asymmetrical for all three conditions (figure 2). The greatest torques were applied

during stance in the direction of internal (positive) rotation. The general pattern is external rotation under small external torque post heel-strike to mid stance. At mid stance, the foot is relatively immobile in the transverse plane, but the torque reaches its maximum internal value. From mid-stance to toe-off, the torque declines, again with minimal angular displacement. During swing phase, the foot rotates internally back to its neutral orientation under no torque. The notable exception to this pattern is the inside-right foot (during right turns). In this condition, the foot angle changes at a more constant rate over the whole gait cycle. The ranges from the human data can be compared to the ranges of the TRAs, but the shapes of the loops cannot since the human subjects impose a different input time history. The average peak torques and maximum excursions during stance while turning are reported in table 2.

The mechanical test torque vs. displacement curves exhibited both linear and non-linear characteristics (figure 3). All of the curves start at the origin and proceed in a clockwise direction. The Endolite TT, Endolite Demountable, and Century XXII Total Shock torque was nearly directly proportional to displacement indicating a linear response (figures 2a, 2b & 2e). The Otto Bock Delta Twist and 4R39 torque increased rapidly at the initial position and at the extreme range of motion indicating a non-linear response (figures 2c & 2d). The trials at the higher rotational velocity (60 °/s) and with axial loading generated plots nearly identical to the unloaded pseudo-static trials (data not shown).

The curves from the same manufacturers comprise a family of curves differentiated by the spring constant. Despite the narrower range, the Endolite TT pylon data lie on top

of the Endolite Demountable TRA. These two TRAs also display the same nearly linear behavior over the range of travel, but differ from the performance listed in the users' guide. Additionally, there is little performance difference between the different Endolite elastomers. The Otto Bock TRAs are likewise similar to each other but notably increase in stiffness towards the limits of the range and have high stiffness values near the neutral position.

Total energy lost and the percent of energy lost to friction are given in table 3. The total energy lost per cycle cannot be compared between adaptors under this experimental design since each adaptor was rotated through its maximum range. Adaptors with larger ranges will have larger energy losses simply because the distance term in the energy equation is larger. The percent of total energy loss due to friction, however, can be compared since the method was the same for each adaptor. The Endolite TT pylon had by far the highest percentage of energy loss due to friction with the rest of the adaptors clustered around each other.

DISCUSSION

This study establishes the baseline performance for TRAs from human subject testing and compares them to the mechanical behavior derived from the MTS testing on currently available TRAs.

The main difference between human performance and TRA mechanical performance lies in the asymmetry of the physiological data. The maximum physiological range of rotation is 26° (table 2). However, the foot rotates internally very little beyond the angle

at heel strike. Nearly all of the foot rotation occurs externally relative to the angle at heel strike (figure 2). The physiological range of torques is also highly asymmetrical, with higher internal torques for all activities. Internal torque ranges from 1.7 times greater than external torque for the left leg during right turns to 6.6 times greater for the right leg during right turns. During linear walking, this asymmetry persists, with internal torque 2.2x higher than external torque (table 2).

In order to accommodate the asymmetrical rotation, the device would need to rotate at least 26° externally from its angle during the swing phase. Other maneuvers may necessitate more rotation or may involve more internal rotation from the angle at heel strike. All the adapters tested have equal rotation, both internal and external, relative to their resting position (where the device would be at heel strike). Given this, the necessary full range for the maneuvers tested in this study would be 52° (twice the maximum external rotation of 26°). If matching the physiological rotational range is the critical performance measure, then only the Endolite adaptors meet the needs indicated by this study.

Another performance measure is the adaptors' response to the torque generated by the human subjects. It is important that the amputee never reaches the end of the rotation, at which point an abrupt stop and a torque spike would occur. The physiological mean peak torque is 11.8 Nm internally. If this torque were applied to the adaptors with the middle or stiffest elastomers installed, none would reach their maximum rotation. With the softest elastomers installed, the Endolite TT and the Century XXII reach the end of their rotation at that torque value. The Delta Twist allows for different elastomers on the

internal and external sides of the adaptor. This may be of value in matching the corresponding asymmetry in the physiological torque data.

The angle of the prosthetic foot in the transverse plane also affects the torque generated in the pylon. Transverse plane prosthetic foot alignment modulates transverse torque since the moment is generated from the instantaneous center of pressure of the foot during stance. If the foot is angled externally, an environmental external torque will result (as will a balancing, subject generated, internal torque) due to the moment created as the foot contacts the floor. This effect is as yet unexplored, so it could not be included in this estimate of the actual rotation and torque required in a TRA.

The energy absorption values may also translate into tangible effects for the amputee. It is important to remember that the absolute energy lost is over the entire range of the device. Thus, devices with greater angular range will necessarily have greater energy losses at the same friction values. However, the higher the percentage of energy loss due to friction, the greater the resistance in the adaptor to changes in direction. If the friction is sufficiently high, the motion will be stepped (resulting in a "sticky" feeling) since a minimum torque must be applied before the adaptor begins to rotate. The MTS in this study was under displacement control, so the torque was always sufficiently high to keep the adaptors rotating. Further tests under low torque would verify the presence or absence of stepped motion.

Several other conclusions can be drawn from the data that may be of interest to the prosthetist. Firstly, the Endolite adaptors differ from the performance listed in the users' guide, and there is very little performance difference between the elastomers. Secondly,

the non-linear (Otto Bock adaptors) vs. linear (all other adaptors) profiles may have clinical significance. It is possible that increased stiffness near the ends of the range serves to help prevent an abrupt stop when the amputee reaches the end of the rotation. And lastly, the high stiffness values of the Otto Bock adaptors around the neutral position (figures 3c & 3d) may reject small moments and help to keep the foot centered in a neutral position with respect to the socket.

Data that describe the mechanical performance of prosthetic components create a structure for conversations between amputees and prosthetists. These data allow the prosthetist to interpret qualitative issues raised by the amputee and direct him/her to the correct rotation adaptor and/or elastomer setup. While, for these reasons, this study will be helpful to prosthetists seeking the correct prescription for TRAs, it also points us in the direction of considering transverse-plane controllable rotation adaptors. The patterns of torsion and torque generation from the human subject data illustrate not only the range of stiffness values, but also consistent changes in the hysteresis loop pattern with turning. Ultimately, the performance criteria of interest are the tissue shear on the residual limb and the ability to perform desired maneuvers. The data from this study will be useful in addressing these criteria and in modeling a controllable TRA that can respond appropriately as the amputee maneuvers within their environment.

NOTES TO CHAPTER THREE

Dillingham, T. R., L. E. Pezzin, et al. (2001). "Use and satisfaction with prosthetic devices among persons with trauma-related amputations: a long-term outcome study." Am J Phys Med Rehabil **80**(8): 563-71.

Ehde, D. M., J. M. Czerniecki, et al. (2000). "Chronic phantom sensations, phantom pain, residual limb pain, and other regional pain after lower limb amputation." Arch Phys Med Rehabil **81**(8): 1039-44.

Hagberg, K. and R. Branemark (2001). "Consequences of non-vascular trans-femoral amputation: a survey of quality of life, prosthetic use and problems." Prosthet Orthot Int **25**(3): 186-94.

Lamoureux, L. W. and C. W. Radcliffe (1977). "Functional analysis of the UC-BL shank axial rotation device." Prosthet Orthot Int **1**(2): 114-8.

Legro, M. W., G. Reiber, et al. (1999). "Issues of importance reported by persons with lower limb amputations and prostheses." J Rehabil Res Dev **36**(3): 155-63.

Marshall, H. M., M. P. Jensen, et al. (2002). "Pain site and impairment in individuals with amputation pain." Arch Phys Med Rehabil **83**(8): 1116-9.

Nielsen, C. C. (1991). "A survey of amputees: functional level and life satisfaction, information needs, and the prosthetist's role." Journal of Prosthetics and Orthotics **3**(3): 125-129.

Sadeghi, H., P. Allard, et al. (2000). "Symmetry and limb dominance in able-bodied gait: a review." Gait & Posture **12**: 34-45.

Schoppen, T., A. Boonstra, et al. (2001). "Factors related to successful job reintegration of people with a lower limb amputation." Arch Phys Med Rehabil **82**(10): 1425-31.

Van der Linden, M. L., N. Twiste, et al. (2002). "The biomechanical effects of the inclusion of a torque absorber on trans-femoral amputee gait, a pilot study." Prosthet Orthot Int **26**(1): 35-43.

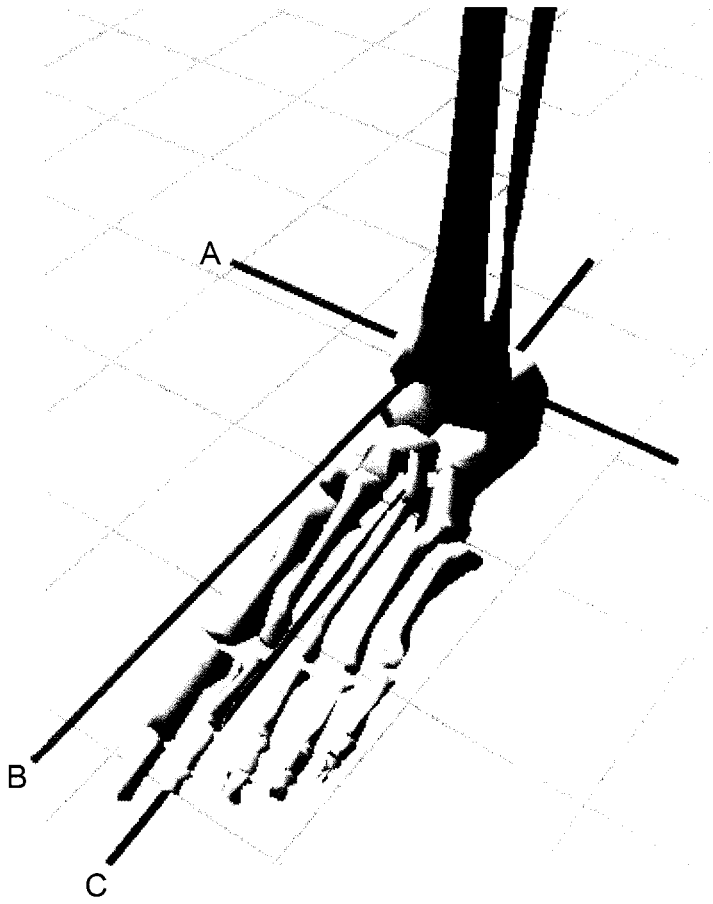

Figure 3.1. Diagram of axes used in calculating foot-tibia angle. The foot-tibia angle is the angle between (B) and (C) in the transverse plane. A: trans-malleolar axis, B: axis perpendicular to (A) through the ankle centre, C: axis from heel to second ray

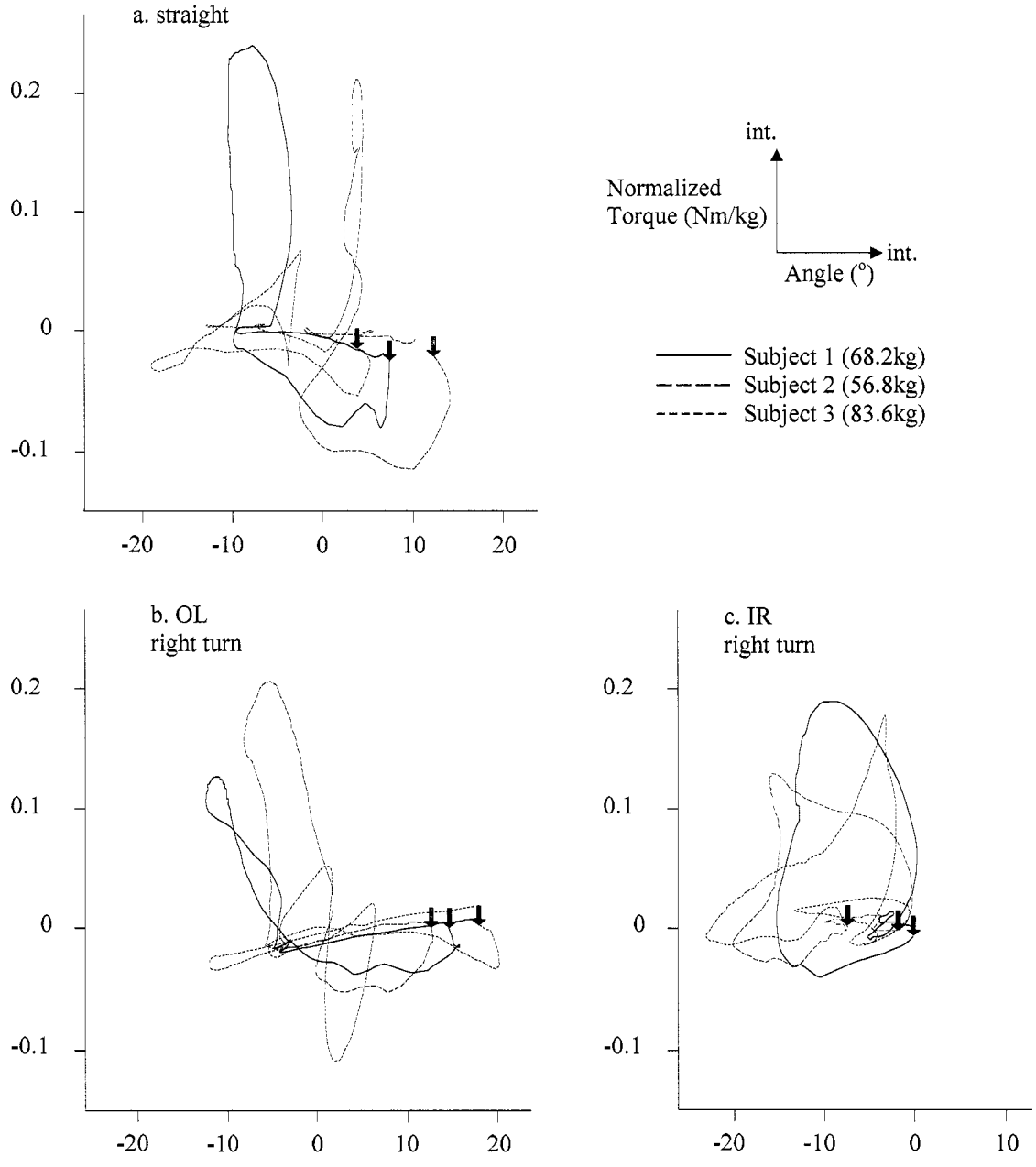

Figure 3.2. Normalized torque vs. displacement for human subjects. Average data from five trials are presented for each subject. Each trace begins at the heel strike (arrow) and proceeds clockwise. Internal angles and torques are positive. 1a.) data taken from the right leg while subjects walked in a straight line 1b.) data taken from the outside left (OL) leg while subjects initiated right turns 1c.) data taken from the inside right (IR) leg while subjects initiated right turns. Additional data are not shown for clarity.

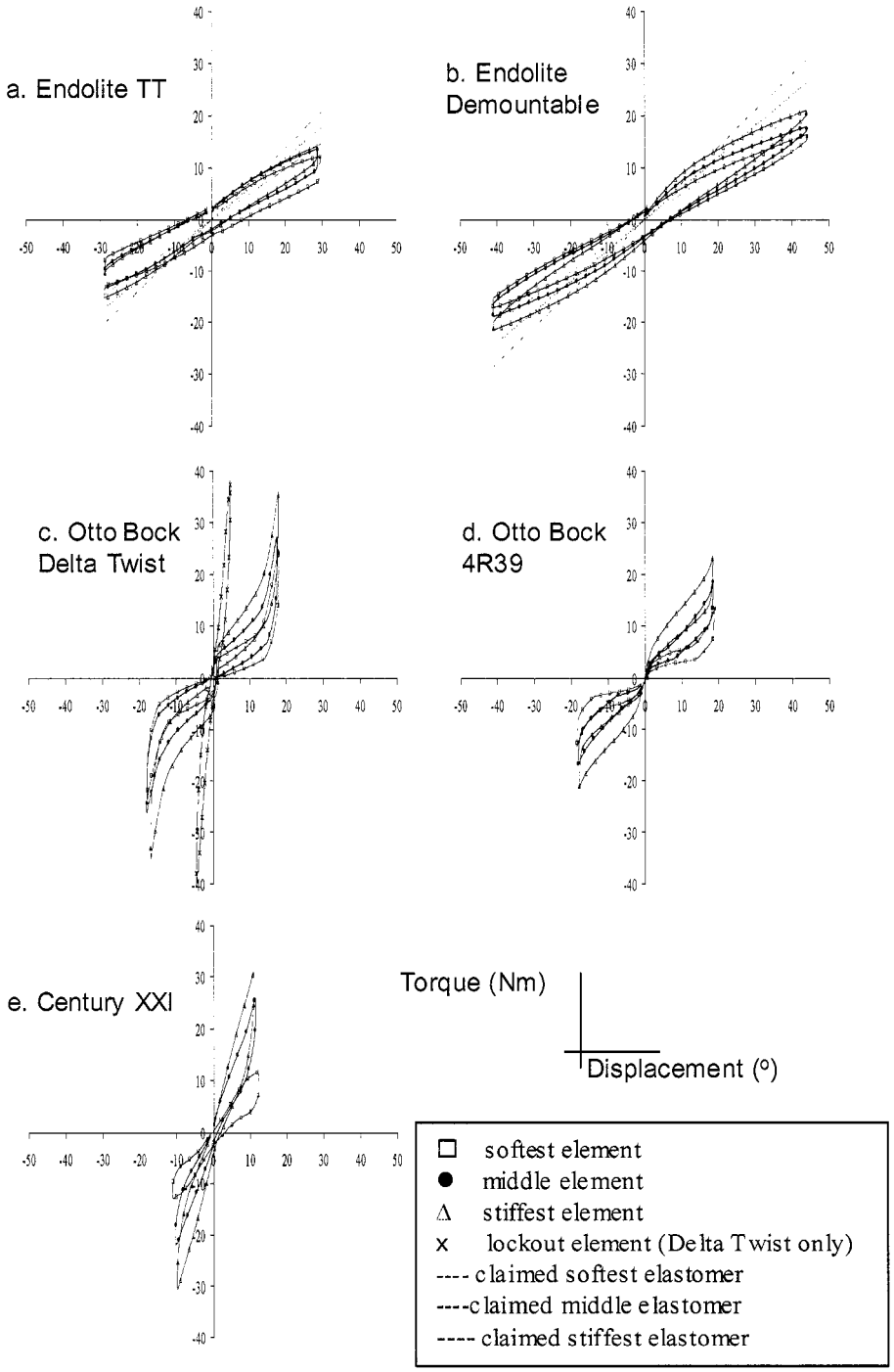

Figure 3.3. Torque vs. displacement for all adaptors and all elastomers. Each trial begins at the origin and traces clockwise.

Table 3.1. Rotation adaptor properties. Documented performance properties from the users' manuals of all devices tested. The Delta Twist was the only device that came with a listed weight. The other devices were weighed in our lab without couplers.

Make/Model	Mass	Tuneable elements	Properties	Range
Endolite TT Pylon (www.endolite.com)	379g[1]	One dot bar Two dot bar Three dot bar	0.5 Nm/° 0.6 Nm/° 0.7 Nm/°	±30°
Endolite Demountable Torque Absorber	225g 359g[2]	Red bar White bar Purple bar	0.5 Nm/° 0.6 Nm/° 0.7 Nm/°	±45°
Century XXII Total Shock (www.ossur.com)	301g	Black elastomer Red elastomer Yellow elastomer	40-65kg user 65-90kg user 90-100kg user	Not listed
Otto Bock 4R39	415g[3]	Screw adjuster	7-10 Nm	±20°
Otto Bock Delta Twist (www.ottobock.com)`	≥325g[4] 376g[5]	Red elastomer Yellow elastomer Green elastomer Black elastomer	<75kg user 75-100kg user 10-125kg user lock-out	±20°

[1]tube cut to 70mm [2]with 143mm carbon fiber tube and tube clamp adapter [3]tube cut to 149mm [4]listed in users' manual [5]tube cut to 95mm

Table 3.2. Human subject peak torque and displacement. Mean peak internal and external torques and angular ranges for human subject data. Each value is the mean of the three subjects. (Ti: internal torque, Te: external torque, range: |max internal angle| + |max external angle|)

Activity	$\overline{\text{peak Ti}}$	$\overline{\text{peak Te}}$	$\overline{\text{range}}$
Straight, right leg	11.4 Nm	5.2 Nm	19.7°
Right turn, left leg	8.2 Nm	4.8 Nm	26.0°
Right turn, right leg	11.8 Nm	1.8 Nm	20.0°

Table 3.3. Rotation adaptor energy losses. Total energy loss per one complete cycle through the maximum range and the percent contribution of friction. [1]The springs are permanently installed so no separate measure of friction could be made.

Make/Model	ΔE (Nm)	Frictional ΔE
Endolite TT Pylon	4.68	73%
Endolite Demountable Torque Absorber	7.23	21%
Century XXII Total Shock	2.39	26%
Otto Bock 4R39	2.01	Not testable[1]
Otto Bock Delta Twist	4.19	32%

Chapter Four: Finite element modeling of the residual limb: effects of turning gait and rotation adaptor use

INTRODUCTION

Residual limb pain and injury is one of the most prevalent and critical problems lower-limb amputees face (chapters 2 & 3). Unlike the bottom of the foot, where non-amputees bear gait forces, the residual limb is not adapted to the forces applied to it by amputees while standing still or walking. Because of these forces on the residual limb, amputees complain of prosthesis comfort and are troubled by residual limb pain (Nielsen 1991; 1998; Legro, Reiber et al. 1999; Ehde, Czerniecki et al. 2000; Hagberg and Branemark 2001). In comparison to walking straight ahead, it is likely that behaviors like turning and obstacle avoidance are associated with higher forces on the residual limb, and that these higher forces are associated with greater residual limb pain and injury. However, little attention has been paid to turning, despite evidence that one in five steps involves turning (Sedgman, Goldie et al. 1994). There are commercially available rotation adaptors designed to lessen the turning-related forces on the residual limb, and we know that some of these adaptors encompass the range of rotation and forces measured in an intact ankle (chapter 3). What we do not know about these rotation adaptors is whether or not they lessen residual limb tissue strain, and the associated pain and injury.

Determining the efficacy of rotation adaptors is challenging because residual limb tissue strain is exceedingly difficult to measure. With human subjects, it isn't ethically feasible to surgically implant strain gauges, and skin mounted strain gauges are

inaccurate due to the forces applied to them by the prosthetic socket. Measures of pain and injury are also difficult to obtain for humans. We currently have no data on the rate or duration of residual limb torsion that produces pain or injury. One approach to this problem is to use finite element (FE) modeling to simulate results under different dynamic conditions. For a review of the efforts to make a useable FE model of the residual limb, see (Mak, Zhang et al. 2001). Early research on the subject focused on validating FE data with instruments built into experimental prosthetic sockets (Sanders and Daly 1993). The authors found that the FE results were not within instrument error and suggested the improved estimates of residual limb properties and better numerical techniques would yield better simulations. More recent efforts produced the same conclusion (Zhang and Roberts 2000). Another group of researchers introduced slippage between the skin and prosthetic liner in their FE models. Other effort has concentrated on parametric analysis of the effects of the various necessary components of FE models (SilverThorn and Childress 1996).

All of the previous FE models suffer from two problems: soft tissue material properties need to be accurately determined under multi-axial loading conditions, and the models of these soft tissues need to be improved. Regarding the soft tissue material properties, unfortunately, most of those data come from indentor tests in which a rod is pressed into the leg to estimate an effective modulus for all of the tissue between the bone and indentor (Zheng and Mak 1999; Zheng, Mak et al. 1999; Tonuk and Silver-Thorn 2003). Indentor tests give poor estimates of the dynamic behavior of the tissue, no information about the mechanical behavior of individual tissue types, and no information

about mechanical behavior of the tissue under shear or tension. Regarding the second shortcoming, all early work and some current research uses linear models. Now it is more common to find non-linear tissue models, but better models would enhance multiple load path predictions. Because of these shortcomings, FE models fall short of their goal to simulate the dynamics of residual limbs.

While it is impossible to accurately simulate tissue strains with FE models, it is possible to use a model with all of the flawed assumptions to do numerical experiments on the changes associated with turning. High fidelity soft tissue models and accurate material properties are clearly missing, but this research establishes a rough model to explore large differences in rotation adaptor properties and their effects on the residual limb tissue.

In this chapter, I address the need to design prosthetic devices that will minimize the residual limb forces associated with turning. I have developed a finite element (FE) model of the below-knee residual limb and prosthetic socket that can be used to predict *changes* in tissue strains for turning steps compared to straight steps and for turning steps with and without the aid of a rotation adaptor. This FE model extends the work in this area by applying forces from straight and turning steps and incorporating the mechanical behavior of a virtual device similar to the rotation adaptors studied in chapter three. I also explore the possible benefits of an adaptive, rotation adaptor that would act to reduce the twisting of the residual limb. Again, I sidestep the obvious limitations of not having good estimates of the soft tissue behavior by comparing the FE model to itself under

different load cases. The model cannot predict tissue strain in a residual limb, but it can predict changes under the different conditions tested.

MATERIALS AND METHODS

Force Data

In order to apply the correct forces to the distal end of the prosthesis, kinetic data were collected from two amputee subjects. Both subjects were left below-knee (BK) amputees with no musculoskeletal or neurological problems by self-report. The University of Washington human subjects institutional review board approved the protocol and all subjects gave their informed consent to participate. Each subject underwent five trials walking straight and five trials turning around a 1m-radius circle. For each trial, the subjects were required to step on a forceplate (Kistler, Winterhur, CH, 600 Hz sampling frequency, 100Hz anti-aliasing filter) that was mounted flush with the floor. I used Matlab's spline function to reduce the 600 Hz forceplate data to 20 Hz (to lessen the computational time needed for the FE model) and averaged the data for all trials and subjects (fig. 4.3). Stance time is defined as the time when the upward ground reaction force (GRFz) is greater than 10N. The axes relate to the subjects as follows (fig 4.1): the X-axis corresponds to subject left/right (positive forces push medially on the pylon), the Y-axis corresponds to subject forward/backward (positive forces push posteriorly on the pylon) and the Z-axis corresponds to subject up/down (positive forces push up on the pylon).

Geometry

The data presented were generated and solved with Marc/Mentat (MSA Software, Los Angeles, California) finite element analysis software, version 2003. The geometry is an idealized, spherical representation of a BK residual limb. The diameter of the limb at the top of the prosthetic socket is 12cm. This tapers to 8cm at the bottom of the residual limb. The bones and soft tissue taper on the same function so that the cross sectional area relationships are constant. The prosthetic socket consisted of a carbon fiber socket, a liner, and a pylon. The liner was fixed to the socket, and the soft tissue was fixed to the liner. Between these three layers, no slippage or loss of contact was allowed. The pylon included a layer of elements that represented a rotation adaptor.

The three dimensional geometry was created by creating a single 2D cross section at the top of the socket (fig 4.2). This geometry was automeshed to 4 noded hexahedral elements. I expanded this layer of 2D elements distally to form the residual limb and prosthetic socket and proximally to form the portion of the residual limb above the socket. Expanding the 2D elements created eight-noded, hexahedral, solid elements. At the distal end of the limb, the layers were closed over each other to create a continuous layer of soft tissue around the bottom of the tibia and fibula (sagittal cross section figure). The completed model had 17577 nodes and 16226 elements. See appendix D for the procedure file.

Material Properties

The material properties of the soft tissue, liner, socket and pylon were assumed to be isotropic, homogeneous, and linearly elastic. The exact values used are given in table

4.1. The rotation adaptor was given damping characteristics by sequentially testing values for the stiffness matrix multiplier until the energy loss in one step approximated the magnitude of the energy lost in one cycle through the range of rotation of the adaptors tested in chapter three (table 3.3).

Boundary Conditions

Zero displacement conditions were applied to the bones. The forces and moments (6 degrees of freedom) recorded from the human subjects were distributed across the bottom of the prosthetic pylon. The top of the soft tissue was unconstrained, which was acceptable because the residual limb was extended far enough from the edge of the prosthetic socket to avoid edge effects from the distal boundary. Model predictions were collected over the complete history of the simulation from two points, one in front of the tibia and the other behind the fibula. These correspond to regions near strain maxima that were used in previous research (Sanders and Daly 1993; Zhang and Roberts 2000). The "ideal" rotation adaptor tissue strains were generated by eliminating the Moment in the Z-axis. In other words, the twisting force around the long axis of the pylon was removed, as if the "ideal" rotation adaptor could somehow dissipate it entirely. This isn't theoretically possible since we require some ground reaction force in order to rotate our bodies during a turn, but it gives a limit to the possible benefits of a "smart", microprocessor controlled rotation adaptor.

RESULTS

The model was used to compare differences in tissue strain between different experimental loads. The loads tested were one straight step, one turning step, and a turning step with and without a virtual rotation adaptor. All plots are in normalized time, from the moment of heel contact, to toe off. Actual average stance time is .74s for straight, and .81s for turning.

straight vs. turning

The differences in equivalent total tissue strain (non-directional sum of strain in all directions at a given point) between straight and turning steps can be seen throughout the stance. After a period of nearly identical onset, the turning step tissue strain drops off more sharply than the straight step tissue strain. In the middle of the stance, the tissue strains are nearly identical again. Near the end of the stance, the turning step tissue strain exceeds the straight step tissue strain, especially for the location near the fibula (fig. 4.4).

turning with RA vs. turning without RA

There is essentially no difference in the tissue strains predicted for rigid vs. RA equipped pylons. The RA equipped model predicts slightly lower tissue strains throughout the entire step (fig. 4.5).

turning with "ideal" RA

Compared to the effect of the commercially available RA the "ideal" RA demonstrates a reduction and smoothing of the tissue strain over the entire stance (fig. 4.6).

DISCUSSION

The goal of prosthesis research and development is to eliminate or reduce amputee pain and injury while increasing the range of possible activities. Amputees routinely find their residual limbs problematic, and these data support the hypothesis that the forces associated with turning are higher and are likely linked to higher rates of pain and injury. These numerical experiments do not accurately simulate tissue strains in residual limbs, but they do show differences in tissue strains between turning and straight walking and for prostheses with and without rotation adaptors.

In general, the pattern of tissue strain follows the development of the vertical component of the ground reaction force (fig. 4.3). This force is the largest of all six applied to the pylon, so it is no surprise that it is the major determinant of the shape of the resultant tissue stress curve. Additionally, the tissue strain pattern at the two locations in the residual limb chosen for analysis represented the same pattern found elsewhere in the residual limb. From location to location, there were small differences in the relative magnitudes and timings of the two peaks, but the basic shape was the same.

The differences between straight and turning forces predict several differences in the resulting tissue forces. The differences are clear in the results (fig. 4.4) but we are limited in our interpretation of their significance. We know very little about the way residual limb skin adapts to the new forces imposed upon it (Wang and Sanders 2003) and there are no data that correlate tissue strain with pain and injury. Until we understand what features of the tissue strain are damaging, we cannot evaluate the differences between walking straight and turning.

While the manufacturers of the currently available rotation adaptors may be dismayed by the results, the comparison of tissue strain with and without the rotation adaptor is not surprising. For amputees, nearly all of the forces from the ground are transmitted to the residual limb whether there is a rotation adaptor installed or not. There are losses associated with frictional damping in rotation adaptors (table 3.3), but when these energy are distributed throughout the entire residual limb, the effect in any one place is very small (fig. 4.5).

The ultimate goal of this work is to use the FE model to predict tissue strains under forces modulated by a virtual rotation adaptor. A small step in that direction is to establish the maximum reduction possible in a case where all the rotational forces in the transverse plane are eliminated. While this is theoretically impossible, (imagine trying to turn on a lazy-susan) it does establish an estimate of the limit of tissue strain reduction possible to achieve with a rotation adaptor. The results with the "ideal" rotation adaptor show a smoothing of the sharp transient at the end of the first peak and a reduction in the amplitude of the second peak. If a real rotation adaptor could accomplish 20% of this ideal reduction, it would certainly be an improvement over the current rotation adaptors and may prove useful in reducing pain and injury for amputees.

More than anything, this work presents us with testable hypotheses. We can experimentally validate the hypotheses that tissue strains are different while turning, and we can test the hypothesis that tissue strains are unaffected by currently available rotation adaptors. Additionally, it provides us with an experimental platform to test reductions in tissue strain in response to new rotation adaptor designs.

NOTES TO CHAPTER FOUR

Ehde, D. M., J. M. Czerniecki, et al. (2000). "Chronic phantom sensations, phantom pain, residual limb pain, and other regional pain after lower limb amputation." Arch Phys Med Rehabil **81**(8): 1039-44.

Legro, M. W., G. Reiber, et al. (1999). "Issues of importance reported by persons with lower limb amputations and prostheses." J Rehabil Res Dev **36**(3): 155-63.

Nielsen, C. C. (1991). "A survey of amputees: functional level and life satisfaction, information needs and the prosthetist's role." Journal of Prosthetics and Orthotics **3**(3): 125-129.

(1998). The Fourier Transform in Biomedical Engineering. T. M. Peters and J. Williams. Boston, MA, Birkhauser**:** 35-38, 194.

Ehde, D. M., J. M. Czerniecki, et al. (2000). "Chronic phantom sensations, phantom pain, residual limb pain, and other regional pain after lower limb amputation." Arch Phys Med Rehabil **81**(8): 1039-44.

Hagberg, K. and R. Branemark (2001). "Consequences of non-vascular trans-femoral amputations: a survey of quality of live, prosthetic use and problems." Prosthet Orthot Int **25**(December): 186-194.

Legro, M. W., G. Reiber, et al. (1999). "Issues of importance reported by persons with lower limb amputations and prostheses." J Rehabil Res Dev **36**(3): 155-63.

Mak, A. F. T., M. Zhang, et al. (2001). "State-of-the-art research in lower-limb prosthetic biomechanics-socket interface: A review." Journal Of Rehabilitation Research And Development **38**(2): 161-173.

Nielsen, C. C. (1991). "A survey of amputees: functional level and life satisfaction, information needs and the prosthetist's role." Journal of Prosthetics and Orthotics **3**(3): 125-129.

Sanders, J. E. and C. H. Daly (1993). "Normal And Shear Stresses On A Residual Limb In A Prosthetic Socket During Ambulation - Comparison Of Finite-Element Results With Experimental Measurements." Journal Of Rehabilitation Research And Development **30**(2): 191-204.

Sedgman, R., P. Goldie, et al. (1994). "Development of a measure of turning during walking." Advancing Rehabilitation conference proceedings, La Trobe University, Melbourne, AU: 26-31.

SilverThorn, M. B. and D. S. Childress (1996). "Parametric analysis using the finite element method to investigate prosthetic interface stresses for persons with trans-tibial amputation." Journal Of Rehabilitation Research And Development **33**(3): 227-238.

Tonuk, E. and M. B. Silver-Thorn (2003). "Nonlinear elastic material property estimation of lower extremity residual limb tissues." Ieee Transactions On Neural Systems And Rehabilitation Engineering **11**(1): 43-53.

Wang, Y. N. and J. E. Sanders (2003). "How does skin adapt to repetitive mechanical stress to become load tolerant?" Medical Hypotheses **61**(1): 29-35.

Zhang, M. and C. Roberts (2000). "Comparison of computational analysis with clinical measurement of stresses on below-knee residual limb in a prosthetic socket." Medical Engineering & Physics **22**(9): 607-612.

Zheng, Y. P. and A. F. T. Mak (1999). "Extraction of quasi-linear viscoelastic parameters for lower limb soft tissues from manual indentation experiment." Journal Of Biomechanical Engineering-Transactions Of The Asme **121**(3): 330-339.

Zheng, Y. P., A. F. T. Mak, et al. (1999). "Objective assessment of limb tissue elasticity: Development of a manual indentation procedure." Journal Of Rehabilitation Research And Development **36**(2): 71-85.

Table 4.1: Finite Element Material Properties

Material Type	Young's Modulus (Mpa)	Poisson's Ratio	Mass Density (kg/m^3)
Bone	2.1e4	.49	400
Soft Tissue	9.7	.49	1000
Liner	1.7	.39	700
Socket	1.4e5	.49	955
Pylon	2e5	.49	400
Elastomer	20	.49	1000

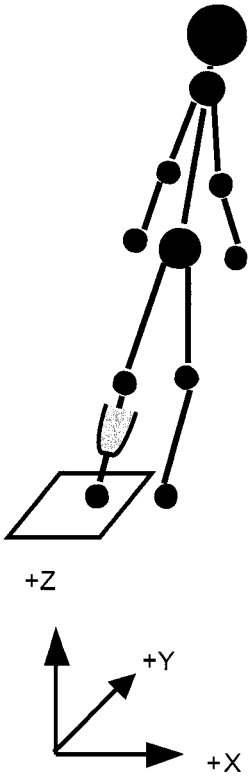

Figure 4.1. Axis definition and sign convention.

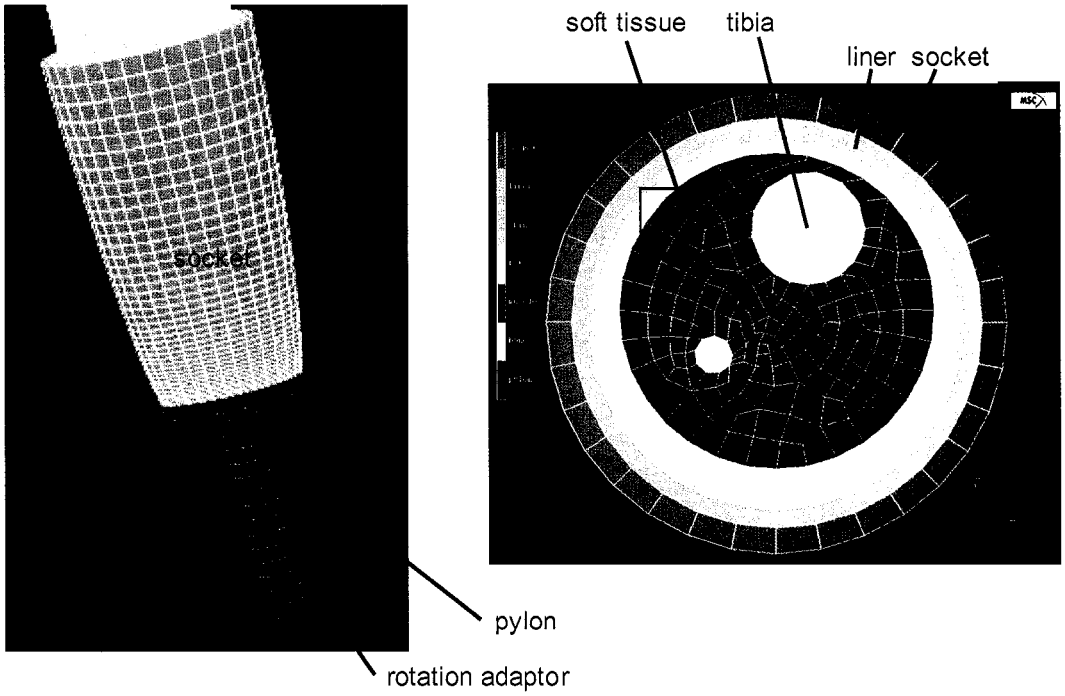

Figure 4.2. Diagram of exterior and cross section of FE model limb and socket.

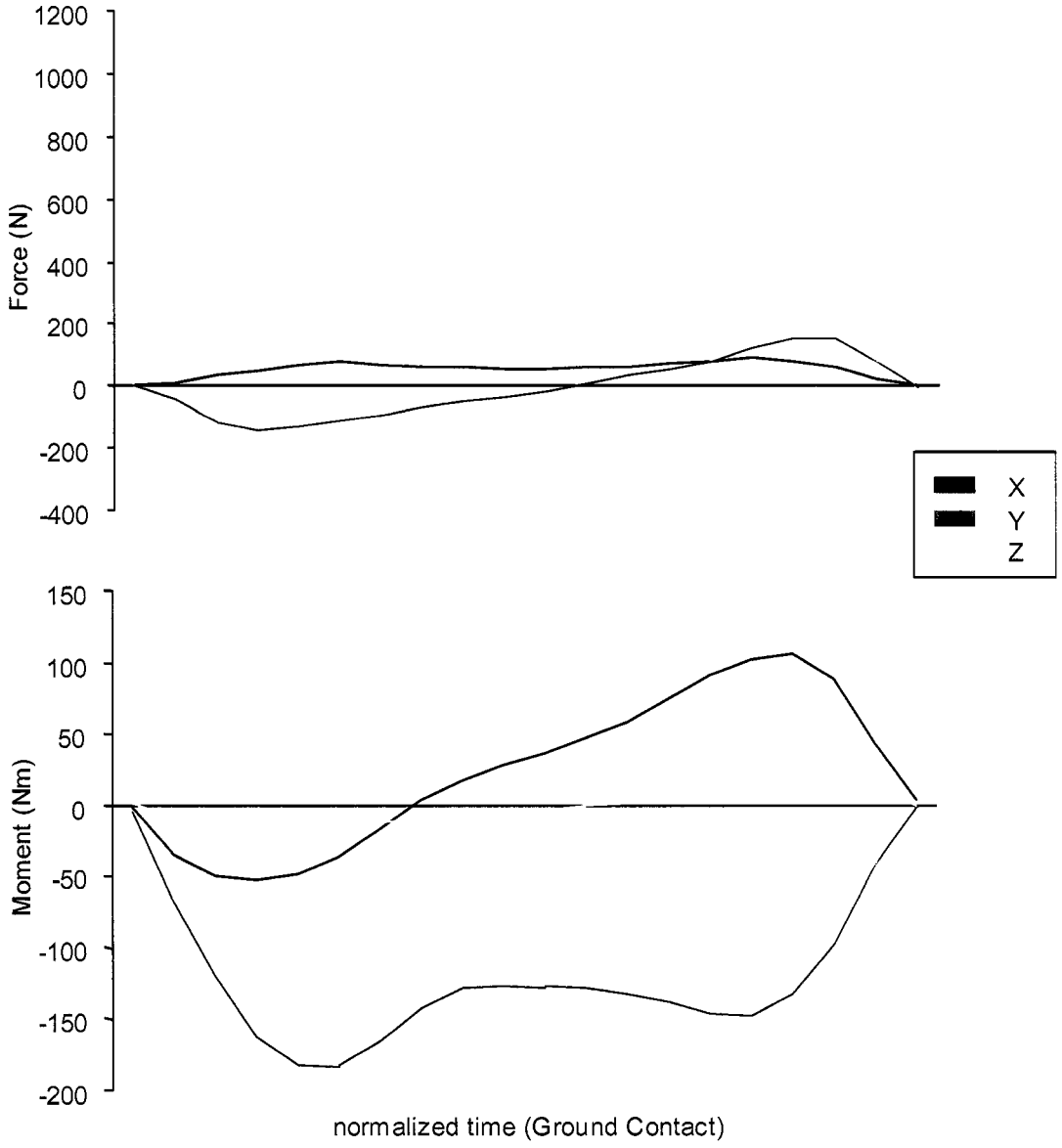

Figure 4.3. Measured ground reaction forces. The normalized time starts at heel strike and continues to toe off. Each line is average data (n = 2 subjects, 5 trials each).

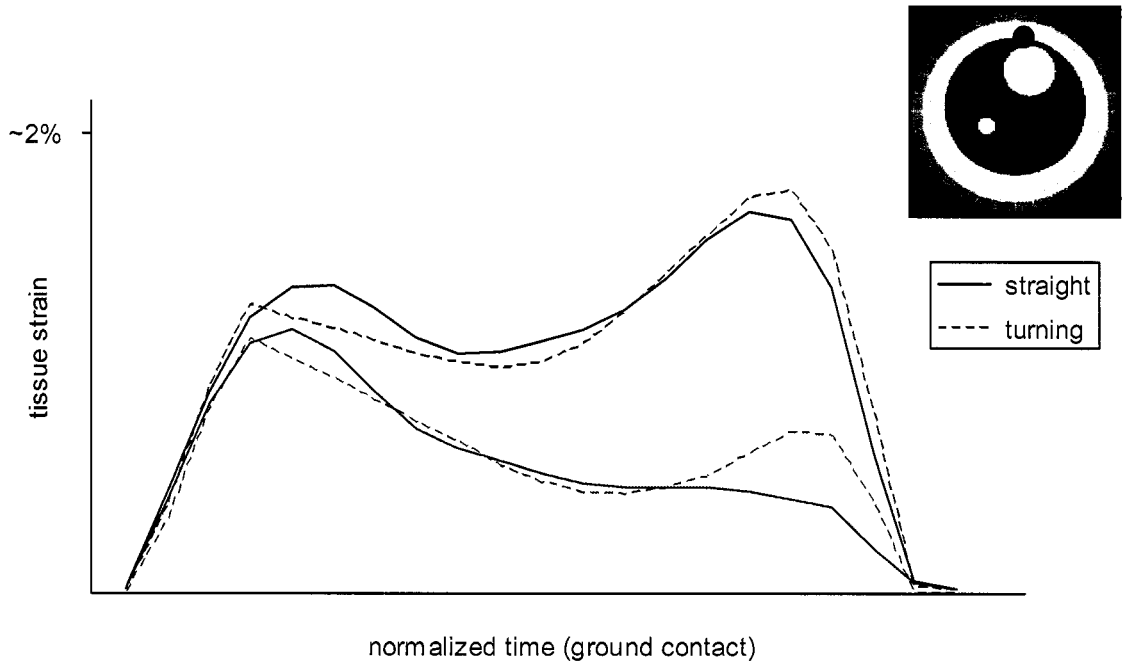

Figure 4.4. Residual limb tissue strain for straight vs. turning.

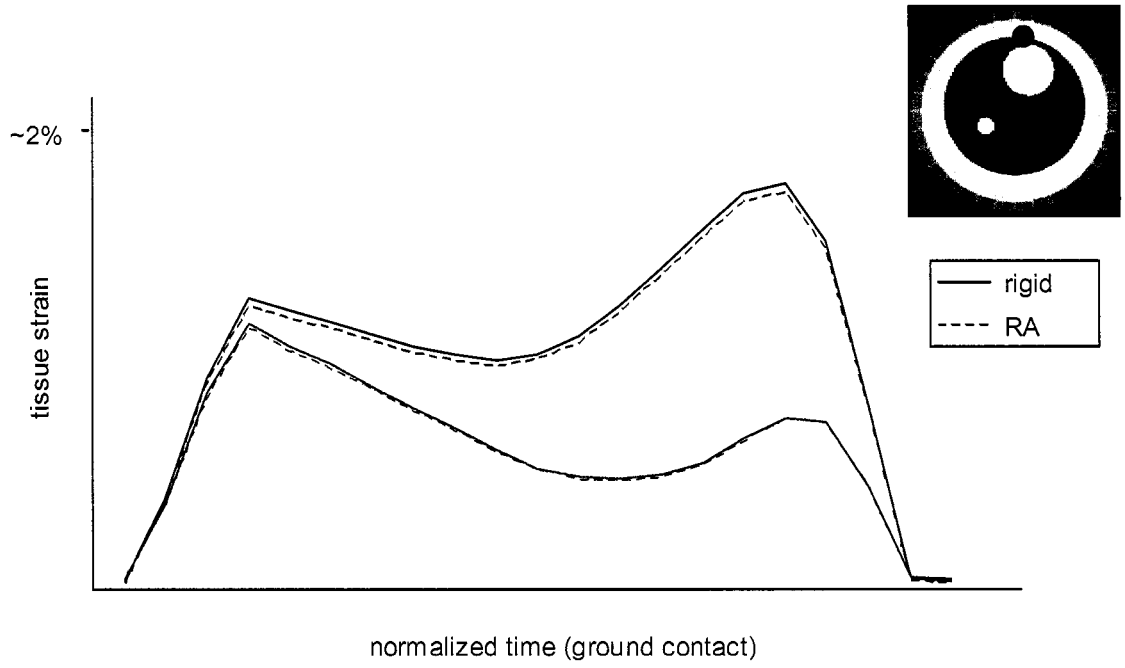

Figure 4.5. Residual limb tissue strain for rigid vs. RA equipped pylons

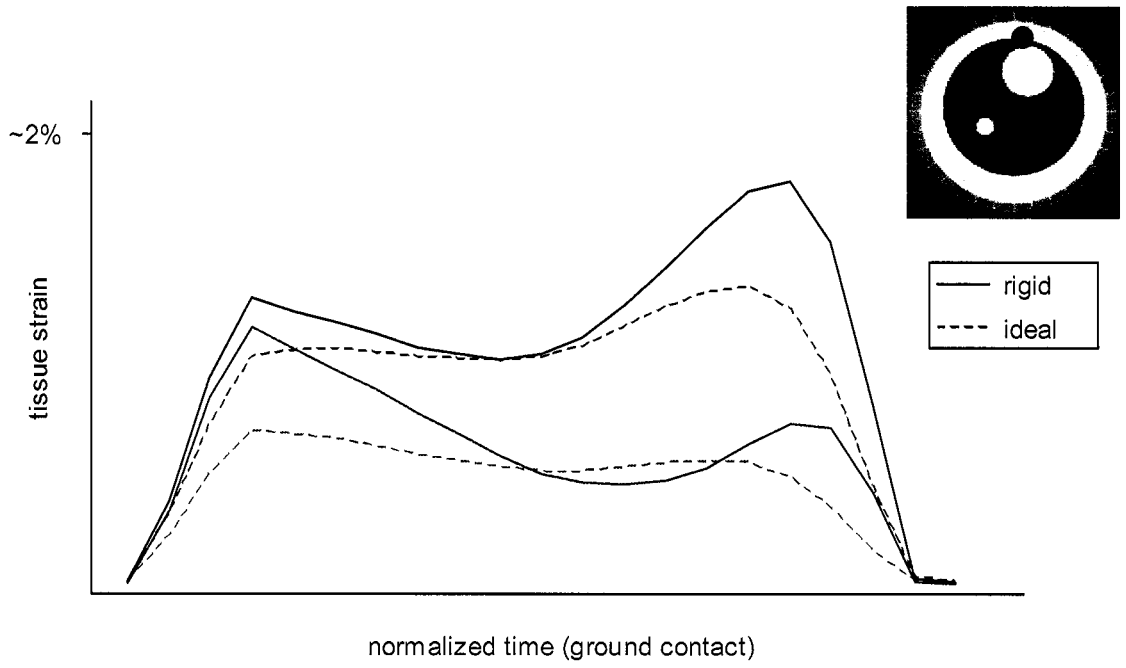

Figure 4.6. Residual limb tissue strain for rigid vs. ideal RA equipped pylons.

BIBLIOGRAPHY

Abramowitch, S. D., T. D. Clineff, et al. (1999). Effects of restricted ankle dorsiflexion on plantar pressure distributions. 23rd Annual Meeting of the American Society of Biomechanics, Pittsburgh, PA.

Arshavksy Yu, I., G. N. Orlovsky, et al. (1989). "Control of Locomotion in Marine Mollusc Clione-Limacina Vii. Reexamination of Type 12 Interneurons." Experimental Brain Research **78**(2): 398-406.

Arshavskii Yu, I., T. G. Delyagina, et al. (1989). "Neural Control of Heart Beating in the Pteropodial Mollusc Clione-Limacina." Neirofiziologiya **21**(2): 185-192.

Arshavsky, Y. I., T. G. Deliagina, et al. (1993). "Pharmacologically induced elements of the hunting and feeding behavior in the pteropod mollusk Clione limacina: II. Effects of physostigmine." Journal of Neurophysiology Bethesda **69**(2): 522-532.

Arshavsky, Y. I., T. G. Deliagina, et al. (1993). "Pharmacologically induced elements of the hunting and feeding behavior in the pteropod mollusk Clione limacina: I. Effects of GABA." Journal of Neurophysiology Bethesda **69**(2): 512-521.

Arshavsky, Y. I., T. G. Deliagina, et al. (1997). "Pattern generation." Current Opinion in Neurobiology **7**(6): 781-789.

Arshavsky, Y. I., T. G. Deliagina, et al. (1991). Locomotion of *Clione limacina* in relation to various types of behavior. Simpler nervous systems. D. A. Sakharov and W. Winlow. Manchester, UK, Manchester University Press**:** 290-315.

Arshavsky, Y. I., G. N. Orlovsky, et al. (1985). "Control of Locomotion in the Marine Mollusk Clione-Limacina 5. Photoinactivation of Efferent Neurons." Experimental Brain Research **59**(1): 203-205.

Arshavsky, Y. I., G. N. Orlovsky, et al. (1993). "Neuronal control of swimming locomotion: Analysis of the pteropod mollusc Clione and embryos of the amphibian Xenopus." Trends in Neurosciences **16**(6): 227-233.

Arshavsky Yu, I., I. N. Beloozerova, et al. (1985). "Control of Locomotion in Marine Mollusk Clione-Limacina 1. Efferent Activity During Actual and Fictitious Swimming." Experimental Brain Research **58**(2): 255-262.

Arshavsky Yu, I., I. N. Beloozerova, et al. (1985). "Control of Locomotion in Marine Mollusk Clione-Limacina 3. the Origin of Locomotory Rhythm." Experimental Brain Research **58**(2): 273-284.

Arshavsky Yu, I., I. N. Beloozerova, et al. (1985). "Control of Locomotion in Marine Mollusk Clione-Limacina 4. Role of Type 12 Interneurons." Experimental Brain Research **58**(2): 285-293.

Arshavsky Yu, I., T. G. Deliagina, et al. (1986). "Control of Locomotion in Marine Mollusk Clione-Limacina Vi. Activity of Isolated Neurons of Pedal Ganglia." Experimental Brain Research **63**(1): 106-112.

Arshavsky Yu, I., T. G. Deliagina, et al. (1992). "Interneurones Mediating the Escape Reaction of the Marine Mollusc Clione-Limacina." Journal of Experimental Biology **164**: 307-314.

Arshavsky Yu, I., S. Grillner, et al. (1991). "Central Generators and the Spatio-Temporal Pattern of Movements."

Benfield, M. C., C. S. Davis, et al. (1996). "Video plankton recorder estimates of copepod, pteropod and larvacean distributions from a stratified region of Georges Bank with comparative measurements from a MOCNESS sampler." Deep-Sea Research **43**(7-8): 1925-1945.

Bryan, P. J., W. Y. Yoshida, et al. (1995). "Ecological role for pteroenone, a novel antifeedant from the conspicuous Antarctic pteropod Clione antarctica (Gymnosomata: Gastropoda)." Marine Biology **122**: 271-277.

Camhi, J. (1970b). "Sensory control of abdomen posture in flying locusts." Journal of Experimental Biology **52**: 533-537.

Chan, W. P. and M. H. Dickinson (1996). "In vivo length oscillations of indirect flight muscles in the fruit fly Drosophila virilis." Journal Of Experimental Biology **199**(12): 2767-2774.

Chan, W. P., F. Prete, et al. (1998). "Visual input to the efferent control system of a fly's "gyroscope"." Science **280**(5361): 289-292.

Combes, S. A. and T. L. Daniel (2003). "Flexural stiffness in insect wings I. Scaling and the influence of wing venation." Journal Of Experimental Biology **206**(17): 2979-2987.

Combes, S. A. and T. L. Daniel (2003). "Flexural stiffness in insect wings II. Spatial distribution and dynamic wing bending." Journal Of Experimental Biology **206**(17): 2989-2997.

Combes, S. A. and T. L. Daniel (2003). "Into thin air: contributions of aerodynamic and inertial-elastic forces to wing bending in the hawkmoth Manduca sexta." Journal Of Experimental Biology **206**(17): 2999-3006.

Conover, R. J. and C. M. Lalli (1972). "Feeding and growth in Clione limacina (Phipps), a pteropod mollusc." J. exp. mar. Biol. Ecol. **9**: 279-302.

Conover, R. J. and C. M. Lalli (1974). "Feeding and Growth in Clione limacina (Phipps), a Pteropod Mollusk. II. Assimilation, Metabolism, and Growth Efficiency." J. exp. mar. Bio. Ecol. **16**: 131-154.

Courtine, G. and M. Schieppati (2003). "Human walking along a curved path. I. Body trajectory, segment orientation and the effect of vision." Eur J Neurosci **18**(1): 177-90.

Courtine, G. and M. Schieppati (2003). "Human walking along a curved path. II. Gait features and EMG patterns." Eur J Neurosci **18**(1): 191-205.

Daniel, T. L. (1984). "Unsteady Aspects Of Aquatic Locomotion." American Zoologist **24**(1): 121-134.

Daniel, T. L. and S. A. Combes (2002). "Flexible wings and fins: Bending by inertial or fluid-dynamic forces?" Integrative And Comparative Biology **42**(5): 1044-1049.

Daniel, T. L., J. G. Kingsolver, et al. (1989). "Mechanical Determinants Of Nectar-Feeding Energetics In Butterflies - Muscle Mechanics, Feeding Geometry, And Functional Equivalence." Oecologia **79**(1): 66-75.

Daniel, T. L. and E. Meyhofer (1989). "Size Limits In Escape Locomotion Of Carridean Shrimp." Journal Of Experimental Biology **143**: 245-265.

Daniel, T. L. and M. S. Tu (1999). "Animal movement, mechanical tuning and coupled systems." Journal Of Experimental Biology **202**(23): 3415-3421.

Deliagina, T. G., Y. I. Arshavsky, et al. (1998). "Control of spatial orientation in a mollusc." Nature London **393**(6681): 172-175.

Deliagina, T. G., G. N. Orlovsky, et al. (1999). "Neuronal mechanisms for the control of body orientation in Clione I. Spatial zones of activity of different neuron groups." Journal of Neurophysiology Bethesda **82**(2): 687-699.

Deliagina, T. G., G. N. Orlovsky, et al. (2000). "Asymmetrical effect of GABA on the postural orientation in Clione." Journal of Neurophysiology Bethesda **84**(3): 1673-1676.

Deliagina, T. G., G. N. Orlovsky, et al. (2000). "Neuronal mechanisms for the control of body orientation in Clione. II. Modifications in the activity of postural control system." Journal of Neurophysiology Bethesda **83**(1): 367-373.

Denny, M. W., T. L. Daniel, et al. (1985). "Mechanical Limits To Size In Wave-Swept Organisms." Ecological Monographs **55**(1): 69-102.

Dickinson, M. (2001). "Solving the mystery of insect flight - Insects use a combination of aerodynamic effects to remain aloft." Scientific American **284**(6): 48-57.

Dickinson, M. (2003). "Animal locomotion: How to walk on water." Nature **424**(6949): 621-622.

Dickinson, M., J. Birch, et al. (2001). "Deconstructing the aerodynamics of insect flight." American Zoologist **41**(6): 1428-1428.

Dickinson, M. H., C. T. Farley, et al. (2000). "How animals move: An integrative view." Science **288**(5463): 100-106.

Dickinson, M. H. and K. G. Gotz (1993). "Unsteady Aerodynamic Performance Of Model Wings At Low Reynolds-Numbers." Journal Of Experimental Biology **174**: 45-64.

Dickinson, M. H. and K. G. Gotz (1996). "The wake dynamics and flight forces of the fruit fly Drosophila melanogaster." Journal Of Experimental Biology **199**(9): 2085-2104.

Dickinson, M. H., F. O. Lehmann, et al. (1998). "The control of mechanical power in insect flight." American Zoologist **38**(4): 718-728.

Dickinson, M. H., F. O. Lehmann, et al. (1993). "The Active Control Of Wing Rotation By Drosophila." Journal Of Experimental Biology **182**: 173-189.

Dickinson, M. H. and M. S. Tu (1997). "The function of dipteran flight muscle." Comparative Biochemistry And Physiology A-Physiology **116**(3): 223-238.

Dillingham, T. R., L. E. Pezzin, et al. (2001). "Use and satisfaction with prosthetic devices among persons with trauma-related amputations: a long-term outcome study." Am J Phys Med Rehabil **80**(8): 563-71.

Eaves, G. N. (1984). "Preparation of the Research-Grant Application: Opportunities and Pitfalls." Grants Magazine **7**(3): 151-157.

Ehde, D. M., J. M. Czerniecki, et al. (2000). "Chronic phantom sensations, phantom pain, residual limb pain, and other regional pain after lower limb amputation." Arch Phys Med Rehabil **81**(8): 1039-44.

Farmer, W., M. "Swimming Gastropods (Opisthobranchia and Prosobranchia)." The Veliger **13**(1): 73-89.

Fiege, D. (1990). "Morphology of the wings of Euthecosomatous pteropods." American Malacological Bulletin **8**(1): 27-36.

Flick, K. (1999). "Control of aquatic flight in Clione limacina." American Zoologist **39**(5): 56A-57A.

Flick, K. C., M. S. Tu, et al. (2001). "Flight control by steering muscles in Manduca sexta." American Zoologist **41**(6): 1445.

Foster, B. A. (1987). "Composition and Abundance of Zooplankton Under the Spring Sea-Ice of Mcmurdo Sound Antarctica." Polar Biology **8**(1): 41-48.

Full, R. J. and D. E. Koditschek (1999). "Templates and anchors: Neuromechanical hypotheses of legged locomotion on land." Journal Of Experimental Biology **202**(23): 3325-3332.

Ghoussayni, S., C. Stevens, et al. (2004). "Assessment and validation of a simple automated method for the detection of gait events and intervals." Gait & Posture **20**: 266-272.

Gilmer, R. W. (1974). "Some aspects of feeding in thecosomatous pteropod molluscs." J. exp. mar. Biol. Ecol. **15**: 124-144.

Gilmer, R. W. (1990). "In situ observations of feeding behavior of thecosome pteropod molluscs." American Malacological Bulletin **8**(1): 53-59.

Gotz, K., B. Hengstenberg, et al. (1979). "Optomotor control of wing beat and body posture in *Drosophila*." Biol Cybern **35**: 101-112.

Hagberg, K. and R. Branemark (2001). "Consequences of non-vascular trans-femoral amputations: a survey of quality of live, prosthetic use and problems." Prosthet Orthot Int **25**(December): 186-194.

Hansen, A. H., D. S. Childress, et al. (2002). "A simple method for determination of gait events." Journal of Biomechanics **35**: 135-138.

Hase, K. and R. B. Stein (1999). "Turning strategies during human walking." J Neurophysiol **81**(6): 2914-22.

Hreljac, A. and R. N. Marshall (2000). "Algorithms to determine event timing during normal walking using kinematic data." Journal of Biomechanics **33**: 783-786.

Kohn, A. J. (1961). "Chemoreception in Gastropod Molluscs." Am. Zoologist **1**: 291-308.

Lafortune, M. A., P. R. Cavanagh, et al. (1994). "Foot inversion-eversion and knee kinematics during walking." Journal of Orthopaedic Research **12**(3): 412-20.

Lalli, C. M. (1970). "Structure and Function of the Buccal Apparatus of Clione limacina (Phipps) with a Review of Feeding in Gymnosomtous Pteropods." J. exp. mar. Biol. Ecol. **4**: 101-118.

Lamoureux, L. W. and C. W. Radcliffe (1977). "Functional analysis of the UC-BL shank axial rotation device." Prosthet Orthot Int **1**(2): 114-8.

Latash, M. L. and V. M. Zatsiorsky (1993). "Joint stiffness: myth or reality." Human Movement Science **12**: 653-692.

Legro, M. W., G. Reiber, et al. (1999). "Issues of importance reported by persons with lower limb amputations and prostheses." J Rehabil Res Dev **36**(3): 155-63.

Legro, M. W., G. D. Reiber, et al. (1998). "Prosthesis evaluation questionnaire for persons with lower limb amputations: assessing prosthesis-related quality of life." Arch Phys Med Rehabil **79**(8): 931-8.

Lehmann, F. O. and M. H. Dickinson (2001). "The production of elevated flight force compromises manoeuvrability in the fruit fly Drosophila melanogaster." Journal Of Experimental Biology **204**(4): 627-635.

Mak, A. F. T., M. Zhang, et al. (2001). "State-of-the-art research in lower-limb prosthetic biomechanics-socket interface: A review." Journal Of Rehabilitation Research And Development **38**(2): 161-173.

Marshall, H. M., M. P. Jensen, et al. (2002). "Pain site and impairment in individuals with amputation pain." Arch Phys Med Rehabil **83**(8): 1116-9.

May, M. and R. Hoy (1990). "Leg-Induced Steering in Flying Crickets." J. exp. Biol. **151**: 485-488.

Meijer, K., T. M. Libby, et al. (2000). "Passive stability provided by the musculo-skeletal properties of an insect leg." American Zoologist **40**(6): 1129-1130.

Mickelborough, J., M. L. van der Linden, et al. (2000). "Validity and reliability of a kinematic protocol for determining foot contact events." Gait & Posture **11**: 32-37.

Nester, C. (2000). "The relationship between transverse plane leg rotation and transverse plane motion at the knee and hip during normal walking." Gait Posture **12**(3): 251-6.

Nester, C. J., A. F. Findlow, et al. (2003). "Transverse plane motion at the ankle joint." Foot Ankle Int **24**(2): 164-8.

Nielsen, C. C. (1991). "A survey of amputees: functional level and life satisfaction, information needs and the prosthetist's role." Journal of Prosthetics and Orthotics **3**(3): 125-129.

Nordt, W. E., 3rd, P. Lotfi, et al. (1999). "The in vivo assessment of tibial motion in the transverse plane in anterior cruciate ligament-reconstructed knees." Am J Sports Med **27**(5): 611-6.

Norekian, T. P. (1999). "GABAergic excitatory synapses and electrical coupling sustain prolonged discharges in the prey capture neural network of Clione limacina." Journal of Neuroscience **19**(5): 1863-1875.

Panchin, Y. V., Y. I. Arshavsky, et al. (1996). "Control of locomotion in the marine mollusc Clione limacina: XI. Effects of serotonin." Experimental Brain Research **109**(2): 361-365.

Panchin, Y. V., Y. I. Arshavsky, et al. (1995). "Control of locomotion in marine mollusk Clione limacina: IX. Neuronal mechanisms of spatial orientation." Journal of Neurophysiology Bethesda **73**(5): 1924-1937.

Panchin, Y. V., G. N. Gamkrelidze, et al. (1994). "Neuronal basis of hunting and feeding behaviour in the pteropod mollusc Clione limacina." Netherlands Journal of Zoology **44**(3-4): 170-183.

Panchin, Y. V., L. B. Popova, et al. (1995). "Control of locomotion in marine mollusk Clione limacina. VIII. Cerebropedal neurons." J Neurophysiol **73**(5): 1912-1923.

Panchin, Y. V., R. I. Sadreev, et al. (1995). "Control of locomotion in marine mollusc Clione limacina X. Effects of acetylcholine antagonists." Experimental Brain Research **106**(1): 135-144.

Peham, C., M. Scheidl, et al. (1999). "Limb locomotion - speed distribution analysis as a new method for stance phase detection." Journal of Biomechanics **32**: 1119-1124.

Pena de Ortiz, S. and Y. I. Arshavsky (2001). "DNA recombination as a possible mechanism in declarative memory: A hypothesis." Journal of Neuroscience Research **63**(1): 72-81.

Robertson, R. M. and A. G. Johnson (1993). "Collision Avoidance of Flying Locusts: Steering Torques and Behavior." J. exp. Biol. **183**: 35-60.

Sadeghi, H., P. Allard, et al. (2000). "Symmetry and limb dominance in able-bodied gait: a review." Gait & Posture **12**: 34-45.

Sanders, J. E. and C. H. Daly (1993). "Normal And Shear Stresses On A Residual Limb In A Prosthetic Socket During Ambulation - Comparison Of Finite-Element

Results With Experimental Measurements." Journal Of Rehabilitation Research And Development **30**(2): 191-204.

Sanders, J. E., C. H. Daly, et al. (1992). "Interface shear stresses during ambulation with a below-knee prosthetic limb." J Rehabil Res Dev **29**(4): 1-8.

Sanders, J. E. and B. S. Goldstein (2001). "Collagen fibril diameters increase and fibril densities decrease in skin subjected to repetitive compressive and shear stresses." J Biomech **34**(12): 1581-7.

Sanders, J. E., B. S. Goldstein, et al. (1995). "Skin response to mechanical stress: adaptation rather than breakdown--a review of the literature." J Rehabil Res Dev **32**(3): 214-26.

Sanders, J. E., J. M. Greve, et al. (1998). "Material properties of commonly-used interface materials and their static coefficients of friction with skin and socks." Journal of Rehabilitation Research & Development **35**(2): 161-76.

Sanders, J. E., R. A. Miller, et al. (1997). "A modular six-directional force sensor for prosthetic assessment: a technical note." J Rehabil Res Dev **34**(2): 195-202.

Sane, S. P. and M. H. Dickinson (2001). "The control of flight force by a flapping wing: Lift and drag production." Journal Of Experimental Biology **204**(15): 2607-2626.

Satterlie, R. A. (1993). "Neuromuscular organization in the swimming system of the pteropod mollusc Clione limacina." Journal of Experimental Biology **181**(0): 119-140.

Satterlie, R. A., G. E. J. Goslow, et al. (1990). "Two Types of Striated Muscle Suggest Two-Geared Swimming in the Pteropod Mollusc Clione-Limacina." Journal of Experimental Zoology **255**(2): 131-140.

Satterlie, R. A., M. Labarbera, et al. (1985). "Swimming in the Pteropod Mollusk Clione-Limacina I. Behavior and Morphology." Journal of Experimental Biology **116**: 189-204.

Satterlie, R. A. and T. P. Norekian (1996). "Modulation of swimming speed in the pteropod mollusc, Clione limacina: Role of a compartmental serotonergic system." Invertebrate Neuroscience **2**(3): 157-165.

Satterlie, R. A. and A. N. Spencer (1985). "Swimming in the Pteropod Mollusk Clione-Limacina Ii. Physiology." Journal of Experimental Biology **116**: 205-222.

Schoppen, T., A. Boonstra, et al. (2001). "Factors related to successful job reintegration of people with a lower limb amputation." Arch Phys Med Rehabil **82**(10): 1425-31.

Sedgman, R., P. Goldie, et al. (1994). "Development of a measure of turning during walking." Advancing Rehabilitation conference proceedings, La Trobe University, Melbourne, AU: 26-31.

SilverThorn, M. B. and D. S. Childress (1996). "Parametric analysis using the finite element method to investigate prosthetic interface stresses for persons with trans-tibial amputation." Journal Of Rehabilitation Research And Development **33**(3): 227-238.

Soom, A. and M. Lee (1983). "Optimal design of linear and nonlinear vibration absorbers for damped systems." Journal of Vibration, Acoustics, Stress, and Reliability in Design **105**: 112-119.

Tarsitano, M. and M. Dickinson (2000). "Visual-olfactory fusion in the flight behavior of Drosophila." American Zoologist **40**(6): 1229-1229.

Tonuk, E. and M. B. Silver-Thorn (2003). "Nonlinear elastic material property estimation of lower extremity residual limb tissues." Ieee Transactions On Neural Systems And Rehabilitation Engineering **11**(1): 43-53.

Townsend, M. A. (1981). "Dynamics and coordination of torso motions in human locomotion." J Biomech **14**(11): 727-38.

Townsend, M. A. (1985). "Biped gait stabilization via foot placement." J Biomech **18**(1): 21-38.

Tu, M. S. and T. L. Daniel (2004). "Cardiac-like behavior of an insect flight muscle." Journal Of Experimental Biology **207**(14): 2455-2464.

Tu, M. S. and T. L. Daniel (2004). "Submaximal power output from the dorsolongitudinal flight muscles of the hawkmoth Manduca sexta." Journal Of Experimental Biology **207**(26): 4651-4662.

Tu, M. S. and M. H. Dickinson (1994). "Modulation Of Negative Work Output From A Steering Muscle Of The Blowfly Calliphora-Vicina." Journal Of Experimental Biology **192**: 207-224.

Tu, M. S. and M. H. Dickinson (1996). "The control of wing kinematics by two steering muscles of the blowfly (Calliphora vicina)." Journal Of Comparative Physiology A-Sensory Neural And Behavioral Physiology **178**(6): 813-830.

Van der Linden, M. L., N. Twiste, et al. (2002). "The biomechanical effects of the inclusion of a torque absorber on trans-femoral amputee gait, a pilot study." Prosthet Orthot Int **26**(1): 35-43.

Vukobratovic, M., A. A. Frank, et al. (1970). "On the stability of biped locomotion." IEEE Trans Biomed Eng **BME-17**(1): 25-36.

Wall, J. C. and J. Crosbie (1996). "Accuracy and reliability of temporal gait measurement." Gait & Posture **4**: 293-296.

Wang, Y. N. and J. E. Sanders (2003). "How does skin adapt to repetitive mechanical stress to become load tolerant?" Medical Hypotheses **61**(1): 29-35.

Zachariah, S. G. and J. E. Sanders (2000). "Finite element estimates of interface stress in the trans-tibial prosthesis using gap elements are different from those using automated contact." Journal Of Biomechanics **33**(7): 895-899.

Zanker, J. M. (1988). "How does lateral abdomen deflection contribute to flight control of *Drosophila melanogaster*?" J. Comp. Physiol. A **162**: 581-588.

Zhang, M., M. Lord, et al. (1995). "Development Of A Nonlinear Finite-Element Modeling Of The Below-Knee Prosthetic Socket Interface." Medical Engineering & Physics **17**(8): 559-566.

Zhang, M. and C. Roberts (2000). "Comparison of computational analysis with clinical measurement of stresses on below-knee residual limb in a prosthetic socket." Medical Engineering & Physics **22**(9): 607-612.

Zhang, M. and V. C. Roberts (1993). "The effect of shear forces externally applied to skin surface on underlying tissues." J Biomed Eng **15**(6): 451-6.

Zhang, M., A. R. Turner-Smith, et al. (1994). "The reaction of skin and soft tissue to shear forces applied externally to the skin surface." Proc Inst Mech Eng [H] **208**(4): 217-222.

Zhang, M., A. R. TurnerSmith, et al. (1996). "Frictional action at lower limb prosthetic socket interface." Medical Engineering & Physics **18**(3): 207-214.

Zheng, Y. P. and A. F. T. Mak (1999). "Extraction of quasi-linear viscoelastic parameters for lower limb soft tissues from manual indentation experiment." Journal Of Biomechanical Engineering-Transactions Of The Asme **121**(3): 330-339.

Zheng, Y. P., A. F. T. Mak, et al. (1999). "Objective assessment of limb tissue elasticity: Development of a manual indentation procedure." Journal Of Rehabilitation Research And Development **36**(2): 71-85.

Appendix A: Biased random walk Matlab code

Introduction

This code simulates the search pattern of a predator hunting for a single, stationary prey item. The distance units are cm, and the time steps are in seconds. Each iteration allows the predator 1 hour to encounter the prey item, starting ~15cm outside of the detection radius (the area around the prey item in which the predator can detect the prey). The predator can move at 1cm/s or stay still. The hunting behavior is random, except when the predator comes within the detection radius of the prey. Within that radius, the predator is more likely to continue in the direction it was going when it first entered the detection radius. This is accomplished by establishing seven bins of varying sizes to represent one centimeter of travel in +/-[x,y,z] or staying still. The bin representing the biased direction is enlarged by the parameter, "bias", and the other six bins are made equally smaller. For each time step, a random number is generated and the bin in which it fits determines the animal's direction. I do not intend this behavior to have any fidelity to the way *Clione* actually hunts; it is a thought experiment designed to demonstrate the difficulty of visually detecting small biases in behavior.

Code

```
close all
clear all
time = 3600; % number of seconds per iteration
iterations = 1; % number of times to run simulation
prey=[17.5 17.5 17.5]; % initial prey location
r=15; % distance to prey that predator can detect prey
bias=.03; % 0-1
encounterdistance = 2.6; % one body length (cm)
```

```
biasm = bias*6+1; % turn bias into a number between 1 and 7

%start each iteration
for n=1:iterations

 %set the initial conditions and build blank matrices for each iteration
 pos=[0 0 0];
 condition=1; % predator not detecting prey
 counter=0; % counts number of encounters with prey
 stepmat = zeros(time-1,3);  % keep track of steps taken by predator

 for i=2:time

  % calculate the distance between predator and prey
  xdist = (prey(1)-pos(1));
  ydist = (prey(2)-pos(2));
  zdist = (prey(3)-pos(3));
  dist = sqrt(xdist^2 + ydist^2 + zdist^2);

  % check distance and increment counter if contact is made
  if dist<encounterdistance
   counter=counter+1;
  end

  if dist>r % predator outside of detection radius
   prob = [1/7 1/7 1/7 1/7 1/7 1/7 1/7];
   condition = 1;

  elseif dist<r & condition==1 % predator moving from outside to inside the
detection radius
   % find the direction the animal was heading in the i-1 time
   s = stepmat(i-1,:); % direction in previous second
   if s == [1 0 0]
    index=1;
   elseif s == [-1 0 0]
    index=2;
   elseif s == [0 1 0]
    index=3;
   elseif s == [0 -1 0]
    index=4;
   elseif s == [0 0 1]
    index=5;
   elseif s == [0 0 -1]
```

```
    index=6;
   else
    index=7;
   end

   %bias in favor of stepmat(i-1,:)
   prob(index) = (1/7)*biasm;
   prob(setdiff([1:7],index)) = (1-prob(index))/6;
   condition=2;

  else
   condition=2; % predator within detection distance of prey
  end

  %determine the next direction
  rn = rand;
  if rn < prob(1)
   step = [1 0 0];
  elseif rn>=sum(prob(1)) & rn <sum(prob(1:2))
   step = [-1 0 0];
  elseif rn>=sum(prob(1:2)) & rn <sum(prob(1:3))
   step = [0 1 0];
  elseif rn>=sum(prob(1:3)) & rn <sum(prob(1:4))
   step = [0 -1 0];
  elseif rn>=sum(prob(1:4)) & rn <sum(prob(1:5))
   step = [0 0 1];
  elseif rn>=sum(prob(1:5)) & rn <sum(prob(1:6))
   step = [0 0 -1];
  else
   step = [0 0 0];
  end

  % Generate the next position and add to the step matrix
  pos = pos +step;
  stepmat(i,:) = step;
 end

 % set the results vector for each iteration and write it to a file
 % This is overkill and time consuming, but it keeps the data intact if
 % the computer crashes in the middle of a large batch of iterations.
 results(n) = counter;
 writetextfile('brwalkloop',results);

end
```

Appendix B: Random walk Matlab code

INTRODUCTION

This code shares its function with the biased random walk code from Appendix A, except that the predator always behaves randomly. That is implemented by keeping the bins that represent the predator's possible motion the same size (see description in Appendix A). Again, I do not intend this behavior to have any fidelity to the way *Clione* actually hunts; it is a thought experiment designed to demonstrate the difficulty of visually detecting small biases in behavior.

CODE

```
close all
clear all

time = 3600; % number of seconds per iteration
iterations = 1; % number of times to run simulation
prey=[17.5 17.5 17.5]; % initial prey location
encounterdistance = 2.6; % one body length (cm)

for n=1:iterations
 counter=0; % counts number of encounters with prey
 pos=[0 0 0]; % initial predator location

 for i=2:time

  % calculate the distance between predator and prey
  xdist = (prey(1)-pos(1));
  ydist = (prey(2)-pos(2));
  zdist = (prey(3)-pos(3));
  dist = sqrt(xdist^2 + ydist^2 + zdist^2);

  % check distance and increment counter if contact is made
  if dist<encounterdistance
   counter=counter+1;
```

```
  end

  % generate the random direction
  rn = rand;
  if rn < (1/7)
    step = [1 0 0];
  elseif rn>=(1/7) & rn <(2/7)
    step = [-1 0 0];
  elseif rn>=(2/7) & rn <(3/7)
    step = [0 1 0];
  elseif rn>=(3/7) & rn <(4/7)
    step = [0 -1 0];
  elseif rn>=(4/7) & rn <(5/7)
    step = [0 0 1];
  elseif rn>=(5/7) & rn <(6/7)
    step = [0 0 -1];
  else
    step = [0 0 0];
  end

  %generate the new position
  pos = pos +step;

 end

 % set the results vector for each iteration and write it to a file
 % This is overkill and time consuming, but it keeps the data intact if
 % the computer crashes in the middle of a large batch of iterations.
 results(n) = counter;
 writetextfile('rwalkloop',results);

end
```

Appendix C: Methods validation: gait lab boundary types

INTRODUCTION

In designing laboratory experiments whose results are used to predict how prosthetic components will function under daily living conditions, researchers must design the experiments so that the subjects behave in the lab as they would anywhere else. The easy method to direct subjects in a gait lab trial is to mark either the path itself or its boundaries on the floor with tape. This may influence the findings, however, because the subject must look at the floor to navigate the path. Taped paths also omit important features of real objects. Because the upper body is wider than stance width, a taped path allows subjects to push parts of their upper body through space where the wall would be without crossing the tape boundary with their feet. More realistic behavior can be provoked in the laboratory by forcing the subjects to keep their upper bodies on the correct side of the wall boundary.

This study measures how experimental subjects alter their paths around a 90° corner, depending on whether or not walls are present, and whether the walls are transparent or opaque. Of course, the closest approximation to natural behavior is to build an actual hallway corner in the lab. Unfortunately, opaque walls reduce the area visible to any one camera. Because accurate kinematic data collection requires as many overlapping camera views as possible, opaque walls are problematic. This study is designed to explore the tradeoffs between more or less realistic hallway boundaries.

MATERIALS AND METHODS

To test different wall types, a hallway corner frame was constructed from 1" diameter copper pipe (fig.1). The frames were positioned to create an ADA compliant 42" wide, 90° hallway corner. Each wall section was 8' tall by 10' long. Plastic gardening mesh (1/2" square) was stretched onto the frame. The mesh gives a visual cue to the subjects but doesn't block the camera views. Three wall types were tested: black tape marking the boundary on the floor, wall frames with mesh, and wall frames with white sheets covering the entire inside wall and 4' of the outside wall (fig.2). Covering outside wall and maintaining sufficient camera overlap to capture the markers in a large enough data acquisition volume was impossible. With the outside wall completely opaque, the cameras had to be mounted very close to the wall. Doing so narrowed the view angles enough that only a very small volume in the center of the corner was visible to all cameras.

Ten non-amputee subjects, free from musculoskeletal and neurological problems by self-report, participated in this study. All subjects gave their informed consent to participate in this UW institutional review board approved protocol. During data collection, subjects wore a headband with four reflective markers. The markers were arranged asymmetrically so that every video frame would indicate subject orientation. Prior to collecting data, the subjects walked back and forth though the hallway to adjust to the task. Subjects were instructed to maintain a comfortable pace, walk through the corner as naturally as possible, and to register any touches to the wall (in which case the trial was re-run). Each subject walked around each wall type 16 times, four each: turning

right, leading with the left foot; turning right, leading with the right foot; turning left, leading with the left foot; and turning left, leading with the right foot. For each trial, subjects started with their toes on a line on the floor 2 meters away from the end of the hallway. A staff member gave the cue for the subject to start when ready and with which foot to lead. Data were not collected during the first and last 2-3 steps to avoid recording transient gait behavior.

Data were collected and organized with off-the-shelf-software and hardware, and analyzed with custom Matlab code on a PC. A ten-camera Vicon 612 system recorded the three-dimensional coordinates of the markers at 120 Hz. The 3D position data for each marker was collected with Vicon Workstation software (Vicon, Oxford Metrics, Oxford, UK). Subsequent analysis was done with custom Code written in Matlab and statistical analysis was done with StatView. The Matlab analysis algorithm is: 1) replace a single occluded marker in any frame by minimizing the error in the sum distances between the occluded marker and the other three markers, 2) find the centroid of the four markers and save the locations in time to a text file, and 3) measure the distance between the inside corner and the path of the head centroid, as the subject crosses the line between the corner vertices (see fig. 3). The difference between direction, starting foot, and wall type were assessed with a repeated measures ANOVA and a Tukey/Kramer post-hoc test.

RESULTS

The experimental design allowed for testing variability in the data with respect to turn direction, starting foot and wall type. Of the three factors, the only one that caused a

significant difference was wall type. Both the opaque and transparent walls caused the subjects to keep the same distance to the inside corner, and the tape allowed the subjects to cut further inward by approximately 10cm (fig. C.3).

DISCUSSION

Replicating real world conditions in the laboratory is an exercise in establishing where returns-per-effort start to diminish. In this case, using completely opaque walls would have required additional cameras and very time-intensive setup. The time expense is multiplied by the need to repeatedly return the lab to the original setup for other concurrent experiments. Fortunately, the data did not point us in that direction and a relatively low effort solution proved satisfactory. Keeping the walls transparent to the cameras while visible to the subjects was relatively easy. It required no camera movement, and only several minutes to move the walls into place prior to testing.

The easy method of using tape to mark a boundary on the floor proved flawed in this design. At the center of the turn, the tape boundary allowed subjects to come closer to the inside corner. This changes the subjects' trajectory, as well as their gait kinematics and kinetics. Tape on the floor does not create an adequate boundary to force subjects to walk around a corner as they would in the real world. Tape boundaries may suffice for straight trajectories, provided it could be shown that looking down for the pathway didn't influence gait.

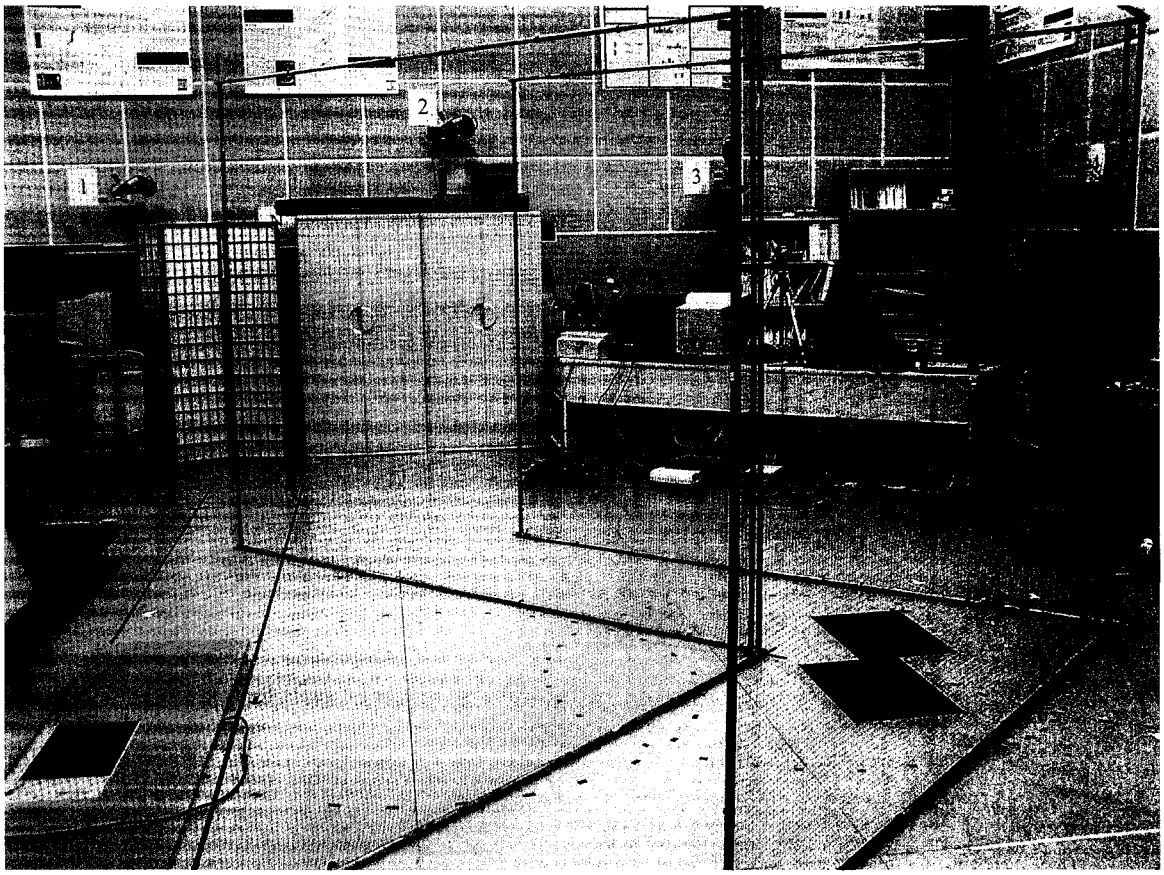

Figure C.1. Hallway corner frame. The mesh is in place, but nearly invisible. Four of the ten cameras used can be seen mounted to the walls in the background. While the forceplates in the center of the corner were on, subjects were told neither to aim for them nor avoid them.

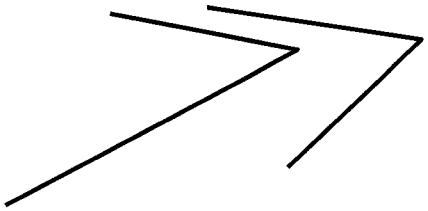

Treatment 1: Tape on Floor

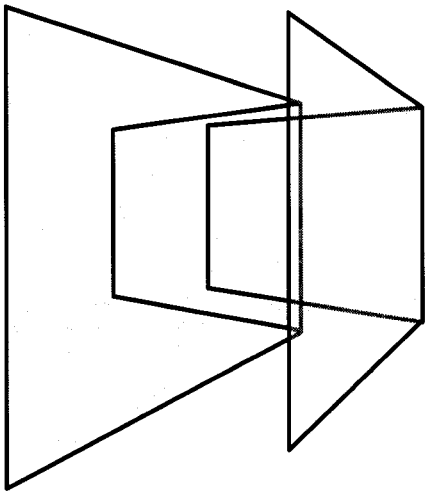

Treatment 2: Transparent Walls

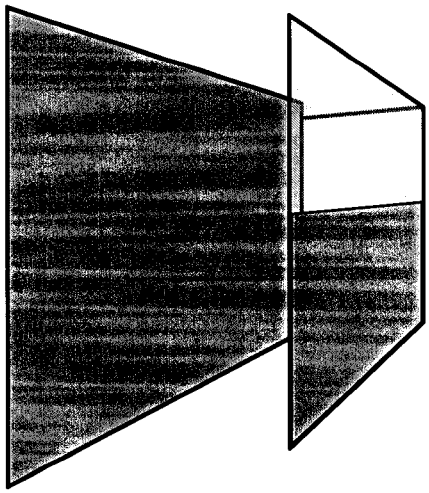

Treatment 3: Opaque Walls

Figure C.2. Wall types.

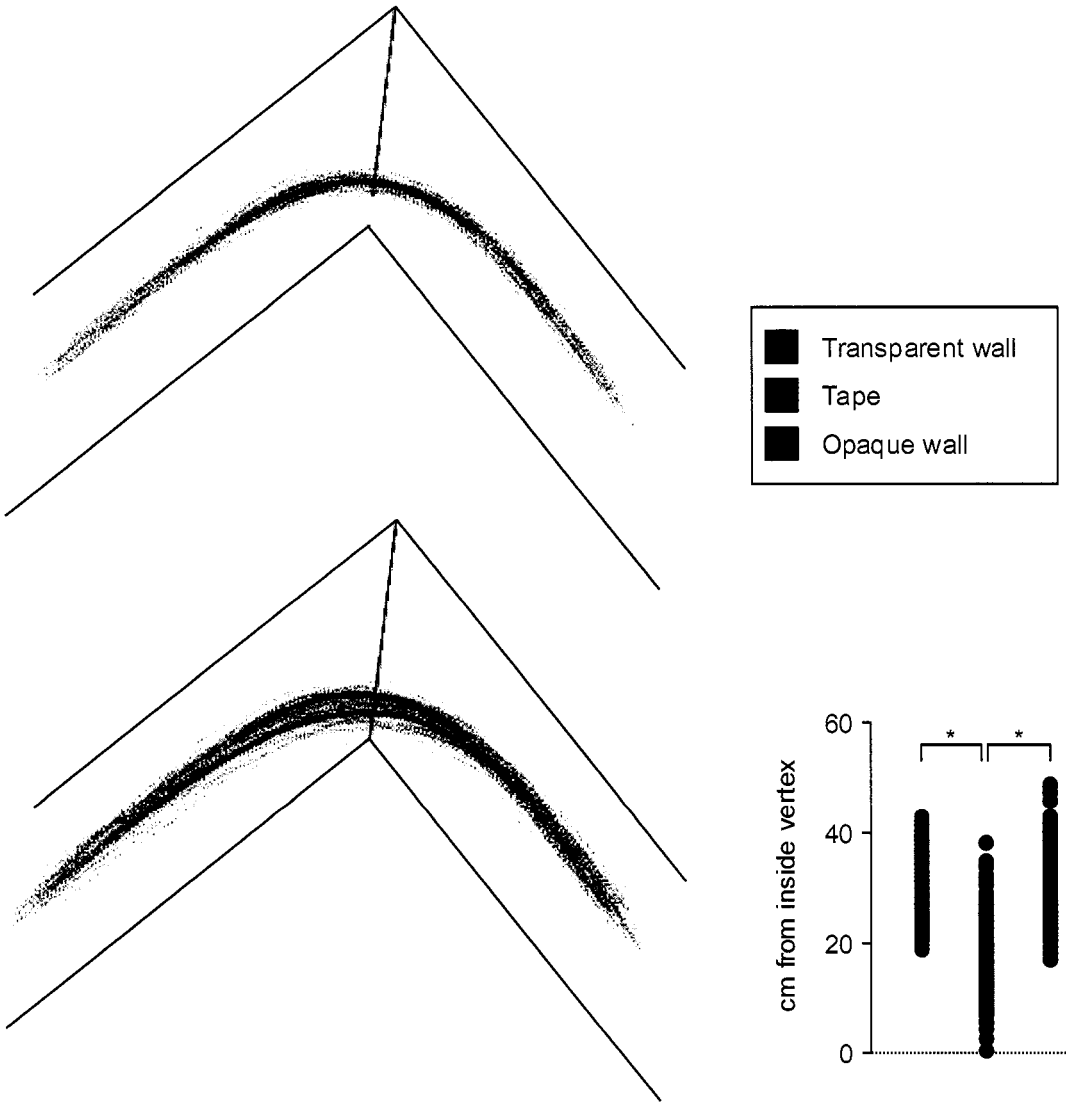

Figure C.3. Walking paths vs. wall type. The two left-most diagrams show the hallway corner (to scale) and the 160 paths taken by ten subjects. For clarity, only left turns are shown. The mean path (wherever all subjects had data) are shown in solid lines and the individual trials are dashed lines. The scatter plot in the lower right shows the distance from the inside corner along the line connecting the vertices for each trial (as represented by the yellow line in the upper diagram). For the scatter plot, the left and right turns are shown together, since there was no difference between them.

Appendix D: Automated gait event detection

INTRODUCTION

The timings of heel strike (HS) and toe off (TO) are important indices for many common measurements taken in gait labs. Variables are measured at these times, and variables are plotted over normalized time from stride to stride.

Many methods exist for establishing the timing of heel strike and toe off. There are foot switches in the shoe, force plates, kinematic methods, and hand rating events from video, kinetic, or kinematic data. Each method has benefits and drawbacks. Foot switches are excellent timing devices, but cannot be used in all situations due to wiring and shoe types. Force plates are very accurate, but can only be used for the steps that hit the plate itself (most gait experiments use only one or two force plates). Kinematic methods are slightly less accurate, but easier to automate, and hand-determined timing depends on the skill of the individual and is very time consuming.

Several authors have developed different methods to determine HS and TO. In each case, forceplate data are the gold-standard for comparison. Using (then new) video de-interlacing(Wall and Crosbie 1996), no difference was found between hand-rated video and forceplate data, but it was also shown that footswitches underestimated stance time. Mickelborough and van der Linden et al. (2000) found that between 88 and 98% hand rated gait events from foot marker velocity data were within 30 ms of forceplate data (Mickelborough, van der Linden et al. 2000). A study using horses showed that the mode velocity of one marker on the hoof could be used to indicate stance phase (Peham, Scheidl et al. 1999). This method, on average, was within 10.8 ms stance duration

determined with forceplate data. Excellent agreement with forceplate data (4.7 ms for HS and 5.6 ms for TO) were found with an automated, kinematic-data-only algorithm (Hreljac and Marshall 2000), but this method relies on the third derivative of position data for foot markers, and analyzed a small sample set of three subjects performing four steps each. Differences of 8 ms for HS and 16 ms for TO (Hansen, Childress et al. 2002) were found with a combination of kinematic data and a pressure mat vs. forceplate data. Lastly, a recently developed simple automated model (Ghoussayni, Stevens et al. 2004) yielded a 16.7 ms difference in HS and a 100 ms difference for TO.

Until now, no automated method that relied solely on kinematic data has been validated with amputee subjects. In this study, I will present a new automated, kinematics only method and give data on its fidelity to an established gait analysis method.

Materials and Methods

Data from twenty subjects (10 non-amputee, 5 left below knee amputees (BKs), and 5 right BKs) were extracted from previous studies. Each subject was free from musculoskeletal and neurological problems by self-report. All subjects gave their informed consent to participate in one of our UW institutional review board approved protocols. In each case, thirty-six reflective markers were placed on the subject according to the Plug In Gait model (Vicon, Oxford Metrics, Oxford, UK). A ten-camera Vicon 612 system recorded the three-dimensional coordinates of the markers at 120 Hz. A force plate or plates mounted flush with the laboratory floor recorded the kinetic data.

Each subject walked in a straight line across the force plates. Two trials were analyzed for each subject, giving a total of 40 trials.

Due to its ubiquity in gait labs, Vicon's Workstation software was used to establish HS and TO timings for a standard of comparison. This system establishes the vertical position of the foot markers at the start of contact (force >10N) with the force plate (HS) and the end of contact (force<10N) with the force plate (TO). The software then scans the kinematic data collected and assigns HS and TO events to the rest of the trial (fig. D.1). All of these records require a hand check for errors. If there are errors, they are fixed either by adjusting parameters and re-running the analysis, or by assigning HS and TO timings by hand via the animation of the recorded kinematics.

The novel automated algorithm (FootFlick) determines HS and TO timings by features of the ankle joint center (AJC) vertical velocity. A trough in the AJC vertical velocity aligns with HS and the subsequent peak aligns with TO (fig. D.2). FootFlick performs the following steps in establishing HS and TO timings (see code section):

1) A ten-point averaging filter is applied to the three dimensional path of the left and right AJCs. The filter runs forward and backward to eliminate any phase change.
2) The AJC vertical velocity is calculated in discrete time steps at the sampling frequency (120Hz).
3) The inflection points (slope = 0) in the AJC velocity trace are found using Tom McMurray's (mcmurray@teamcmi.com) function, "peakdetect.m."

4) TO events are defined as positive peaks within 30% of the height of the highest positive peak, to eliminate regions of noisy data.

5) HS events are defined as negative peaks that occur within a region around the average of all negative peaks that occur between –48 cm/s and 12 cm/s. The region is defined as a percentage of range of peak values above and below the mean.

6) HS and toe off events within the first or last 5 frames of data collection are discarded since this is an error prone region for Vicon.

7) The HJC velocity time series is plotted, with indicators for the HS and TO timings established (fig D.3).

8) A user scans the plots and corrects those with missing or incorrect data.

RESULTS

In no case was the absolute value of the difference between FootFlick and Vicon greater than 8 frames, or 66.7 milliseconds. The true average differences (not the absolute differences) were less than the absolute average differences, but there was no constant trend that could be used to rectify the data. Hereafter, the differences all refer to absolute differences. The mean differences varied from 15 to 27 milliseconds. Because the average time from one heel strike to the following heel strike on the same side for the control subjects is 127 frames (1.06seconds), the mean differences represent 1.4% to 2.5% of the approximate stride time. FootFlick missed or erroneously identified 0/374 TOs identified by Vicon. FootFlick missed or erroneously identified 45/271 (16%)

amputee HSs identified by Vicon and 6/108 (5.6%) non-amputee HSs identified by Vicon. Taking the HSs and TOs together, the overall error rate (either missed, erroneously identified or extraneously added data) was 51 events per 753 (6.8%). These 51 events took 30 minutes to correct.

DISCUSSION

FootFlick's fidelity to Vicon's data is comparable to or better than other kinematic only methods of HS and TO detection. Unfortunately, none of these studies compared their results to Vicon data. Nonetheless, each study uses a well-validated method to generate comparison data.

While the error rate for detecting HSs was much higher than that for detecting TOs, the mean differences for TOs were lower and the histograms show a more accurate distribution. The TO peaks were easy to automatically identify because they were higher than any other peaks (fig D.2). The HS troughs, however, were more problematic since they were in the same range as the noisiest part of the data. Nonetheless, once identified, the average HS differences were smaller. Another contributing factor to this is the difficulty of accurately establishing TO in Vicon. Because our Vicon model does not include a marker at the tip of the toe, where the foot leaves contact with the ground, the other markers only provide an approximation. Additionally, when Vicon's data must be hand corrected, the accuracy of the TO determination depends on the operator. Even experienced gait lab technicians have difficulty clearly defining the "by hand" method of TO detection.

FootFlick provides an easy way to correct erroneous data. The AJC velocity data are plotted for each trial with symbols superimposed on the graph for HSs and TOs. After analyzing all of the data, an operator need only look at the plots and close all of the plot windows in which no errors occurred. Once I was accustomed to the task, this process took only several seconds per plot. For the remaining trials, the Matlab zoom feature can be used to quickly identify the location of an inaccurately identified HS or TO. A companion function can be written to identify the row of data in which the error occurred, and the data can be corrected by manually entering the new value in Matlab's array editor. Manually entering corrected data takes approximately the same time as hand correcting Vicon data. Because the data are stored in rows by trial, experimental protocol and subject, the row corresponding to a particular trial will depend on the experimental design. The row finding companion function (rowfind.m) for the data used in this experiment is included in the code section.

CODE

footfalls.m

```
% footfalls.m
% This file takes exported data from Vicon on the z position of the feet markers and determines the
% timings of heel strikes and toe offs
%
% bug free 2/31/05  KCF

close all
clear all

cd('C:\Documents and Settings\Kevin Flick\My Documents\Documents\VA\turning project\hallway2 text files')
```

```
% Vectors of filename components
subj = ['S1';'S2';'S3';'S4';'S5';'S6';'S7';'S8';'S9';'S10';'S11'];
dir = ['Left' 'Right'];
foot = dir;

% turn plotting on and off (plotter = 1 is on)
plotter = 1;

% define filter
points = 10;
filtvector = ones(1,points)/points;  % n point averaging filter

% Threshhold parameter for positive peaks
posfactor = .7;

% threshhold parameters for negative peaks
lowfactor = -1;
highfactor = .05;

% Initialize data matrix for saving
footmat = [];

% Increment the filenames and read them in one at a time
for s=[1 2 3 4 5 6 7 8 10 11]
 for d = 1:2
  for f = 1:2
   for tr = [1 2 3 5]

    % read in the file
    file = [subj(s,:) ' ' dir(4*d-3:5*d-1) ' ' foot(4*f-3:5*f-1) ' Foot 0' num2str(tr) '.txt']
    a = dlmread (file,'\t',9, 0);

    % Vicon does not export all the data.  It only exports from the frame when one
of the exported
    % markers first appears
    startrow = a(1,1);
    if startrow~=1
     a = [zeros(startrow-1,length(a(1,:)));a];
    end

    % identify the correct components
    left = a(:,29);
    right = a(:,26);
```

```
        [rleft,cleft] = size(left);
        [rright,cright] = size(right);

        % find index to first non-zero elements
        leftnums = find(left ~= 0);
        rightnums = find(right ~= 0);
        leftfirstnum = leftnums(1);
        rightfirstnum = rightnums(1);
        leftlastnum = leftnums(end);
        rightlastnum = rightnums(end);

        % filter (only on non-zero elements so the averaging filter doesn't
        % smear out the ends with zeros)
        left(leftfirstnum:leftlastnum) = filtfilt(filtvector,1,left(leftfirstnum:leftlastnum));
        right(rightfirstnum:rightlastnum) =
filtfilt(filtvector,1,right(rightfirstnum:rightlastnum));

        % replace zeros with NaNs to make velocity calculations easier
        left(1:leftfirstnum-1)=NaN; left(leftlastnum+1:end) = NaN;
        right(1:rightfirstnum-1)=NaN; right(rightlastnum+1:end) = NaN;

        %
================================================================ %
        % ============== process the left footstrikes ============== %
        %
================================================================ %

        % calculate the velocity (cv)
        leftv = [];
        for n = 1:length(left) - 1
          leftv(n,:) = left(n+1,:) - left(n,:);
        end
        leftv = [NaN; leftv];

        % recreate numerical data for peakdetect function
        leftv(isnan(leftv))=0;

        % call function peakdetect to find the peaks in the velocity data
        [pospeakind,negpeakind]=peakdetect(leftv);

        % find peak indices over threshhold for positive peaks
        threshhold = posfactor * max(leftv);
        threshpeakfinder = find(leftv(pospeakind)>threshhold);
        threshpeaks = pospeakind(threshpeakfinder);
```

```
        % Eliminate the first and last peaks identified if they fall within
        % a defined margin (measured in frames)
        margin = 10;
        if threshpeaks(1) <= leftfirstnum + margin;
          threshpeaks = threshpeaks(2:end);
        end
        if threshpeaks(end) >= leftlastnum - margin;
          threshpeaks = threshpeaks(1:end-1);
        end

        % find peak indices over threshhold for negative peaks
        middlepeaks = leftv(negpeakind(find(leftv(negpeakind) > -4 &
leftv(negpeakind) < 2)));
        mprange = max(middlepeaks)-min(middlepeaks);
        high = mean(middlepeaks) + highfactor * mprange;
        low = mean(middlepeaks) + lowfactor * mprange;
        threshpeakfinderneg = find(leftv(negpeakind) > low & leftv(negpeakind) <
high);
        threshpeaksneg = negpeakind(threshpeakfinderneg);

        % Eliminate the first and last peaks identified if they fall within
        % a defined margin (measured in frames)
        margin = 5;
        if threshpeaksneg(1) <= leftfirstnum + margin
          threshpeaksneg = threshpeaksneg(2:end);
        end
        if threshpeaksneg(end) >= leftlastnum - margin
          threshpeaksneg = threshpeaksneg(1:end-1);
        end

        if plotter==1
          % Plot the raw data
          figure
          set (gcf, 'numbertitle','off','name', [file ' (left events)'])
          plot(leftv,'b'); hold on; %plot(left,'k')
          % Plot the threshhold lines
          plot (zeros(size(leftv)) + low,'g');
          plot (zeros(size(leftv)) + high);
          % Plot the identified peaks

plot(threshpeaks,leftv(threshpeaks),'r^',threshpeaksneg,leftv(threshpeaksneg),'ro')
          drawnow
        end
```

```
% pad the peak vectors with NaN for matrix construction
threshpeaks(end+1:10) = NaN;
threshpeaksneg(end+1:10) = NaN;

% Insure that they are row vectors
if size(threshpeaks,1) == 10
  threshpeaks = threshpeaks';
end
if size(threshpeaksneg,1) == 10
  threshpeaksneg = threshpeaksneg';
end

% append data to the matrix
footmat = [footmat;threshpeaks;threshpeaksneg];

% ================================================== %
% ============== process the right footstrikes ============== %
% ================================================== %

% calculate the velocity (cv)
rightv = [];
for n = 1:length(right) - 1
  rightv(n,:) = right(n+1,:) - right(n,:);
end

% recreate numerical data for peakdetect function
rightv(isnan(rightv))=0;

% call function peakdetect to find the peaks in the velocity data
[pospeakind,negpeakind]=peakdetect(rightv);

% find peak indices over threshhold for positive peaks
threshhold = posfactor * max(rightv);
threshpeakfinder = find(rightv(pospeakind)>threshhold);
threshpeaks = pospeakind(threshpeakfinder);

% Eliminate the first and last peaks identified if they fall within
% a defined margin (measured in frames)
margin = 10;
if threshpeaks(1) <= rightfirstnum + margin;
  threshpeaks = threshpeaks(2:end);
end
if threshpeaks(end) >= rightlastnum - margin;
```

```
        threshpeaks = threshpeaks(1:end-1);
      end

      % find peak indices over threshhold for negative peaks

   middlepeaks = rightv(negpeakind(find(rightv(negpeakind) > -4 & rightv(negpeakind)
< 2)));
      mprange = max(middlepeaks)-min(middlepeaks);
      high = mean(middlepeaks) + highfactor * mprange;
      low = mean(middlepeaks) + lowfactor * mprange;
      threshpeakfinderneg = find(rightv(negpeakind) > low & rightv(negpeakind) <
high);
      threshpeaksneg = negpeakind(threshpeakfinderneg);

      % Eliminate the first and last peaks identified if they fall within
      % a defined margin (measured in frames)
      margin = 5;
      if threshpeaksneg(1) <= rightfirstnum + margin
        threshpeaksneg = threshpeaksneg(2:end);
      end
      if threshpeaksneg(end) >= rightlastnum - margin
        threshpeaksneg = threshpeaksneg(1:end-1);
      end

      if plotter ==1
        % Plot the raw data
        figure
        set (gcf, 'numbertitle','off','name', [file ' (right events)'])
        plot(rightv,'b'); hold on; %plot(right,'k')
        % Plot the threshhold lines
        plot (zeros(size(rightv)) + low,'g');
        plot (zeros(size(rightv)) + high);
        % Plot the identified peaks

plot(threshpeaks,rightv(threshpeaks),'r^',threshpeaksneg,rightv(threshpeaksneg),'ro')
        drawnow
      end

      % pad the peak vectors with NaN for matrix construction
      threshpeaks(end+1:10) = NaN;
      threshpeaksneg(end+1:10) = NaN;

      % Insure that they are row vectors
      if size(threshpeaks,1) == 10
```

```
        threshpeaks = threshpeaks';
      end
      if size(threshpeaksneg,1) == 10
        threshpeaksneg = threshpeaksneg';
      end

      % append data to the matrix
      footmat = [footmat;threshpeaks;threshpeaksneg];
    end
  end
 end
end

% the variable name "FootMats" doesn't exist.  This is to safeguard against
% saving new data over already processed data.
% cd('C:\Documents and Settings\Kevin Flick\My
Documents\Documents\VA\turning project\Event Data')
% save('footfalls','FootMats')
% save('footfalls ','FootMats','-ASCII', '-TABS')
```

peakdetect.m

```
function [pospeakind,negpeakind]=peakdetect(signal)

%     PEAKDETECT peak detection
%
%     [pospeakind,negpeakind]=peakdetect(signal)
%
%     The positive and negative polarity (concave down and up) peak index vectors
are
%     generated from the signal vector and graphically displayed.  Positive and
negative
%     polarity peaks occur at points of positive to negative and negative to positive
%     slope adjacency, respectively.  The typically rare contingencies of peaks
%     occurring at the lagging edges of constant intervals are supported.  Complex
%     signals are modified to the modulus of the elements.  If unspecified, the signal
%     vector is entered after the prompt from the keyboard.

%     Implemented using MATLAB 6.0.0
%
%     Examples:
%
%     È [p,n]=peakdetect([-1 -1 0 1 0 1 0 -1 -1])
%
```

```
%     p =
%
%        4    6
%
%     n =
%
%        1    5    8
%
%     È [p,n]=peakdetect(cos(2*pi*(0:999999)/500000))
%
%     p =
%
%              1      500001     1000000
%
%     n =
%
%          250001      750001
%
%     Copyright (c) 2001
%     Tom McMurray
%     mcmurray@teamcmi.com

%     if signal is not input, enter signal or return for empty outputs

if ~nargin
  signal=input('enter signal vector or return for empty outputs\n');
  if isempty(signal)
    pospeakind=[];
    negpeakind=[];
    return
  end
end
sizsig=size(signal);

%     while signal is unsupported, enter supported signal or return for empty outputs

while isempty(signal)|~isnumeric(signal)|~all(all(isfinite(signal)))...
    |length(sizsig)>2|min(sizsig)~=1
  signal=input(['signal is empty, nonnumeric, nonfinite, or nonvector:\nenter '...
      'finite vector or return for empty outputs\n']);
  if isempty(signal)
    pospeakind=[];
    negpeakind=[];
    return
```

```
  end
  sizsig=size(signal);
end

%     if signal is complex, modify to modulus of the elements

if ~isreal(signal)
  signal=abs(signal);
end

%     if signal is constant, return empty outputs

if ~any(signal-signal(1))
  pospeakind=[];
  negpeakind=[];
  disp('constant signal graph suppressed')
  return
end
sizsig1=sizsig(1);
lensig=sizsig1;

%     if signal is a row vector, modify to a column vector

if lensig==1
  signal=signal(:);
  lensig=sizsig(2);
end
lensig1=lensig-1;
lensig2=lensig1-1;

%     if signal length is 2, return max/min as positive/negative polarity peaks

if ~lensig2
  [sig,pospeakind]=max(signal);
  [sig,negpeakind]=min(signal);
  disp('2 element signal graph suppressed')
  return
end

%     generate difference signal

difsig=diff(signal);

%     generate vectors corresponding to positive slope indices
```

```
dsgt0=difsig>0;
dsgt00=dsgt0(1:lensig2);
dsgt01=dsgt0(2:lensig1);

%       generate vectors corresponding to negative slope indices

dslt0=difsig<0;
dslt00=dslt0(1:lensig2);
dslt01=dslt0(2:lensig1);

%       generate vectors corresponding to constant intervals

dseq0=difsig==0;
dseq01=dseq0(2:lensig1);
clear difsig

%       positive to negative slope adjacencies define positive polarity peaks

pospeakind=find(dsgt00&dslt01)+1;

%       negative to positive slope adjacencies define negative polarity peaks

negpeakind=find(dsgt01&dslt00)+1;

%       positive slope to constant interval adjacencies initiate positive polarity peaks

peakind=find(dsgt00&dseq01)+1;
lenpeakind=length(peakind);

%       determine positive polarity peak terminations

for k=1:lenpeakind
  peakindk=peakind(k);
  l=peakindk+1;

%       if end constant interval occurs, positive polarity peak exists

  if l==lensig
    pospeakind=[pospeakind;peakindk];

%       else l<lensig, determine next nonzero slope index

  else
```

```
    dseq0l=dseq0(l);
    while dseq0l&l<lensig1
      l=l+1;
      dseq0l=dseq0(l);
    end

%     if negative slope or end constant interval occurs, positive polarity peaks exist

    if dslt0(l)|dseq0l;
      pospeakind=[pospeakind;peakindk];
    end
  end
end

%     negative slope to constant interval adjacencies initiate negative polarity peaks

peakind=find(dslt00&dseq01)+1;
lenpeakind=length(peakind);
clear dseq01

%     determine negative polarity peak terminations

for k=1:lenpeakind
  peakindk=peakind(k);
  l=peakindk+1;

%     if end constant interval occurs, negative polarity peak exists

  if l==lensig
    negpeakind=[negpeakind;peakindk];

%     else l<lensig, determine next nonzero slope index

  else
    dseq0l=dseq0(l);
    while dseq0l&l<lensig1
      l=l+1;
      dseq0l=dseq0(l);
    end

%     if positive slope or end constant interval occurs, negative polarity peaks exist

    if dsgt0(l)|dseq0l;
      negpeakind=[negpeakind;peakindk];
```

```
    end
  end
end
clear dsgt0 peakind

%     if initial negative slope occurs, initial positive polarity peak exists

if dslt00(1)
  pospeakind=[1;pospeakind];

%     elseif initial positive slope occurs, initial negative polarity peak exists

elseif dsgt00(1)
  negpeakind=[1;negpeakind];

%     else initial constant interval occurs, determine next nonzero slope index

else
  k=2;
  dseq0k=dseq0(2);
  while dseq0k
    k=k+1;
    dseq0k=dseq0(k);
  end

%     if negative slope occurs, initial positive polarity peak exists

  if dslt0(k)
    pospeakind=[1;pospeakind];

%     else positive slope occurs, initial negative polarity peak exists

  else
    negpeakind=[1;negpeakind];
  end
end
clear dsgt00 dslt0 dslt00 dseq0

%     if final positive slope occurs, final positive polarity peak exists

if dsgt01(lensig2)
  pospeakind=[pospeakind;lensig];

%     elseif final negative slope occurs, final negative polarity peak exists
```

```
elseif dslt01(lensig2)
  negpeakind=[negpeakind;lensig];
end
clear dsgt01 dslt01

%      if peak indices are not ascending, order peak indices

if any(diff(pospeakind)<0)
  pospeakind=sort(pospeakind);
end
if any(diff(negpeakind)<0)
  negpeakind=sort(negpeakind);
end

%      if signal is a row vector, modify peak indices to row vectors

if sizsig1==1
  pospeakind=pospeakind.';
  negpeakind=negpeakind.';
end

%      plot signal peaks

% plot(0:lensig1,signal,pospeakind-1,signal(pospeakind),'b^',negpeakind-1,...
%    signal(negpeakind),'bv')
% xlabel('Sample')
% ylabel('Signal')
% grid
```

rowfind.m

```
% This file finds the correct row number in the footmat data file for any
% trial

s = 1;
d = 2;
f = 2;
tr = 2;

% translate trials [1 2 3 5] to [1 2 3 4]
trials = [1 2 3 NaN 4];
t = trials(tr);
```

```
% pull desired event data
lto = (s-1)*64 + (d-1)*32 + (f-1)*16 + (t-1)*4 + 1
lhs = (s-1)*64 + (d-1)*32 + (f-1)*16 + (t-1)*4 + 2
rto = (s-1)*64 + (d-1)*32 + (f-1)*16 + (t-1)*4 + 3
rhs = (s-1)*64 + (d-1)*32 + (f-1)*16 + (t-1)*4 + 4
```

NOTES TO APPENDIX D

Ghoussayni, S., C. Stevens, et al. (2004). "Assessment and validation of a simple automated method for the detection of gait events and intervals." Gait & Posture **20**: 266-272.

Hansen, A. H., D. S. Childress, et al. (2002). "A simple method for determination of gait events." Journal of Biomechanics **35**: 135-138.

Hreljac, A. and R. N. Marshall (2000). "Algorithms to determine event timing during normal walking using kinematic data." Journal of BIomechanics **33**: 783-786.

Mickelborough, J., M. L. van der Linden, et al. (2000). "Validity and reliability of a kinematic protocol for determining foot contact events." Gait & Posture **11**: 32-37.

Peham, C., M. Scheidl, et al. (1999). "Limb locomotion - speed distribution analysis as a new method for stance phase detection." Journal of Biomechanics **32**: 1119-1124.

Wall, J. C. and J. Crosbie (1996). "Accuracy and reliability of temporal gait measurement." Gait & Posture **4**: 293-296.

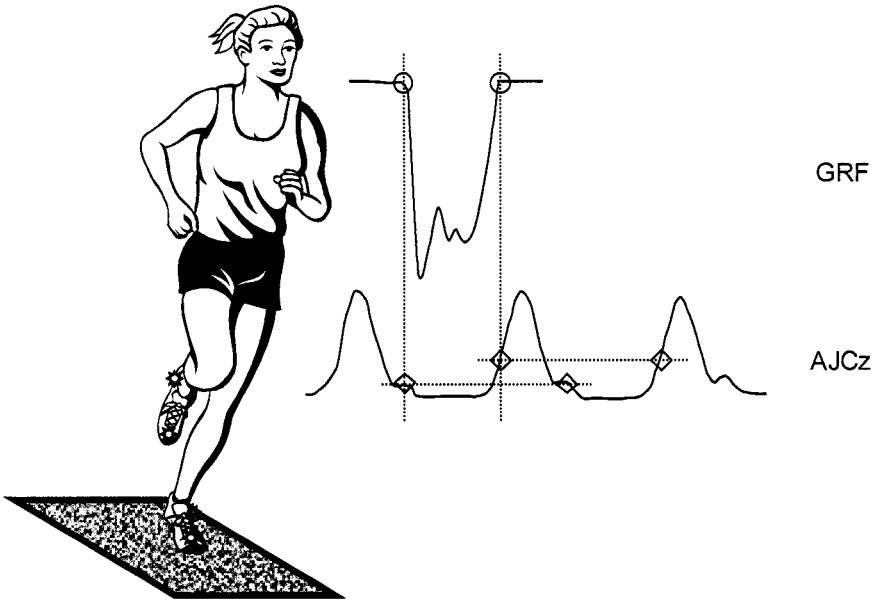

Figure D.1. Vicon gait events. The cartoon shows a subject with lateral heel markers and toe markers stepping on a force plate. The Vicon software package determines the moments of HS and TO (red circles) for one step by ground reaction force (GRF) applied to the forceplate during one step. It then finds the vertical position of the foot at those moments in time (AJCz) and matches foot position on all other steps to extrapolate HS and TO (red diamonds).

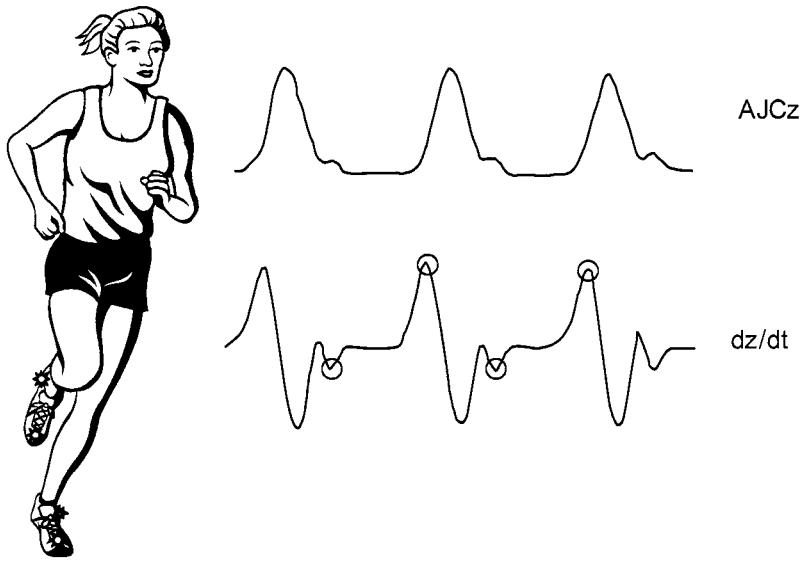

Figure D.2. FootFlick HS and TO determination. The cartoon shows a subject with lateral heel markers and toe markers. FootFlick computes the velocity of the ankle joint center in the vertical axis (AJCz) from kinematic data, then determines HS and TO timings directly from the peaks and troughs in the velocity data for the AJC (dz/dt).

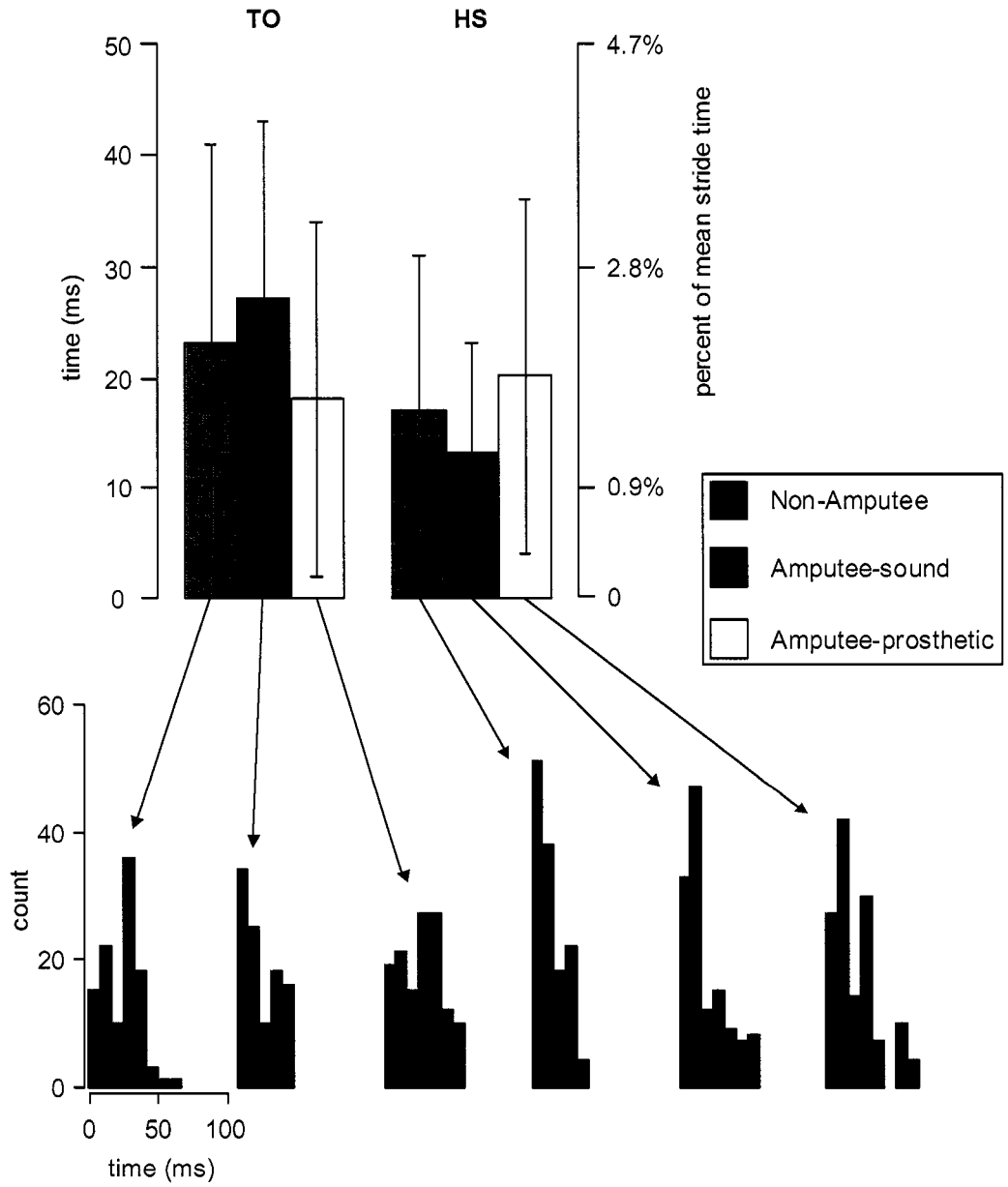

Figure D.3. FootFlick vs. Vicon. The upper bar graph shows the average of all the differences between Vicon and FootFlick HS and TO timings (n = 106, 135, 133, 108, 134, and 137, from left to right). The percentage scale on the right is based on the mean stride time for control subjects. The lower plots are histograms for each case.

Appendix E: Finite element procedure file

INTRODUCTION

This procedure file runs on Marc/Mentat finite element software, version 2003.

CODE

```
|Version : MSC.Marc Mentat 2003 (32bit)

*new_material
*material_name socket
*material_type mechanical:isotropic
*material_value isotropic:youngs_modulus 1.4e11
*material_value isotropic:poissons_ratio .49
*material_value isotropic:mass_density .955e3

*new_material
*material_name liner
*material_type mechanical:isotropic
*material_value isotropic:youngs_modulus 6e8
*material_value isotropic:poissons_ratio .39
*material_value isotropic:mass_density .7e3

*new_material
*material_name skin
*material_type mechanical:isotropic
*material_value isotropic:youngs_modulus 9.7e6
*material_value isotropic:poissons_ratio .49
*material_value isotropic:mass_density 11e3
*material_value isotropic:mass_density 1e3

*new_material
*material_name fat
*material_type mechanical:isotropic
*material_value isotropic:youngs_modulus 9.7e6
*material_value isotropic:poissons_ratio .49
*material_value isotropic:mass_density .9e3

*new_material
*material_name muscle
*material_type mechanical:isotropic
```

```
*material_value isotropic:youngs_modulus 9.7e6
*material_value isotropic:poissons_ratio .49
*material_value isotropic:mass_density 1.06e3

*new_material
*material_name bone
*material_type mechanical:isotropic
*material_value isotropic:youngs_modulus 2.1e10
*material_value isotropic:poissons_ratio .49
*material_value isotropic:mass_density .4e3

*new_material
*material_name pylon
*material_type mechanical:isotropic
*material_value isotropic:youngs_modulus 2e11
*material_value isotropic:poissons_ratio .49
*material_value isotropic:mass_density .4e3

*new_material
*material_name elastomer
*material_type mechanical:isotropic
*material_value isotropic:youngs_modulus 2e11
*material_value isotropic:poissons_ratio .49
*material_value isotropic:mass_density 1000
*material_type damping
*material_value damping:stiffness_mult
.1

*new_md_table 1 1
*table_name
table_Fx_t
*set_md_table_type 1
time
*set_md_table_step_v 1
20
*set_md_table_max_v 1
1
*set_md_table_min_f 1
-200
*set_md_table_max_f 1
1100
*set_md_table_step_f 1
10
*table_add
```

```
0       0       0.05    39.253  0.1     143.85  0.15    204.29  0.2     208.57  0.25    201.01
        0.3     188.95  0.35    176.11  0.4     166.68  0.45    156.21  0.5     152.04  0.55
        155.29  0.6     167.05  0.65    185.15  0.7     205.31  0.75    217.74  0.8     206.06
        0.85    156.48  0.9     65.28   0.95    0.21362         1       0

*new_md_table 1 1
*table_name
table_Fy_t
*set_md_table_type 1
time
*set_md_table_step_v 1
20
*set_md_table_max_v 1
1
*set_md_table_min_f 1
-200
*set_md_table_max_f 1
1100
*set_md_table_step_f 1
10
*table_add
0       0       0.05    -18.18  0.1     -69.907         0.15    -103.71         0.2     -
86.466  0.25    -69.372         0.3     -53.141         0.35    -40.48  0.4     -27.493
        0.45    -10.7   0.5     3.9203  0.55    14.043  0.6     23.679  0.65    36.129  0.7
        52.549  0.75    75.96   0.8     95.707  0.85    99.341  0.9     59.985  0.95    -
2.5589  1       0

*new_md_table 1 1
*table_name
table_Fz_t
*set_md_table_type 1
time
*set_md_table_step_v 1
20
*set_md_table_max_v 1
1
*set_md_table_min_f 1
-200
*set_md_table_max_f 1
1100
*set_md_table_step_f 1
10
*table_add
```

```
0       0       0.05    303.14 0.1     702.06 0.15    988.3  0.2     986.76 0.25    965.01
        0.3     929.09 0.35    890.45 0.4     868.58 0.45    838.63 0.5     830.51 0.55
        845.47 0.6     884.62 0.65    927.95 0.7     949.37 0.75    942.55 0.8     846.66
        0.85    617.1  0.9     268.77 0.95    12.244 1       0

*new_md_table 1 1
*table_name
table_Mx_t
*set_md_table_type 1
time
*set_md_table_step_v 1
20
*set_md_table_max_v 1
1
*set_md_table_min_f 1
-200
*set_md_table_max_f 1
110
*set_md_table_step_f 1
10
*table_add
0       0       0.05    -32.661        0.1     -62.812        0.15    -72.782        0.2
        -60.98  0.25    -46.746        0.3     -35.221        0.35    -25.77  0.4    -
17.197 0.45     -8.2921        0.5     1.6436 0.55    14.478 0.6     30.151 0.65    46.972
        0.7     63.033 0.75    74.1    0.8     78.048 0.85    67.543 0.9     36.053 0.95
        2.2203 1        0

*new_md_table 1 1
*table_name
table_My_t
*set_md_table_type 1
time
*set_md_table_step_v 1
20
*set_md_table_max_v 1
1
*set_md_table_min_f 1
-200
*set_md_table_max_f 1
110
*set_md_table_step_f 1
10
*table_add
```

```
0       0       0.05    -34.976         0.1     -93.676         0.15    -136.48         0.2
        -139.96         0.25    -140.16         0.3     -136.73         0.35    -131.31
        0.4     -127.41         0.45    -122.75         0.5     -122.23         0.55    -
126.68 0.6      -136.4 0.65     -147.34         0.7     -154.75         0.75    -154.88
        0.8     -140.22         0.85    -102.13         0.9     -43.641         0.95    -
1.7741 1        0

*new_md_table 1 1
*table_name
table_Mz_t
*set_md_table_type 1
time
*set_md_table_step_v 1
20
*set_md_table_max_v 1
1
*set_md_table_min_f 1
-200
*set_md_table_max_f 1
110
*set_md_table_step_f 1
10
*table_add
0       0       0.05    -7.4055         0.1     -18.718         0.15    -24.805         0.2
        -20.626         0.25    -17.629         0.3     -14.544         0.35    -11.216
        0.4     -7.7354         0.45    -3.4074         0.5     0.78328         0.55    4.9558
        0.6     9.781   0.65    15.425 0.7      21.733 0.75     28.786 0.8      33.907 0.85
        32.507 0.9      18.463 0.95     0.050949        1       0


*new_apply
*apply_name
fixedbone
*apply_type fixed_displacement
*apply_dof x *apply_dof_value x
0 0 0 0 0 0

*new_apply
*apply_name
GRF_turning
*apply_type point_load
*apply_dof x *apply_dof_value x
-1 1 1 1 1 0
*apply_dof_table x
```

```
table_Fx_t
*apply_dof_table y
table_Fy_t
*apply_dof_table z
table_Fz_t
*apply_dof_table mx
table_Mx_t
*apply_dof_table my
table_My_t
*apply_dof_table mz
table_Mz_t

*color 240
*color 240 1 0 0
*color 218
*color 218 1 0 0
*color 219
*color 219 1 0.969 0.75
*color 217
*color 217 1 0.75 0
*color 220
*color 220 0 0 .5
*color 216
*color 216 0.952 0.539 0.316
*color 215
*color 215 0.794 0.803 1
*color 214
*color 214 0.57 0.57 0.57

*grid_u_domain -.1 .1
*grid_v_domain -.1 .1
*grid_u_spacing .01
*grid_v_spacing .01
*set_grid on
*identify_materials
*elements_solid

*set_curve_type circle_cr
*set_plot_curve_div_high
*add_curves
-2.000000000000e-002 -1.000000000000e-002  0.000000000000e+000 .006
1.000000000000e-002  3.000000000000e-002  0.000000000000e+000 .018
0.000000000000e+000  .004  0.000000000000e+000 .05
0.000000000000e+000  0.000000000000e+000  0.000000000000e+000 .058
```

```
0.000000000000e+000  0.000000000000e+000  0.000000000000e+000 .06
0.000000000000e+000  0.000000000000e+000  0.000000000000e+000 .065
0.000000000000e+000  0.000000000000e+000  0.000000000000e+000 .073
0 0 0 .02

*sweep_all
*remove_unused_nodes
*remove_unused_points
*renumber_all

*set_curve_div_type_fix_ndiv *set_curve_div_num
32
*apply_curve_divisions
3 4 5 6 7
all_selected

*set_curve_div_type_fix_ndiv *set_curve_div_num
16
*apply_curve_divisions
 2
 8
all_selected

*set_curve_div_type_fix_ndiv *set_curve_div_num
8
*apply_curve_divisions
 1
all_selected

*af_planar_quadmesh
 7
 6
all_selected

*af_planar_quadmesh
 6
 5
all_selected

*af_planar_quadmesh
4 5
all_selected

*af_planar_quadmesh
```

```
 4
 3
all_selected

*remove_unused_nodes
*remove_unused_points
*sweep_all
*intersect_curves
all_existing
*clean_2d_loops
all_existing
*set_curve_div_type_fix_avgl
*set_curve_div_type_fix_avgl *set_curve_div_avgl
.01
*set_curve_div_rest_evn
*apply_curve_divisions
 9 11 12 23
 15 17 19 21 24
 13 16
all_selected

*set_curve_div_type_fix_ndiv
*set_curve_div_num
6
*apply_curve_divisions
11
all_selected

*set_curve_div_type_fix_ndiv
*set_curve_div_num
2
*apply_curve_divisions
9
all_selected

*af_planar_quadmesh
 13
 16
 19
all_selected
 19
 15
all_selected
 23
```

```
 9
 12
all_selected
 9
 12
 24
 17
 15
 21
all_selected
 11
 23
all_selected
 3
 13
 16
 17
 24
 11
 21
all_selected

*sweep_all
*remove_unused_nodes
*remove_unused_points
*renumber_all

*edit_material
socket
*add_material_elements
1 to 32
all_selected
*select_clear

*edit_material
liner
*add_material_elements
33 to 64
all_selected
*select_clear

*edit_material
skin
*add_material_elements
```

```
65 to 96
all_selected
*select_clear

*edit_material
fat
*add_material_elements
97 to 128
all_selected
*select_clear

*edit_material
bone
*add_material_elements
129 to 165 166 167 210 211 212 213 214
all_selected
*select_clear

*select_mode_invert
*select_elements_material
bone
fat
skin
liner
socket
*edit_material
muscle
*add_material_elements
all_unselected
*select_clear

*set_duplicate_scale_factors
1 1 1
*set_duplicate_translations
0 0 0.01
*set_duplicate_repetitions
1
*select_elements_material
skin fat muscle bone
*duplicate_elements
all_selected
*select_clear

*set_duplicate_scale_factors
```

```
.097276/.146 .097276/.146 1
*set_duplicate_translations
0 0 -.254017
*set_duplicate_repetitions
1
*select_elements
 1 to 316
*duplicate_elements
all_selected
*select_clear

*set_expand_scale_factors
.9899 .9899 .95
*set_expand_translations
0 0 -.014
*set_expand_repetitions
40
*select_elements
1 to 316
*expand_elements
all_selected
*select_clear

*set_expand_scale_factors
1 1 1
*set_expand_translations
0 0 .014
*set_expand_repetitions
10
*select_elements
317 to 568
*expand_elements
all_selected
*select_clear

*select_mode_and
*select_method_user_box
*select_elements
-.1
.1
-.1
.1
.005
.2
```

```
*set_move_translations
0 0 -.01
*set_move_scale_factors
1 1 1
*move_elements
all_selected
*select_clear
*select_reset

*edit_material
pylon
*select_elements
569 to 884
*add_material_elements
all_selected
*select_clear

*set_expand_scale_factors
1 1 1
*set_expand_translations
0 0 -.01
*set_expand_repetitions
1
*select_elements_material
pylon
*expand_elements
all_selected
*select_clear
*sweep_all

*set_duplicate_scale_factors
1 1 1
*set_duplicate_translations
0 0 -.01
*set_duplicate_repetitions
15
*select_elements
 16210 16211 16213 16212 16214 16222 16229 16223 16226 16234 16233 16225 16224
16232 16205 16206 16209 16208
 16207 16204 16221 16230 16228 16227 16231 16220 16219 16218 16217 16216 16215
16236 16235 16240 16249 16237
 16238 16243 16244 16245 16246 16251 16253 16248 16239 16250 16241 16247 16252
16242
all_selected
```

```
*duplicate_elements
all_selected
*select_clear
*sweep_all

*select_elements_material
pylon
*set_move_translations
0 0 .01
*set_move_scale_factors
1 1 1
*move_elements
all_selected
*select_clear
*select_reset

*sweep_all
*remove_unused_nodes
*remove_unused_points
*renumber_all

*add_surfaces
 point(-8.000000000000e-002, 8.000000000000e-002, -.245)
 point( 8.000000000000e-002, 8.000000000000e-002, -.245)
 point( 8.000000000000e-002,-8.000000000000e-002, -.245)
 point(-8.000000000000e-002,-8.000000000000e-002, -.245)

*edit_material
muscle
*select_method_surface_dist
*select_mode_and
*select_elements_material
bone
*select_mode_intersect
*set_select_distance
.045
*select_elements
 1
*add_material_elements
all_selected
*select_clear

*edit_material
fat
```

```
*select_mode_and
*select_elements_material
muscle
*select_mode_intersect
*set_select_distance
.025
*select_elements
 1
*add_material_elements
all_selected
*select_clear

*edit_material
skin
*select_clear
*select_mode_and
*select_elements_material
fat
*select_mode_intersect
*set_select_distance
.015
*select_elements
 1
*add_material_elements
all_selected
*select_clear

*edit_material
liner
*select_clear
*select_mode_and
*select_elements_material
skin
*select_mode_intersect
*set_select_distance
.013
*select_elements
 1
*add_material_elements
all_selected
*select_clear

*edit_material
socket
```

```
*select_clear
*select_mode_and
*select_elements_material
liner
*select_mode_intersect
*set_select_distance
.008
*select_elements
 1
*add_material_elements
all_selected
*select_clear

*edit_material
elastomer
*add_material_elements
 15484 15499 15514 15529 15544 15559 15574 15589 15604 15619 15634 15649 15664
 15679 15694 15709 15724 15739 15754 15769 15784 15799 15814 15829 15844 15859
 15874 15889 15904 15919 15934 15949 15964 15979 15994 16009 16024 16039 16054
 16069 16084 16099 16114 16129 16144 16159 16174 16189 16204 16219
all_selected
*select_clear

*new_icond
*icond_type displacement
*icond_dof x *icond_dof_value x
*icond_dof y *icond_dof_value y
*icond_dof z *icond_dof_value z
*icond_dof rx *icond_dof_value rx
*icond_dof ry *icond_dof_value ry
*icond_dof rz *icond_dof_value rz
*add_icond_nodes
all_existing

*new_icond
*icond_type velocity
*icond_dof x *icond_dof_value x
*icond_dof y *icond_dof_value y
*icond_dof z *icond_dof_value z
*icond_dof thx *icond_dof_value thx
*icond_dof thy *icond_dof_value thy
*icond_dof thz *icond_dof_value thz
*add_icond_nodes
all_existing
```

```
*edit_apply
fixedbone
*select_mode_and
*select_elements_material
bone
*select_nodes_elements
all_selected
*add_apply_nodes
all_selected
*select_clear

*add_nodes
0 0 -.40417
*new_rbe2
*rbe2_name
pylon_base
*rbe2_ret_node
 17577
*add_rbe2_tied_nodes
17539 17540 17521 17520 17519 17518 17517 17541 17542 17543 17530 17531 17532
17534 17535
17536 17537 17538
all_selected
*rbe2_tied_dof 1
*rbe2_tied_dof 2
*rbe2_tied_dof 3
*rbe2_tied_dof 4
*rbe2_tied_dof 5
*rbe2_tied_dof 6

*edit_apply
GRF_turning
*add_apply_nodes
17577
all_selected

*set_applys off
*regenerate

*geometry_type mech_three_solid
*geometry_option assumedstrn:on
*add_geometry_elements
all_existing
```

```
*loadcase_type dynamic_transient
*loadcase_value nsteps
20

*job_class mechanical
*element_type 7
all_existing

*add_job_loadcases lcase1

*job_option large:off
*loadcase_type dynamic_transient
*loadcase_option nonpos:on
*loadcase_option initstress:none

*add_post_tensor cauchy
*add_post_tensor strain
*add_post_var ecauchy
*add_post_var eel_strain
*add_post_var ee_energy

*job_param memory
3000000

*check_job
```

VITA

Kevin Flick earned a Bachelor of Arts degree in Biology, with a specialization in Marine Biology from Boston University. In 2005, he earned a Doctor of Philosophy at the University of Washington in Zoology.

Had it been up to me, the previous two sentences would be all there is to read on this page. Happily, my wife contributed the following:

Kevin Charles Flick has had many interests in his 35 years that he has pursued with as much passion as he has pursued science. Among these interests are cycling, backpacking, whitewater kayaking, endurance mountain biking, rock climbing, cooking and being a husband and father. Kevin does not approach life tentatively. He pushes himself to limits that are surpassed only by his spirit.

Kevin has been encouraged by two adoring parents to follow his curiosities and endless interests. Their support was resolute from the beginning, despite his interests including videogames and perilous endeavors on bicycles. The same could be said for his graduate school academic advisor.

Kevin has studied science in the Netherlands, at Boston University, and the University of Washington. He has worked at the Veteran's Administration developing prosthetics for the latter part of his graduate work. Prior to graduate school, he worked at TERC in Cambridge, Massachusetts, as a research associate developing teacher education curricula. For the two years prior, Kevin taught science to high school students in New York City. One year was in a bilingual classroom and the other was an honors biology and marine biology classroom.